

**INVESTIGATING EXPRESSION, FUNCTION AND
BIOCOMPATIBILITY OF THE GENETICALLY ENCODED CALCIUM
INDICATOR TN-XXL IN TRANSGENIC MICE**



Dissertation zur Erlangung des Doktorgrades der Naturwissenschaften
an der Fakultät für Biologie
der Ludwig-Maximilians-Universität München

vorgelegt von
Stephan Dörenberger

München, den 19.12.2011

Betreuer:

Dr. Oliver Griesbeck

Erstgutachter:

Prof. Dr. Alexander Borst

Zweitgutachter:

Prof. Dr. Rainer Uhl

Tag der mündlichen Prüfung:

29.03.2012

Table of Contents

Table of Contents	I
Abbreviations	V
1. Abstract.....	- 1 -
2. Introduction	- 3 -
2.1 Fluorescence and Fluorescence Resonance Energy Transfer.....	- 3 -
2.2. The Importance of Calcium Signaling	- 7 -
2.3. Synthetic Calcium Dyes.....	- 10 -
2.4. GFP – the Basis to Develop Genetically Encoded Indicators	- 11 -
2.5. Genetically Encoded Calcium Indicators (GECIs)	- 13 -
2.6. Advances of Calcium Imaging Techniques.....	- 17 -
2.7. TN-XXL - a Suitable GECI for the Generation of Transgenic Mice	- 18 -
2.8. Transgene Promoter Candidates to Drive TN-XXL Expression in Mice.....	- 20 -
2.9. Objective	- 22 -
3. Materials and Methods	- 23 -
3.1. Molecular Biology.....	- 23 -
3.1.1. Polymerase Chain Reaction	- 23 -
3.1.2. DNA Purification	- 24 -
3.1.3. Restriction Digest of DNA.....	- 24 -
3.1.4. Dephosphorylation of Vector DNA.....	- 25 -
3.1.5. Ligation of DNA Fragments	- 26 -
3.1.6. Preparation of Chemically-competent E. coli.....	- 27 -
3.1.7. Transformation of Chemically-competent E. coli.....	- 27 -
3.1.8. Purification of Bacterial DNA.....	- 27 -
3.2. Protein Biochemistry.....	- 28 -
3.2.1. Protein Expression Using the E. coli BL21 Strain.....	- 28 -
3.2.2. Purification of Recombinant Expressed Proteins	- 28 -
3.2.3. SDS Polyacrylamide Gel Electrophoresis.....	- 28 -
3.2.4. Western Blot.....	- 29 -
3.3. Cellular Biology	- 30 -
3.3.1. Preparation of Primary Cell Cultures	- 30 -
3.3.2. Dissection of Sinoatrial Node Explants from Adult Mice	- 30 -
3.3.3. Preparation of Dispersed SAN Cells	- 31 -
3.3.4. Preparation of E8.5 Hearts	- 31 -

TABLE OF CONTENTS

3.3.5. Transfection of Primary Cultured Cells and Dissociated Neurons.....	- 31 -
3.4. Histology and Immunohistochemistry.....	- 32 -
3.4.1 Cryosections of Fixed Mouse Tissues.....	- 32 -
3.4.2. DAPI Staining of Cryosections of Mouse Tissues.....	- 32 -
3.4.3 Immunostaining of Sinoatrial Node Tissue	- 32 -
3.4.4 Antibody Staining of Fixed Mouse Brain Sections	- 33 -
3.5. Imaging Experiments.....	- 34 -
3.5.1. Imaging of Fixed Tissue Sections and Stained Tissues	- 34 -
3.5.2. Fluorescence Recovery after Photo Bleaching (FRAP)	- 34 -
3.5.3. Concentration Determination of TN-XXL Expressing Tissue	- 35 -
3.5.4. Imaging of Primary Cultured Cells	- 35 -
3.5.5. Imaging of Embryonic Hearts.....	- 36 -
3.5.6. Imaging of Sinoatrial Node Explants from Adult Mouse Hearts	- 36 -
3.6. Transgenic Mice.....	- 37 -
3.6.1. Preparations for the Generation of Transgenic Mouse Lines.....	- 37 -
3.6.2. Purification of DNA fragments and pronucleus injection	- 38 -
3.6.3 Creation and Breeding of Transgenic mice.....	- 38 -
3.6.4. Genotyping	- 39 -
3.6.5 Breeding mouse lines for homozygosis.....	- 41 -
3.7. Microarray assays	- 41 -
3.8. Data Generation.....	- 42 -
3.8.1. Image Processing.....	- 42 -
3.8.2. Data Analyses.....	- 42 -
3.9. Materials	- 43 -
3.9.1. Instruments.....	- 43 -
3.9.2. Consumables.....	- 44 -
3.9.3. Buffers, solutions and media.....	- 45 -
3.9.4. Chemicals.....	- 48 -
3.9.5. Plasmids, bacterial strains, cell-lines and mice.....	- 50 -
4. Results	- 51 -
4.1. Transgenic Mice Expressing TN-XXL under the Thy-1.2 Promoter	- 51 -
4.1.1. Generation of Mice Expressing TN-XXL under the <i>Thy1.2</i> Promoter.....	- 51 -
4.1.2. Expression Patterns of <i>Thy1.2</i> TN-XXL Mouse Lines	- 52 -
4.2. Transgenic Mice Expressing TN-XXL under the Control of the TLCN Promoter	- 59 -
4.2.1. Testing the Functionality of pBstN-TLCN3.9:TN-XXL in Dissociated Neurons.....	- 60 -

TABLE OF CONTENTS

4.2.2. Expression Pattern of <i>TLCN3.9</i> TN-XXL Mouse Lines	- 61 -
4.3. Transgenic Mice Expressing TN-XXL under the Control of the β -actin Promoter	- 65 -
4.3.1. Western Blot Analysis of β -actin TN-XXL mice tissues	- 66 -
4.3.2. Observing Fluorescence Expression pattern of β -actin TN-XXL mice	- 66 -
4.3.3. Indicator Concentration, Mobility and Durability Inside Cells	- 69 -
4.3.4. Calcium Responses in Primary Cells Derived from Transgenic Mice.....	- 75 -
4.3.5. Calcium Responses of TN-XXL in Cardiac Tissues	- 76 -
4.3.6. Transcription Profiling of TN-XXL Expression in Transgenic Mice	- 83 -
4.3.7. Behavioral Testing of TN-XXL Mice.....	- 87 -
5. Discussion	- 91 -
5.1. Expression of TN-XXL under the Thy1.2 Promoter	- 92 -
5.2. In vivo Recordings in the Visual Cortex of Thy1.2 Mice Expressing TN-XXL.....	- 94 -
5.3. Transgenic Mice Expressing TN-XXL under the <i>TLCN3.9</i> Promoter	- 97 -
5.4. TN-XXL in Mice under the β -actin Promoter	- 98 -
5.4.1 Ubiquitous TN-XXL Expression.....	- 98 -
5.4.2. Long-term Expression and Performance of TN-XXL in Cultured Cells.....	- 99 -
5.4.3. Calcium Imaging of TN-XXL in Tissues of the Developing and Adult Heart.....	- 101 -
5.4.4. Effects of TN-XXL Expression on Gene Regulation and Animal Behavior	- 102 -
5.5. Conclusion.....	- 105 -
Appendix	- 107 -
References	- 111 -
Acknowledgements.....	i
Curriculum Vitae.....	iii
Versicherung	v

Abbreviations

°C	degree Celsius
Å	Angström
AM	acetomethyl
ATP	adenosine 5'-triphosphate
BAPTA	1,2-bis-[2-aminophenoxy]ethane-N,N,N',N'-tetraacetic acid
BBS	BES-buffered saline
BES	N,N-bis[2-hydroxyethyl]-2-aminoethanesulfonic acid
bp	base pair
bpm	beats per minute
CAG	CMV enhanced early chicken β -actin
CaM	calmodulin
CCD	charged-coupled device
CFP	cyan fluorescent
CMV	cytomegalovirus
cp	circular permuted
DAPI	4',6-diamidino-2-phenylindole
DMEM	Dulbecco's Modified Eagle Medium
DMSO	dimethyl sulfoxide
DNA	deoxyribonucleic acid
E18	embryonic day 18
E8.5	embryonic day 8.5
EDTA	ethylenediamine tetraacetic acid
EGTA	ethylene glycol-bis[β -amino-ethyl ether] N,N,N',N'-tetraacetic acid
ER	endoplasmic reticulum
F	fluorescence intensity emission
FCS	fetal calf serum
FRAP	fluorescence recovery after photobleaching
FRET	fluorescence resonance energy transfer
g	gram
GECI	genetically encoded calcium indicator

ABBREVIATIONS

GFP	green fluorescent protein
h	hour
HBSS	Hank's Balanced Salt Solution
HEK	human embryonic kidney
HEPES	N-(2-hydroxyethyl)piperazine-N'-(2-ethanesulfonic acid)
Hz	hertz
IP ₃	inositol-1,4,5-trisphosphate
IPTG	isopropyl- β -D-thiogalactopyranoside
l	liter
LB	lysogeny broth
M	molar
MCS	multiple cloning site
min	minute
MKF	murine kidney fibroblast
MOPS	3-(N-morpholino)propanesulfonic acid
nt	nucleotide
OGB-1	Oregon green BAPTA -1
PBS	phosphate buffered saline
PBT	phosphate buffered saline with Triton-X 100
PCR	polymerase chain reaction
PMSF	phenylmethylsulfonylfluoride
PMT	photo multiplier tube
R	ratio; YFP/CFP
R _{max}	ratio at highest calcium concentration
R _{min}	ratio at zero calcium concentration
ROS	Reactive oxygen species
RYR	ryanodine receptor
s	second
SAN	sinoatrial node
SDS	sodium dodecyl sulfate
SMC	smooth muscle cell

ABBREVIATIONS

SR	sarcoplasmic reticulum
TAE	tris-acetate-EDTA electrophoresis buffer
TE	tris-EDTA buffer
TG	transgenic
TLCN	telencephalin
TnC	troponin C
WT	wild-type
YFP	yellow fluorescent protein

1. Abstract

Monitoring cellular calcium levels by fluorescent probes has become an important method to visualize cellular signaling processes. The development of genetically encoded calcium indicators (GECIs) strongly contributed to the application of calcium imaging which in contrast to synthetic calcium dyes enables cell-type specific labeling, long-term expression and therefore chronic imaging approaches. Whilst GECI engineering and optimization mainly focused on improving signal strength or calcium affinities and kinetics, little is known about the magnitude of interference of GECIs affecting cellular calcium homeostasis in host organisms. Various previous attempts to genetically express GECIs using calmodulin-based indicators frequently resulted in pathological changes or decreased function of the GECI in the host organism. In contrast to calmodulin-based GECIs, calcium imaging studies in the nervous system of flies and mice expressing troponin C-based GECIs did not display detrimental changes.

In this work, TN-XXL performance was confirmed by transgenic TN-XXL expression in a *Thy1.2* driven mouse line which enabled chronic *in vivo* calcium imaging of sensory evoked calcium transients of layer 2/3 neurons of the visual cortex during monocular deprivation over weeks. In addition, a detailed analysis focused on TN-XXL expression, function, viability and biocompatibility in mice ubiquitously expressing TN-XXL under the β -*actin* promoter. TN-XXL expression was determined in almost all tissues examined and functionality was validated in a variety of cultured cell-types. In addition the applicability of ratiometric indicators for calcium imaging of dynamic and complex tissues was evaluated via the use of explants from developing and adult cardiac tissues. Moreover, the tolerance of long-term expressed TN-XXL was verified on cellular level and along with a genome wide transcriptional analysis and behavioral experiments TN-XXL biocompatibility was investigated with only minor effects on the host genome and behavior.

Together this study not only establishes the first detailed combined observation of function and biocompatibility of a GECI ubiquitously expressed in a mouse model but also has set the foundation criteria necessary for the evaluation of transgenic mouse lines expressing GECIs. Transgenic TN-XXL expression in this β -*actin* mouse line further offers ease of use for calcium signaling studies in a variety of cell-types and tissues of pharmaceutical relevance. Moreover, the facilitated cell line production and the possibility to establish mouse line crossings with existing disease models can open new grounds for investigations of calcium related diseases *in vitro* and *in vivo*.

2. Introduction

Fluorescence microscopy has become an integral part in the field of life science in the last decades. The success of fluorescence microscopy is based on the fundamental principle that the visualization of cells, cellular compartments or protein complexes within cells is achieved with a high contrast by fluorescent probe labeling. The detection of fluorescence with microscopes works with the following principle: an illuminating light beam excites fluorescent particles in a specimen which emit fluorescent light that further is collected by a photon detector (CCD camera, photo diode, etc.). To ensure a high contrast image the excitation and emission pathways are separated by optical filters. Further, the ability to visualize structures situated deep inside tissues with 2-photon microscopes or to resolve sub-diffraction patterns by super-resolution microscopy techniques such as STED, PALM and STORM strongly contributed to the success of fluorescence microscopy.

Furthermore, fluorescence microscopy is not only of use for the visualization cells or cellular compartments but also enables the analysis, monitoring and manipulation of cellular processes by the application of fluorescent sensors, which are either synthetic or genetically encoded in origin.

2.1 Fluorescence and Fluorescence Resonance Energy Transfer

Fluorescence is defined as the characteristic of a molecule to emit photons upon absorption of light. The photoactive part is defined as a 'fluorophore' and consists mostly of aromatic rings that form a π -electron system.

Fluorescence occurs in a fluorophore, when a photon elicited by an external light source excites an electron. This electron transits from a low energy ground state (S_0) to a state of increased energy. Dependent of the energy level of the absorbed photon ($h\nu_{EX}$) the electron can be elevated to different energy states (S_1, S_2, \dots) and subordinated vibrational levels (S_1'). From this excited state 'internal conversion' occurs within femtoseconds causing a relaxation of the electron to the lowest energy level of the excited state (S_1). When the electron falls back from S_1 to its ground state S_0 it emits energy in form of a photon (Figure 1). This process takes place within nanoseconds and defines the fluorescent lifetime of a fluorescent probe. Due to the energy loss during internal conversion, the energy of the emitted photon ($h\nu_{EM}$) is lower and therefore of longer wavelength than of the absorbed photon.

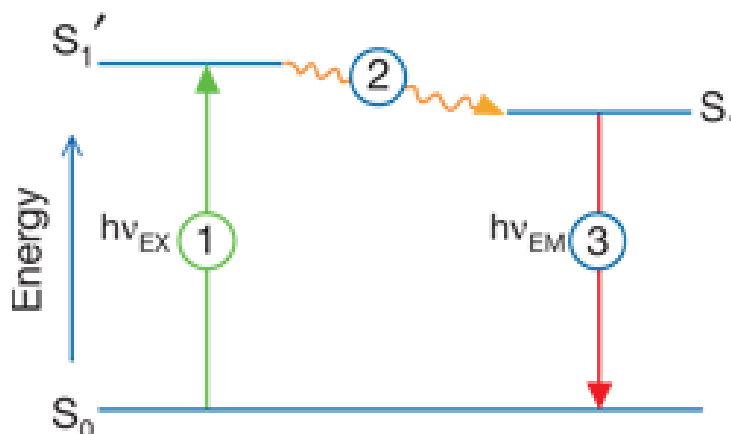


Figure 1: Jablonski diagram illustrating the cycle of fluorescence. An electron of a fluorophore is excited from the ground state (S_0) to an excited state (S_1'). Partially dissipating energy causes the drop to the singlet excited state (S_1) within nanoseconds from where a photon is emitted and the electron returns to its ground state (S_0).

This wavelength difference ($h\nu_{EX} - h\nu_{EM}$) between excitation and emission is called 'Stokes Shift' which allows the use of fluorescence microscopy by the separation of the optical pathway for the excitation and emission channel. Due to the separation of excitation and emission channels a high image quality with high contrast and low background signal is achieved which benefits fluorescence microscopy in contrast to bright-field transmission microscope techniques.

Fluorophores suitable for fluorescence microscopy need to possess a practical brightness which is defined by the extinction coefficient – the proportion of excitation light which is absorbed by a fluorophore – and the quantum efficiency. The quantum efficiency of a fluorophore is defined as the rate of the excitation light that is converted into fluorescence and is calculated from the ratio of emitted to absorbed photons. A higher quantum efficiency of a fluorophore implicates a low rate of non-radiative relaxation during the fluorescence process and therefore a reduced amount of light which is needed to excite the fluorophore. Hence, fluorophores which possess high quantum efficiency are more resistant to photobleaching. Long acquisition times and high light intensities in biological imaging can cause photobleaching, the irreversible chemical destruction of a fluorophore. Thus, the photostability or bleaching resistance is also an important characteristic for the use of fluorophores in fluorescence microscopy. As described above fluorescence is elicited by the emission of photon which is caused by the drop of an electron from excited singlet state (S_1) to the ground state (S_0). In some cases the excited electron can interconvert to an excited triplet state. In the triplet state electrons are trapped for microseconds to seconds and are

prone to incur chemical reactions with surrounding molecules (e.g. oxygen) which lead to photobleaching. Photobleaching is a cumulative effect of fluorophore loss from excitation-emission cycles over time and strongly depends on the excitation intensity (Song et al., 1995).

But the effect of photobleaching is also volitional in fluorescence microscopy. Photobleaching can be used in fluorescence recovery after photobleaching (FRAP) experiments, an optical technique whereby excitation light of high energy irreversible destroys the fluorophores in a defined area of interest. Due to Brownian motion, intact fluorophores from the outside of the bleached area will diffuse and replace the destroyed probes. This method can be applied to investigate diffusion and membrane exchange rates in cells loaded with synthetic dyes or expressing fluorescent proteins (FPs) which are freely diffusible or tagged to membranes or other cellular compartments (Tripathi and Parnaik, 2008; Houtsmuller, 2005; Axelrod et al., 1976).

Apart from the irreversible destruction of a fluorophore by photobleaching, the fluorescence emission intensity of a fluorophore can also be reversibly decreased by quenching of the fluorophore. Quenching occurs by the interaction of fluorophores with ions changing the chemical environment or with other substances interfering with the fluorophore (collision quenching) (Eftink and Ghiron, 1981).

Fluorescence resonance energy transfer (FRET) is a special form of quenching by which dipole-dipole interactions of fluorophores induce a non-radiative energy transmission from the donor to the acceptor fluorophore (Forster, 1946).

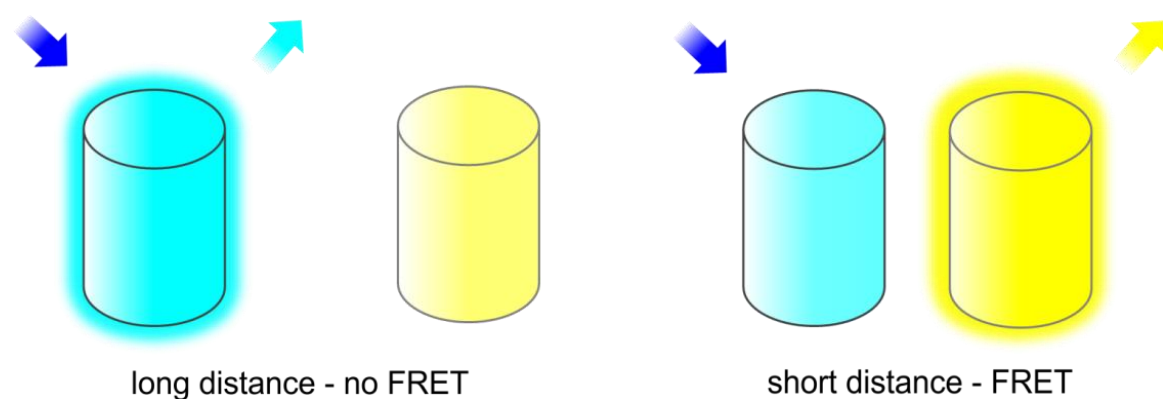


Figure 2: The Principle of FRET. A schematic representation of FRET. The blue arrow indicates the donor excitation. The donor emission when no FRET is occurring and acceptor emission are depicted by the cyan and yellow arrow, respectively.

Whilst the excited donor transfers its energy to an acceptor fluorophore, the acceptor itself becomes excited and emits a photon. Bringing the donor and the acceptor in close proximity induces the interaction of donor and acceptor and leads to a decrease in the donor emission (quenching) and an increase in acceptor emission (Figure 2). In general the FRET efficiency is dependent on three parameters. Firstly, it is determined by the 'spectral overlap integral' which describes the overlap of the donor emission and the acceptor absorption spectrum. Secondly, the FRET efficiency is highly dependent on the intermolecular distance. The quantum mechanical energy transfer can only occur when donor and acceptor fluorophore come to close proximity. The distance by which the energy transfer efficiency is 50% is called 'Förster distance'. Thirdly, the FRET efficiency is influenced by the orientation of dipole moments of donor and acceptor fluorophore to each other. An effect that can be neglected with small, freely rotating synthetic dyes but has to be taken into account with larger sized fluorescent proteins ($\sim 40 \text{ \AA}$) being limited in their orientational distribution (Hink et al., 2003).

Initially, FRET was used as a 'spectroscopic ruler' to measure distances between molecules tagged with fluorescent probes (Figure 2)(Stryer, 1978). Later the principle of FRET was extended to fluorescence microscopy whereby FRET enables ratiometric measurements of a fluorescent probe which emits light at two different wavelengths. The signal is calculated from the ratio of the two emission intensities. This ratiometric readout is more robust to misrepresentations of the investigated sample caused by motion artifacts, labeling differences and fluctuations of the illuminating light source or the recording device (CCD camera/PMT/Photo diode) than single fluorophore measurements (Helmchen, 2011). Due to these advantages FRET-based techniques are wide spread in fluorescence microscopy today and moreover build the basis for the development of FRET-based indicators that are applied in several cell biological disciplines, e.g. observing neuronal function by monitoring glutamate (Hires et al., 2008) and calcium levels (Mank et al., 2008) or by visualizing changes in neuronal membrane potentials (Dimitrov et al., 2007), and further to follow transcription in cells (Friedrich et al., 2010).

2.2. The Importance of Calcium Signaling

Calcium ions impact nearly every phase of cellular life. As the most important second messenger, calcium is involved in secretion, contraction, cellular excitability, gene expression, cell proliferation and cell death (Berridge et al., 2000). In general, calcium acts in different forms on cellular processes. Signaling of calcium can either occur extracellularly through voltage gated calcium channels and receptor activated channels (e.g. ATP, acetylcholine, glutamate) or mediated intracellularly whereby calcium concentrations are controlled by the uptake and release from internal stores of cellular compartments (Figure 3).

A major part of calcium research has been focused on investigating signaling mechanisms underlying neuronal function in the central nervous system (CNS). In neurons of the nervous system calcium influx occurs as a consequence of electric current propagation over the plasma membrane during neuronal activity which triggers the activation of voltage gated calcium channels. Thereby calcium navigates neurotransmitter release from vesicles for signal propagation at the presynapse, gene regulation by activation of further downstream processes at the soma, and synaptic plasticity and memory consolidation at the postsynapse in spines (Limbäck-Stokin et al., 2004). Monitoring and understanding neuronal function became a key role in neuroscience and the direct coupling of the rise of internal calcium concentration with neuronal activity enabled researchers to monitor neuronal activity by measuring intracellular calcium concentrations visualized with synthetic or genetically encoded calcium sensors.

However, calcium signaling is not only important for the maintenance of neuronal function in the brain through calcium influx from the extracellular space. Furthermore, most of the cellular signaling processes are regulated by alteration of intracellular calcium concentrations. Membrane receptors such as receptor tyrosine kinases or G-protein coupled receptors can be activated by numerous hormones which initiate a signaling cascade over activation of phospholipase C. Phospholipase C causes production of inositol-1,4,5-triphosphat (IP_3) which binds the IP_3 receptor (IP_3R) and triggers the release of calcium from the endoplasmic reticulum (ER). This leads to the activation of further downstream mechanisms, including metabolism, cell proliferation and gene regulation (Figure 3). Furthermore, in cardiac and skeletal muscle voltage gated calcium channels trigger the calcium-induced-calcium-release via calcium mediated activation of the ryanodine receptor (RyR) which initiates the calcium release from the sarcoplasmic reticulum (SR) and initiates the contraction process (Chueh and Gill, 1986; Lytton et al., 1992).

INTRODUCTION

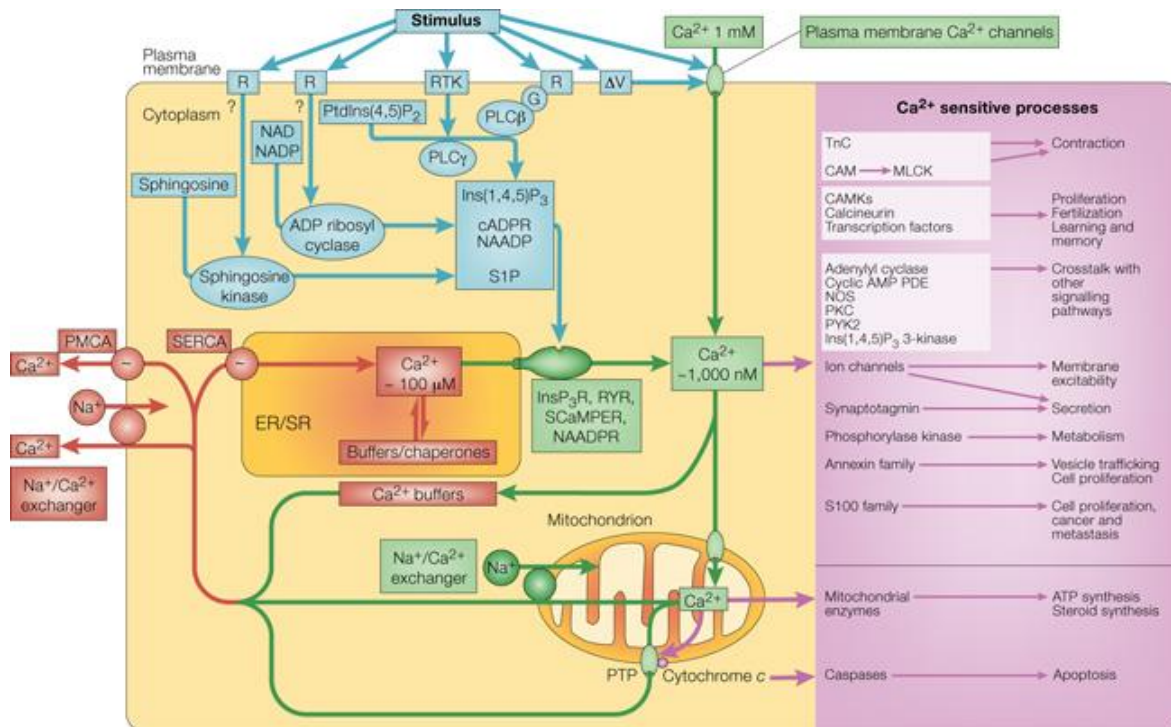


Figure 3: A schematic overview of cellular calcium signaling. Calcium mobilizing signals (blue) are stimulated through a variety of cell-surface receptors (R) including G-protein receptors (G) and receptor tyrosine kinases (RTK). These signals include: generation of Ins(1,4,5)P₃ from phosphatidylinositol-4,5-bisphosphate (PtdIns(4,5)P₂) catalyzed by phospholipase C enzymes (PLC β , PLC γ); cyclic ADP ribose (cADPR) and nicotinic dinucleotide phosphate (NAADP) generated from nicotinamide-adenine dinucleotide (NAD) and its phosphorylated derivative NADP by ADP ribosyl cyclase; sphingosine 1-phosphate (S1P) generated by a sphingosine kinase. The ON mechanisms (green) include calcium influx from voltage or ligand sensitive calcium channels or calcium release through internal channels: Ins(1,4,5)P₃ receptors, ryanodine receptors (RYR), NAADP receptors and sphingolipid Ca²⁺ release-mediating protein of the ER (SCaMPER) which activate cell-type specific calcium sensitive processes (purple). And the OFF mechanisms (red) which pump calcium out of the cytoplasm over Na⁺/Ca²⁺ exchanger and plasma membrane Ca²⁺ ATPases (PMCA) to the extracellular space or via sarco-/endoplasmic reticulum Ca²⁺ ATPase (SERCA) back to ER/SR (TrnC, troponin C; CAM, calmodulin; MLCK, myosin light chain kinase; CAMK, Ca²⁺/calmodulin dependent protein kinase; cAMP PDE, cyclic AMP phosphodiesterase; NOS, nitric oxide synthase; PKC, protein kinase C; PYK2, proline-rich kinase 2; PTP, permeability transition pore). Adapted from (Berridge et al., 2000).

These two systems are also able to co-operate e.g. in pancreatic cells where receptor activated calcium release from the ER is initialized by IP₃R and RYR which regulate fluid and enzyme secretion (Cancela et al., 1999).

High intracellular calcium levels occurring during calcium signaling would be cytotoxic when exposed over a long period of time and can elicit apoptotic mechanisms, therefore the internal calcium concentration is strictly regulated and excessive calcium is pumped out of the cell immediately, is retransferred to internal stores or buffered by calcium binding complexes which induce further signaling steps. The buffering of elevated intracellular

calcium can take place either via passive calcium buffers e.g. parvalbumin, calretinin shaping the amplitude and duration of calcium signals, or active calcium buffers e.g. troponin C (TnC) and calmodulin (CaM) that undergo conformational changes and activate further downstream processes. TnC mediates the interaction of actin and myosin during muscle contraction, whilst CaM is embedded in many general processes, including crosstalk between signaling pathways, ion channel modulation, metabolism and gene transcription.

Furthermore, calcium signaling is not just restricted to single cells or cellular compartments, but can also manifest as information transmission in between cells and propagate over major parts of tissues in form of calcium waves. Intercellular calcium waves can either travel via gap junctions or by the activation of purinergic receptors via extracellular ATP (Osipchuk and Cahalan, 1992) and regulate a variety of processes e.g. trigger cilia movement to expel inhaled contaminants in lung epithelium (Lansley and Sanderson, 1999), coordinate the metabolic function in liver (Gaspers and Thomas, 2005), or modulate neuronal activity and information processing in the CNS when propagating over glial cells (Newman, 2001).

Collapsing of the fine-tuning of calcium regulatory machinery due to exogenous environmental factors or mutations of genes involved in calcium regulation can implicate undesirable effects in the calcium homeostasis and impair calcium signaling. These calcium-signaling abnormalities can have severe pathological consequences, e.g. mutations of the RYR induced dysregulation of intracellular calcium release can cause neuromuscular disorders (Gommans et al., 2002; Treves et al., 2005), dysregulation of intracellular calcium transients during cardiac contraction can diminish force production and decrease cardiac function (Hasenfuss et al., 1992; Wehrens et al., 2005) and farther calcium dysregulations are also involved in neurodegenerative diseases, such as Alzheimer's or Parkinson disease (Wojda et al., 2008).

The role of calcium as global player in regulating cellular functions and its function during the occurrence of diseases was a driving force for the investigations that have been performed to date. Furthermore, researchers began to develop tools to monitor calcium concentrations and to gain superior knowledge in the mechanisms of how calcium regulates physiological processes. The development of synthetic and genetically encoded fluorescent probes to trace calcium levels supported research for a better understanding of mechanisms that involve calcium fluctuations, such as memory consolidation and synaptic formation, but also brought new insights to neurodegenerative, cardiac and muscle diseases and cancer development (Berridge et al., 2003).

2.3. Synthetic Calcium Dyes

Before the development of fluorescent probes that allow tracing of cellular calcium concentrations, researchers were constrained to electrophysiological recordings which are very complex regarding the equipment, time-consuming and recordings from a high number of cells at a time are difficult to achieve. The design and development of synthetic calcium dyes enabled non-invasive recordings of intracellular calcium signals solely with a fluorescence microscope and farther simultaneous monitoring of a high number of cells became possible.

The first generation of synthetic calcium dyes emerged in the 1980's. These versions were all hydrophilic, therefore not membrane-permeable and disadvantageous for non-invasive cell experiments. The breakthrough of synthetic calcium dyes for intracellular imaging began when Roger Tsien and colleagues developed fluorescent dyes fused to acetoxymethyl (AM) esters (Tsien, 1981). These AM-ester fused dyes are hydrophobic, can be bath-applied and are able to cross cell membranes and enter cells. Once infiltrated a cell the inactive esterified dyes become activated by de-esterification of endogenous esterases. The cleavage of the ester turns the dye hydrophilic, cell impermeable and therefore becomes trapped in the cell. Based on this principle numerous synthetic calcium dyes were developed with different calcium dissociation constants (K_d) for monitoring calcium signals of different concentrations. High affinity calcium dyes (e.g. Fura-2, OGB-1, Fluo-4) with low K_d values in the nano-molar range were developed to investigate systems with low calcium transients e.g. neuronal activity (Ohki et al., 2006; Stosiek et al., 2003), whereby affinity calcium dyes with high K_d values in micro molar range (e.g. Fluo-5N, OGB-5N) were constructed to observe calcium dynamics in models with high changes in calcium concentration e.g. in skeletal (DiFranco et al., 2002) and cardiac muscle (Fan and Palade, 1999).

In general, synthetic calcium dyes are very successful in the field of calcium imaging due to the high brightness, bleach resistance, and fast kinetics. However, a major disadvantage of synthetic dyes is that cellular localization cannot be tightly controlled and targeting of particular cell types, subsets of cell or organelles is hardly achievable. The loading via membrane-permanent esters is often difficult or impossible in animals with thick cell walls or cuticles such as in the fruit fly *Drosophila melanogaster* or the nematode *Ceanorhabditis elegans*. Additionally, synthetic calcium dyes tend to compartmentalize and are eventually extruded from the cell during long-term recordings and they diffuse out of cell over time which obstruct the establishment chronic imaging experiments (Palmer and Tsien, 2006). These drawbacks especially manifest in experiments with tissue explants or *in vivo* preparations. Researchers tried different approaches to overcome these drawbacks e.g. by

microinjection of synthetic dyes which limited the recording number to a single cell at a time (Svoboda et al., 1999), electroporation or by bulk loading of cell-populations (Nagayama et al., 2007; Stosiek et al., 2003). But regardless of improvements concerning dye delivery the labeling remained unspecific and temporary.

With the discovery and utilization of the green fluorescent protein (GFP) and numerous color variants researchers could overcome these drawbacks by engineering GFP-based genetically encoded calcium indicators (GECIs), biosensors that exclusively consist of amino acids and can be synthesized by the host cell or organism for a facilitated use to investigate calcium signaling (McCombs and Palmer, 2008).

2.4. GFP – the Basis to Develop Genetically Encoded Indicators

The discovery of GFP in 1962 by Shimomura in the jellyfish *Aequorea victoria* (Shimomura et al., 1962) and subsequent steps in the 1990s of solving the genetic sequence (Prasher et al., 1992), the 3 dimensional structure (Cubitt et al., 1995; Ormö et al., 1996; Yang et al., 1996) and the ability to express cDNA of GFP in bacteria or nematodes (Chalfie et al., 1994) paved the way for the success that GFP holds in research today.

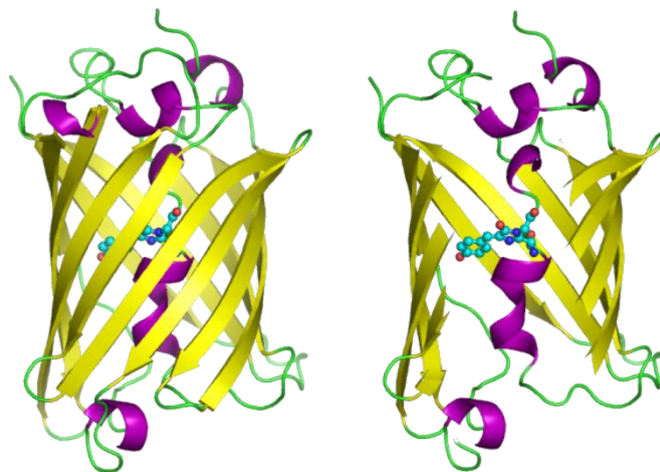


Figure 4: Scheme of the crystal structure of GFP. Side view of the β -barrel (yellow) and the centered fluorophore (Ser65-Tyr66-Gly67) stabilized by α -helices (purple). In the right picture some residues are removed to allow a better view of the fluorophore. Modified from PDB-entry 1GFL (Yang et al., 1996).

During that time researchers elaborated that the formation of the GFP fluorophore under aerobic conditions is accomplished by autocatalytic cyclization of the 3 amino acids Ser65–Tyr66–Gly67 in protection of the surrounding β -barrel consisting of 11 beta sheets (Figure 4)(Tsien, 1998). Rapidly, scientist began to exchange residues surrounding the fluorophore by rational design, random mutagenesis and DNA shuffling eager to improve the wild-type GFP (Cormack et al., 1996; Heim et al., 1994; Cramer et al., 1996). That gave rise to new variants with improved brightness, photostability and spectral properties.

The original GFP, being derived from the cold water jellyfish *Aequorea victoria* exhibited poor folding properties at 37°C. The addition of the mutations F64L which optimized the folding properties of GFP at 37°C and S65T that shifted the original excitation peak of GFP from 395nm to 488nm yielded the brighter and more stable version of GFP named enhanced GFP (EGFP) (Cormack et al., 1996). On the basis of EGFP further mutations broad up a variety of spectral versions. Mutating the residue Y66W gave rise to the cyan fluorescent protein (CFP) with excitation and emission maxima at 432nm and 475nm, respectively (Cormack et al., 1996). The development of the yellow fluorescent protein (YFP) which exhibits maximal fluorescence upon excitation at 514 nm at an emission at 527nm was due to mutations at the coordinating residues S65G and T203F (Wachter et al., 1998). Further mutations of YFP generated Citrine, an improved version to diminish pH, chloride sensitivity and increased photostability and protein folding properties (Griesbeck et al., 2001). The good spectral overlap of CFP and YFP variants rendered them the most successful FRET pair for the deployment to FRET-based biosensors to date (Piston and Kremers, 2007).

The rapid development of GFP variants and the discovery of new orange and red fluorescent proteins (FPs) deriving from different organisms extended the color spectrum of FPs (Shaner et al., 2004). To date researchers can choose from a wide spectrum of FPs with various properties regarding color, brightness, photostability, folding efficiency and pH dependency. Moreover, specific expression of FPs in the cytosol or fused to endogenous cellular proteins allowed studying morphology and cellular dynamics of specific cell types, cellular organelles or compartments. Furthermore, the development of fusion-constructs consisting of FPs and a regulatory subunit of a protein enabled the design of functional single- and dual-wavelength biosensors to monitor a large variety of cellular processes using fluorescence microscopy.

2.5. Genetically Encoded Calcium Indicators (GECIs)

Solely composed of DNA, a variety of genetically encoded sensors can be engineered by deleting, inserting or manipulating parts of the DNA. Furthermore, the use of cellular targeting sequences, cell-type or tissue specific promoters, and transgenic technologies provides methods of non-invasively expressing indicators in tissue of living organisms with cellular and sub-cellular specificity (Caroni, 1997; Hara et al., 2004; Mitsui et al., 2007).

The development of GECIs was profoundly inspired from the desire to study neuronal activity. The coupling of electrical signal propagation during neuronal information transmission with the influx of calcium through voltage gated channels motivated researchers to develop genetically encoded tools to investigate the complexity of neuronal function. The advantages GECIs imply in contrast to synthetic calcium dyes further supported their development (see section 2.3).

In general, GECIs consist of a calcium binding domain which undergoes a conformational change upon binding of calcium ions and is either fused to a single or two fluorescent proteins which transform conformational changes into a fluorescence readout. In single FP sensors the calcium binding modulates the brightness of the FP by changing the degree of protonation of the fluorophore (Figure 5 A), whereas dual FP sensors work on the principle of FRET (see section 2.1) whereby the binding of calcium induces a decrease donor fluorescence emission and an increase the acceptor fluorescence (Figure 5 B).

The development of single FP GECIs rose with the observation that FPs tolerate insertions of large fraction without abolishing the fluorescence (Baird et al., 1999). The insertion of the calcium binding domain calmodulin from *Xenopus* at the position Tyr145 of YFP and further improvements due to folding problems and pH sensitivity by exchanging YFP to Citrine lead to the single FP GECIs Camgaroos, low sensitivity sensors with K_d values of 5-7 μM (Figure 6 A)(Baird et al., 1999; Griesbeck et al., 2001). However, Camgaroos suffered from low fluorescence at basal calcium levels and therefore were difficult to detect when expressed in mammalian cells. A further step towards improved single FP GECIs yielded in the development of the Pericams, sensors whereby calmodulin and its binding peptide M13 were fused to the N- and C-terminal ending of a circular permuted variant of YFP (YFP cp145) (Nagai et al., 2001). The new N-/C-terminal ends were situated in closer proximity to the fluorophore in order to allow a higher interference and higher response range of the sensor to calcium binding. Indeed, Flash pericam exhibited higher calcium affinity with K_d values of 0.2 - 1.7 μM and an increase of intensity upon calcium binding of up to 8-fold.

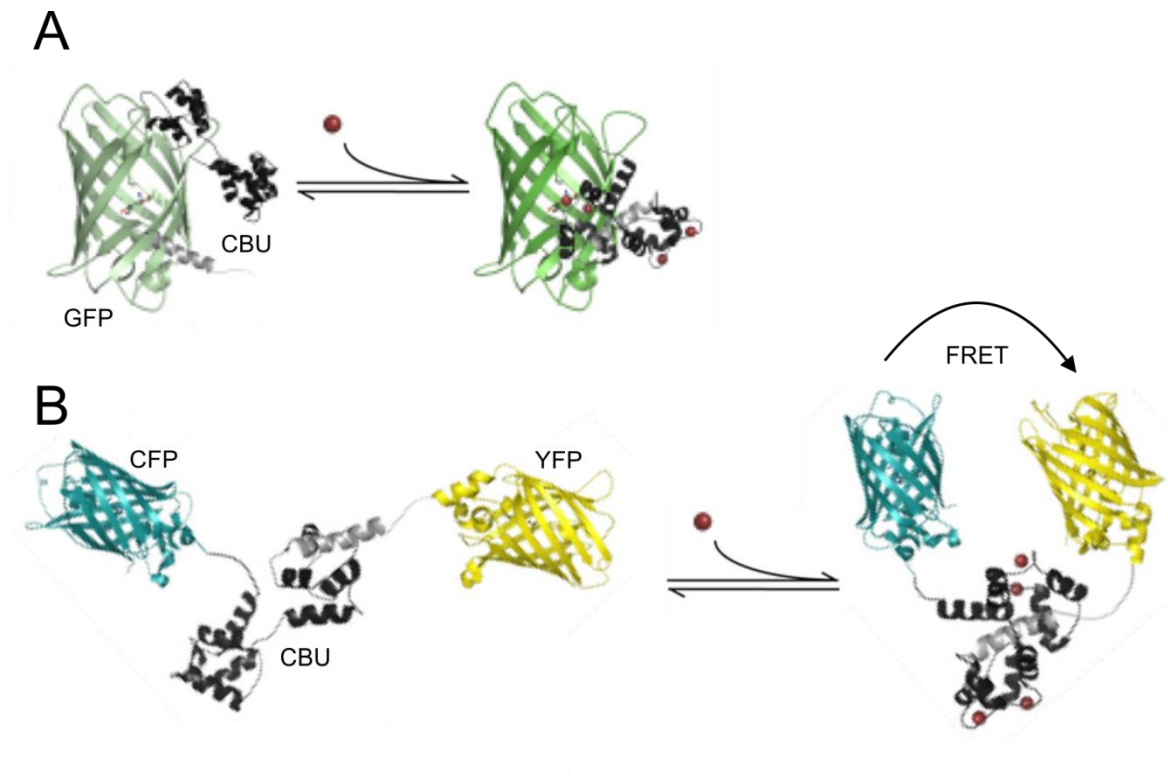


Figure 5: A schematic model of the working principle of single FP and FRET-based GECIs. (A) A single FP sensor consisting of a circularly permuted GFP and a calcium binding unit (CBU). Upon binding of calcium the CBU changes conformation and induces a change in the protonation state of the GFP which leads to a fluorescence increase. (B) A FRET-based calcium indicator consisting of a donor (CFP) and acceptor (YFP) fluorophore fused to a CBU. Calcium binding elicits a conformational change which brings the two FPs in closer proximity and FRET can occur. Modified from McCombs and Palmer, 2008.

However, the low fluorescence at basal calcium levels made expression almost undetectable in cell culture.

On the building principle of the Pericams, a new class of single FP GECIs, the G-CaMPs, revolutionized the field of single FP calcium indicators. In G-CaMPs the fluorescence backbone of YFP was exchanged by a circularly permuted variant of EGFP (EGFP cp149) and the amino acid residues 145-148 were deleted (Nakai et al., 2001). The first version showed similar disadvantages as Camgaroos and Pericams: dim basal fluorescence, pH sensitivity and slow maturation at 37°C. However after incorporation of several mutations new variants showed better folding, increased basal fluorescence, higher signal change upon calcium binding and high calcium affinities with a K_d value up to 150 nM were created (Tian et al., 2009).

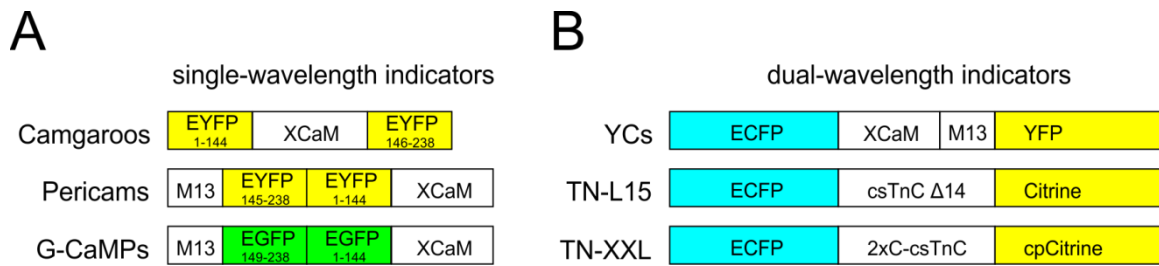


Figure 6: Schematic overview of the major groups of single- and dual wavelength GECIs. (A) Single-wavelength indicators Camgaroos, Pericams and G-CaMPs. In Camgaroos the calcium binding *Xenopus* calmodulin (XCaM) is inserted in between YFP variants. The Pericams use circularly permuted EYFP flanked by an N-terminal M13 peptide and a C-terminal XCaM. G-CaMPs share the same building principle as Pericams but exchanged YFP with GFP. (B) Dual-wavelength GECIs Yellow Cameleons (YC), TN-L15 and TN-XXL consist of either TnC or XCaM/M13 serving as calcium binding domain which is sandwiched between CFP and YFP/Citrine or circularly permuted variants. Modified from Mank and Griesbeck, 2008.

Besides the low fluorescence at basal calcium concentrations single FP sensors are prone to imaging artifacts due to the single channel readout. Motion artifacts elicited by out-of-focus movements, fluctuations of the excitation light source or uneven cellular expression can lead to misinterpretations of the imaging data and distort the experimental outcome.

To overcome these disadvantages dual fluorophore indicators that function on the basis of FRET were developed. The dual-channel ratiometric readout of fluorescence in FRET sensors counteracts imaging artifacts yielding a more consistent imaging readout which plays to the use of FRET-based sensors in moving preparations and *in vivo* experiments (e.g. heartbeat, respiratory movements). Common FRET pairs incorporated in dual FP indicators are of variants of CFP (ECFP, mCerulean (Rizzo et al., 2004), mTurquoise (Goedhart et al., 2010)) and YFP (EYFP, mVenus (Nagai et al., 2002), mCitrine (Griesbeck et al., 2001)) which until to date exhibit the most optimal spectral overlap and exceed the best dynamic range. In general, two versions of dual FP indicators have evolved. On the one hand, the Cameleons, FRET-indicators of which calmodulin/M13 serves as the calcium binding unit that was already used in single FP indicators on the other hand GECI that incorporate troponin C (TnC) as calcium binding moiety (Figure 6 B). *In vitro* experiments with Cameleons show ratio changes up to 600 % and also high calcium affinity with K_d values of 50 – 250 nM. However, exposing calmodulin-based GECIs to *in vivo* conditions most of them exhibited poor performance, most likely a consequence of the interaction of calmodulin with the cellular machinery (Nagai et al., 2004).

Therefore, FRET-based indicators with troponin C serving as calcium binding domain were developed in the research group of Oliver Griesbeck. TnC in contrast to calmodulin is not

INTRODUCTION

endogenously expressed globally in every cell, but expression is restricted to skeletal and cardiac muscle whereby TnC incorporated in the troponin complex consisting of troponin C, I and T, is responsible for calcium binding during muscle contraction. The first TnC-based indicator incorporated a truncated variant of chicken skeletal TnC sandwiched between CFP and Citrine. This indicator, named TN-L15, was successfully expressed in mammalian cells and in transgenic animals where it reliably reported cytosolic calcium changes (Heim and Griesbeck, 2004; Heim et al., 2007). In terms of monitoring small calcium fluctuations which occur during neuronal firing the signal strength and sensitivity to magnesium ions diminished the dynamic range of TN-L15. A first attempt to reduce the magnesium sensitivity by mutating the residues N109D, D111N, N145D and D147N of the C-lobe of TnC gave rise to TN-XL, a high speed but low affinity sensor which turned out to be suitable for systems with high calcium fluctuations but inapplicable to monitor low changes in calcium concentration, e.g. single action potentials (Mank et al., 2006). A second step to increase calcium affinity by keeping low magnesium sensitivity was achieved by rearranging the TnC domain.

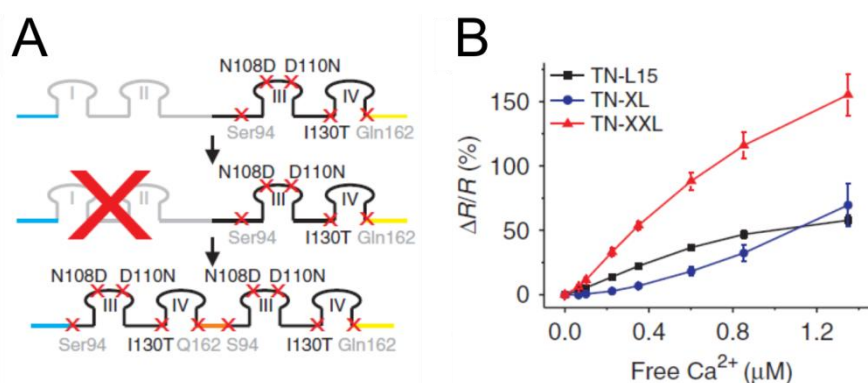


Figure 7: Generation and *in vitro* properties of TN-XXL. (A) Schematic illustration of the rearrangement and substitution of N- and C-terminal domains of TN-XXL. Blue and yellow lines depict the fusion to CFP and cpCitrine, respectively. (B) Calcium affinity titration of TN-L15, TN-XL and TN-XXL. Modified from Mank et al, 2008.

The low-affine N-terminal lobe of TnC (EF-Hand I and II) was replaced by the high affine C-terminal lobe (EF-hand III and IV) resulting in a TnC chimera consisting of two C-terminal lobes (Figure 7 A). Furthermore, two mutations (N145D and D147N) were reversed in each of the C-terminal lobes. This yielded in the upgraded FRET-based GECI TN-XXL which deployed ratio changes of up to 250 % *in vitro* and reported an improved calcium affinity with a *K_d* value in the range of 800 nM (Figure 7 B). TN-XXL was amongst the first FRET-

based GECIs able to resolve single action potentials measured in hippocampal slice preparations. Furthermore, *in vivo* calcium imaging in flies and successful chronic *in vivo* imaging in orientation selective neurons the primary visual cortex of anesthetized mice proved the potential of TN-XXL (Mank et al., 2008).

2.6. Advances of Calcium Imaging Techniques

Early imaging experiments were restricted due to the lack of advanced optical and technical devices suitable for fluorescence imaging. Using wide-field fluorescence microscopy or single photon confocal microscopy limited imaging depth therefore the use of imaging approaches was narrowed down to cell culture experiments or studies in optical transparent organisms like *C. elegans* or the zebrafish larvae. Moreover, intact tissues produce light scattering effects that even with a powerful laser pulse of a laser scanning confocal microscope hindered imaging in regions lying deeper than 50 – 100 μm (Russell, 2011).

With the development of the 2-photon microscope by Winfried Denk and colleagues in the 1990s this depth limit could be broken and functional calcium imaging up to several hundreds of micrometers was possible due to the shift in laser excitation to the infrared which is less prone to light scattering and allows deeper tissue penetration (Denk et al., 1990). As a consequence of this breakthrough optical imaging and computing technologies advanced rapidly in the past decades and enabled the development of increasingly sophisticated imaging approaches from *in vitro* cell experiments to *in vivo* imaging in intact tissues, whole intact anesthetized or even awake animals.

There are two major aspects why *in vivo* application of calcium indicators are mainly restricted to investigations of neuronal activity in the brain. On the one hand the realization to perform *in vivo* calcium imaging experiments was driven by the fact that the brain is surrounded by thick bone which allows fixation of the head and enabled decoupling from body motion artifacts produced by body movements, heart beat or the respiratory system. On the other hand, the lack of knowledge how neuronal function and signal transmission are computed in the CNS encouraged researchers to observe the mechanisms underlying neuronal function, in circuits, synaptic transmission and signal propagation. Therefore, techniques were developed which allowed 2-photon microscopy in anesthetized and head-fixed animals and in addition to record calcium responses e.g. in barrel and visual cortex with synthetic dyes and GECIs (Stosiek et al., 2003; Mrsic-Flogel et al., 2007; Heim et al., 2007; Mank et al., 2008; Wallace et al., 2008). Furthermore, the application of GECIs enabled

chronic calcium imaging experiment in cortical pyramidal neurons of over days and weeks (Mank et al., 2008).

Ongoing improvements of technical equipment either by mounting head-fixed awake mice on a Styrofoam ball (Dombeck et al., 2007) or by the installation of a miniature 2-photon microscope on the head of a freely moving rats (Helmchen et al., 2001) extended the diversity of imaging applications from anesthetized head-fixed animals to awake, freely moving and behaving animals. However, the mentioned 2-photon calcium imaging approaches still suffer from depth restrictions of 200-400 μm depending on the optics and used laser power which limit imaging to upper cortical layers and impair observations of deeper brain region. Improvements the of optical toolbox e.g. the development optical prisms for periscopic imaging (Murayama et al., 2007) or the invention of ultra-small, needle-like gradient index (GRIN) lenses for optical-fibers (Levene et al., 2004) allowed minimally invasive *in vivo* 2-photon calcium imaging on a subcellular resolution in depths up to several millimeters. A non-invasive way enabling the *in vivo* recording of calcium signal in deeper areas was the development of regenerative amplification multiphoton microscopy (RAMM). With this recently developed method spontaneous and sensory-evoked neuronal calcium transients of layer 5 neurons located 800 μm deep in the cortex of anesthetized mice could be recorded *in vivo* (Mittmann et al., 2011).

2.7. TN-XXL - a Suitable GECI for the Generation of Transgenic Mice

The improvements in advanced microscopy techniques during the last decade would benefit from the generation of transgenic animals expressing a GECI since transfection, viral transduction or loading of the calcium indicator would become redundant. This would simplify the design and implementation of calcium imaging experiments. Furthermore, dye loading, transduction of calcium sensors by virus mediated gene transfer or electroporation need additional intervention and subsequently can cause stress for the animal that could distort the experimental outcome. With the generation of transgenic animals these aspects can be avoided. Likewise, the generation of transgenic animals needs a careful decision which promoter has to be selected. One has to take into account a promoter which provides expression in the preferred region of interest and at sufficient expression levels of the transgene to assure the applicability of the transgenic animal.

Moreover, the most appropriate GECI in terms of brightness, dynamic range and cell viability has to be chosen. As mentioned above, *in vivo* imaging studies of calmodulin-based GECIs like G-CaMPs and Yellow Cameleons (YC) showed impairment of the GECI during

long-term expression. Additionally, it has been reported that in some cases the production of transgenic animals expressing calmodulin-based GECIs was accompanied by severe morphological defects, aggregation and loss of function of the indicator (Hasan et al., 2004; Tallini et al., 2006; Tian et al., 2009). The mentioned effects are thought to manifest due to the interaction of the indicators' CaM with endogenous CaM and the interference with downstream signaling pathways. Furthermore, this hypothesis was supported by a study whereby overexpression of CaM in ventricular cardiomyocytes of mice perturbed DNA synthesis during the cell cycle which caused hyperplasia, a pathologic form of enhanced cell proliferation in the adult heart (Colomer et al., 2004).

To avoid interaction of the expressed GECI with endogenous cellular processes a different type of calcium indicators – TnC-based calcium indicators – can be picked for the generation of transgenic animals. Troponin C is solely expressed in muscle tissue and in contrast to CaM its function is restricted to muscle contraction and does not interfere with further signaling processes. It has been shown before that a derivate of the TnC-based calcium indicator TN-L15 was successfully and functionally expressed in mice without deploying any obvious visible cellular defects (Heim et al., 2007).

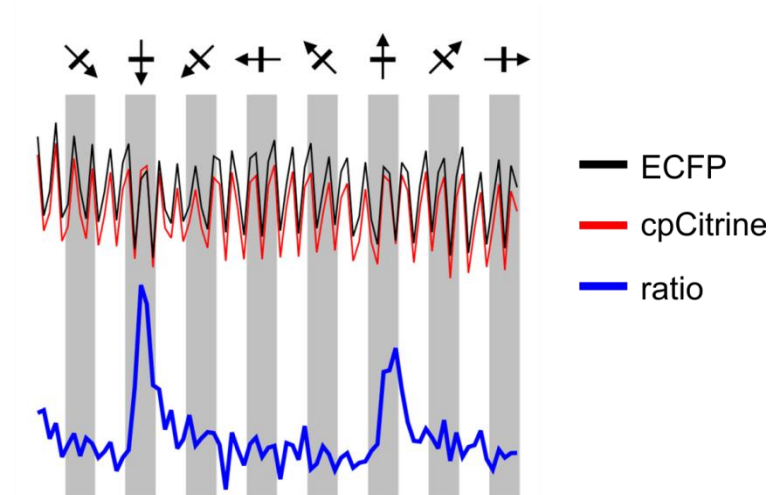


Figure 8: Ratiometric properties of TN-XXL in neurons *in vivo*. Imaging of sensory evoked calcium transients recorded in cortical neurons of the mouse visual cortex to moving bars of different orientations (indicated by arrows). The upper traces display the effect of motion artifacts caused by the respiratory system on the single emission channel readout (ECFP, black; cpCitrine, red). The lower trace (blue) illustrates a distinct orientation selective response to up- and downward motion due to the reduction of motion artifacts by the calculation of the ratio (R) (cpCitrine/ECFP). Alexandre Ferraro Santos unpublished observations.

Its improved version TN-XXL which possesses better calcium affinity and higher dynamic range was already tested in *in vivo* experiments in the mouse visual system whereby chronic calcium imaging from cortical neurons over weeks also yielded reproducible orientation-selective responses without displaying neuronal defects or changes in cell morphology (Mank et al., 2008). Together with the ratiometric readout which facilitates imaging of moving tissues (Figure 8), overcomes fluctuation of the light source or uneven expression levels this characterizes TnC-based calcium indicators in general and TN-XXL in particular as suitable candidate for long-term calcium imaging experiments and the generation of transgenic animals.

2.8. Transgene Promoter Candidates to Drive TN-XXL Expression in Mice

Already mentioned, the TnC-based GECI TN-L15 successfully showed the neuronal expression in transgenic mice under the control of the *Thy1.2* promoter (Heim et al., 2007). Due to the low dynamic range and the low calcium sensitivity of TN-L15 small calcium transients could not be recorded. Therefore, it would be beneficial to transgenically express the improved GECI TN-XXL in mouse lines under the *Thy1.2* promoter. First described by Caroni and colleagues, the *Thy1.2* promoter specifically drives expression of neurons in cortical, hippocampal, thalamic and brainstem regions of the brain in a mosaic manner (Caroni, 1997). This well-studied promoter was further chosen for the expression of several FPs whereby high-level transgene expression was observed (Feng et al., 2000). Although, the *Thy1.2* promoter exhibits high neuronal expression, it is known to favor expression of neurons in layers lying 600 – 800 μm deep in the cortex (layer 4 and 5).

To date, using standard 2-photon microscopes *in vivo* calcium imaging is constrained to depth of 400 μm and calcium imaging of deeper situated cells is just achievable with high-end 2-photon microscope setups, which are not commonly available, yet. Therefore a further approach can be elaborated by using the telencephalin (*TLCN*) promoter, a recently discovered neuronal promoter, which drives transgene expression preferably in upper cortical layers (layer 2/3) in depth of 150 – 300 μm (Mitsui et al., 2007). Expressing TN-XXL driven by the *TLCN* promoter would be more desirable for the use of standard 2-photon microscopy techniques for the study of neuronal activity in cortical regions *in vivo*.

The advances in imaging technology and the improvements of GECIs more than proved the applicability of GECIs to investigate neuronal function and network dynamics. The state of development where GECIs are found today enables first attempts to break the barrier of restricting the application for GECIs to the nervous system where most studies have been reported so far. The ability to produce transgenic animals expressing GECIs under different genomic promoters can open doors for the use of GECIs in more clinical relevant fields. In a previous study the ubiquitously expressing chicken β -actin (CAG) promoter, including an immediate-early cytomegalovirus enhancer and a bovine globin poly-adenylation signal, was used for the generation of mouse lines expressing EGFP in several tissues and cell types (Okabe et al., 1997).

The global expression of a GECI such as TN-XXL with its advantages of ratiometric readout and interoperability in this transgenic background could enable to extend the applicability of calcium imaging. β -actin promoter driven TN-XXL expression would allow calcium imaging in a vast amount of organs to study calcium signaling or dysregulations, e.g. in the cardiovascular, the renal and the hematopoietic system where labeling of synthetic dyes or transfection of GECIs are difficult to achieve. Advantages of a such a 'ready-to-image' mouse would also manifest in the ease of generation and handling of cells and tissues for the preparation of calcium imaging experiments since methods like dye loading, transfection or virus mediated transduction to express calcium dyes or indicators would be redundant. Furthermore, a 'ready-to-image' mouse could be used as model organism for the extraction of different types of primary cell lines or the establishment of stem cell lines that can be used for pharmacological screenings to investigate the effect of drugs on calcium sensitive mechanism.

So far calcium imaging has become essential in neuroscience, cell biology and physiological research. However, *in vivo* studies are restricted to research regarding the nervous system and the potential of GECIs as tool in pharmacological studies has been underachieved.

2.9. Objective

The generation of transgenic mice expressing GECIs under different promoters will become a more and more valuable tool to study calcium dynamics. Therefore, a major goal of this work is the characterization of transgenic mice expressing TN-XXL under different promoters.

A first part of this study will concentrate on the generation and characterization of transgenic mouse lines which express the GECI TN-XXL in the central nervous system under the control of the *Thy1.2* and the *TLCN* promoter. Furthermore, expression patterns and expression levels of TN-XXL will be investigated in the gained mouse models.

A further goal of this work is the examination of the functionality and biocompatibility of long-term expression of TN-XXL in an already existing mouse model whereby TN-XXL is expressed under the *β -actin* promoter which drives transgene expression ubiquitously in various cells and organs. First, levels of TN-XXL expression in different tissues will be observed by fluorescence microscopy. Furthermore, the functionality of TN-XXL will be elaborated with calcium imaging experiments in different kinds of cultured cell types and tissue explants. Moreover, the biocompatibility of TN-XXL will be addressed by investigating the viability of TN-XXL on the cellular level. Lastly, transcriptional profiling and behavioral analyses should clarify global effects on gene expression and animals' behavior of long-term expression of TN-XXL in this mouse model to validate the applicability.

3. Materials and Methods

3.1. Molecular Biology

3.1.1. Polymerase Chain Reaction

Originally developed by Mullis the PCR technique allows the amplification of DNA via the utilization of thermally stable bacterial or archaean polymerases such as Taq or Pfu (Mullis et al., 1986). The different polymerases vary in DNA amplifying speed and accuracy. In this study, Taq polymerase was used for high speed DNA amplifications that allowed mutations due to the low proof-reading capability (e.g. mouse genotyping). Herculase II Fusion, a fusion of an engineered Pfu variant with high affinity DNA binding domain, was used for reactions demanding high yield, superior reliability and short cycling times.

Table 1: The reaction mix of a PCR

Reagent	Volume	Unit
DNA template	0.5-1 μ l	200ng/ μ l
primer #1	1 μ l	50 μ M
primer #2	1 μ l	50 μ M
Herc. II Reaction Buffer	10 μ l	5x
dNTP solution	1 μ l	12.5 mM
Herculase II fusion	0.5 μ l	2 U
DMSO if needed	5 μ l	
add H ₂ O to 50 μ l		

Addition of DMSO to the reaction mix (Table 1) often enhances the yield of DNA obtained by the PCR especially when the reaction initially produces too little DNA, when added the water volume was reduced to the respective volume. All reagents were added on ice and the reaction was initialized with the 95°C incubation step (Table 2). Hot start increases specificity and reduces primer dimerization.

Table 2: The temporal order for the PCR reaction

Reaction step	Temp.	Time
1. Hot start	95°C	5 min
2. Denaturation	95°C	30 s
3. Annealing	55°C	1 min
4. Elongation	68°C	1-2 min
29x repetition of step 2.-4.		
5. Final elongation	68°C	5 min
6. Final hold	15°C	forever

3.1.2. DNA Purification

The Purification of DNA fragments > 100 nt was performed with the QIAquick PCR Purification Kit. In addition, to separate DNA fragments of different sizes (> 70 nt) on an agarose gel, the QIAquick Gel Extraction Kit was applied. The kits were used according to the manufacturer's protocol.

3.1.3. Restriction Digest of DNA

Restriction endonucleases recognize a specific sequence of nucleotides and produce a cut in the DNA. The target sequence for restriction enzymes – a restriction site – mostly consists of a short palindromic DNA sequence that has a length of 4 – 8 bp. In cloning, restriction endonucleases are used to bind to their target site and cut DNA. This characteristic offers a molecular tool to specifically recombine DNA fragments. Both the vector backbone and the insert are digested with two different restriction enzymes. The restricted DNA fragments were used as substrates for the subsequent ligation reaction (Table 4). Restriction digest were also used to check for the successful insertion of a DNA fragment into the vector backbone (Table 3).

MATERIALS AND METHODS

Table 3: Protocol for analytical digest to determine the successful insertion of DNA

Reagent	Volume	Unit
DNA template	1 - 2 μ l	100-200 ng
restriction enzyme	0.1 - 0.3 μ l	~2 U
BSA	0.2 μ l	100 x
restriction buffer	2 μ l	10 x
Add H ₂ O to 20 μ l total volume		
Incubate for 1 h at 37°C		

Table 4: Protocol for Preparative digests for subsequent cloning

Reagent	Volume	Unit
DNA template	2 - 10 μ l	2-10 μ g
restriction enzyme	1 - 3 μ l	~10 U
BSA	0.5 μ l	100 x
restriction buffer	5 μ l	10 x
Add H ₂ O to 50 μ l total volume		
Incubate for 3 h to 16 h at 37°C.		
(depending on restriction enzyme used)		

3.1.4. Dephosphorylation of Vector DNA

Dephosphorylation of a digested vector is used to avoid self-ligation of the opened vector. The removal of 5'-phosphate groups from DNA that is required for a successful ligation reaction is catalyzed by phosphatases. The Antarctic Phosphatase is the enzyme of choice because it can be heat-inactivated and the vector can be used for ligation without any further purification step (Table 5).

MATERIALS AND METHODS

Table 5: Protocol for the dephosphorilation reaction

Reagent	Volume	Units
digested DNA vector	50 μ l	100-200 ng
Antarctic Phosphatase buffer	6 μ l	10x
Antarctic Phosphatase	1 μ l	1U/ μ l
Add H ₂ O to a total volume of 60 μ l		
Incubation at 37°C for 2 h		

To inhibit the dephosphorylating reaction the samples were incubated at 70°C for 10 min.

3.1.5. Ligation of DNA Fragments

DNA ligases catalyze the fusion of two DNA fragments with complementary sequences. Treatment of the vector backbone and the insertion fragment with the same set of restriction enzymes enables the directed introduction of the desired fragment into the vector backbone (Table 6).

Table 6: Protocol for the ligation reaction

Reagent	Volume	Unit
vector DNA	0.5 - 1 μ l	50 ng
insert DNA	1 - 3 μ l	150 - 250 ng
T4 Ligase Buffer	1.5 μ l	10 x
T4 DNA ligase	0.75 μ l	(300 U)
Add H ₂ O to 15 μ l total volume		
Incubate for 1 h to 16 h at room temperature.		

3.1.6. Preparation of Chemically-competent *E. coli*

For the preparation of chemically competent cells, *E. coli* strains (XL1 Blue, BL21 gold) cell were processed following a modified protocol according to Inoue (Inoue et al., 1990). In brief, cells were inoculated and grown over night in 4 ml LB medium at 37°C. After the first hour of growth tetracycline (10µg/ml) was added to the solution. The following day, the culture was transferred to 300 ml LB medium and grown until a OD₆₀₀ of 0.5 - 0.6 was reached. The cell suspension was placed on ice for 20 min and followed by centrifugation at 2500 g for 20 min (4°C). The supernatant was discarded and the pellet was resuspended in 60-80 ml of chilled Inoue transformation buffer. After an additional centrifugation step at 2500 g for 15 min (4°C) the cells were resuspended in 20 ml Inoue transformation buffer supplemented with 1.5 ml DMSO. The cell suspension incubated on ice for 10 min containing the chemically competent *E. coli* was aliquoted (50 µl) and stored at -80°C until usage.

3.1.7. Transformation of Chemically-competent *E. coli*

An aliquot of chemically competent cells (XL1 Blue, BL21 gold; see above) was thawed for 5 min on ice and plasmid DNA (5 µl of a ligation reaction; 100 ng of purified vector DNA) was added. Cells were incubated on ice for 20 - 30 min and heat-shocked for 1 min at 42°C. After the heat-shock, cells were kept on ice for 2 min. For bacteria transformed with plasmids carrying an ampicillin resistance the bacteria were immediately plated. An additional step was necessary, when other antibiotics were used. To overcome the inhibition of protein synthesis caused by antibiotics 150 µl of LB-medium was added to the bacterial suspension and incubated for 1 h at 37°C without antibiotics before plating them onto LB-agar plates containing the respective antibiotic.

3.1.8. Purification of Bacterial DNA

Plasmid DNA expressed in bacteria was extracted and purified. Smaller amounts with a DNA yield of up to 10 µg from 2 ml bacterial culture were gained using the QIAprep Miniprep Kit. Processing was accomplished following the manufacturer's protocol. Larger amounts and higher purity of DNA were achieved with the PureYield™ Plasmid Midiprep System. From 200 ml bacterial culture up to 500 µg of DNA could be isolated. After purification DNA was stored at -20 °C.

3.2. Protein Biochemistry

3.2.1. Protein Expression Using the *E. coli* BL21 Strain

Protein expression vectors (pRSET, pET-28A) carrying the gene of interest were transformed with the *E. coli* strain BL21. A starting culture of transformed bacteria culture was grown over-night at 37°C in 5 ml of LB medium containing the corresponding antibiotic (100 µg/ml). The day after the culture was transferred to 400 ml LB medium containing antibiotics (100 µg/ml) and let grow until an OD₆₀₀ of 0.6 to 0.8 was reached. To induce expression 0.5 mM IPTG was added and the culture was incubated for 3 – 8 h at 37°C. Bacterial cells were harvested by centrifugation at 6000 g for 10 min (4°C).

3.2.2. Purification of Recombinant Expressed Proteins

A bacterial pellet was resuspended with 10 ml of protein resuspension buffer containing 1 mM PMSF, 5 µg/ml Pepstatin and 1 µg/µl Leupeptin to inhibit protease activity. To induce cell lysis the cell suspension was incubated at -80°C for 10 min. After thawing, lysozyme (1 mg) was added and incubated for 30 min on ice followed by addition of Triton-X-100 (0.1 %), DNaseI (5 µg/ml) and RNase (5 µg/ml) and ultra-sonication for 20 min on ice. The sample was centrifuged for 30 min at 13.000 rpm, the supernatant containing the protein of interest was transferred to a new tube and 300 µl of Ni-NTA agarose was added. Binding of the N-terminal 6 x His-tag to the Ni-NTA agarose was allowed for 2 h at 4°C. The protein/Ni-NTA agarose complex was put in a polypropylene column and washed with 20 ml protein resuspension buffer. After washing the protein was eluted with protein elution buffer.

3.2.3. SDS Polyacrylamide Gel Electrophoresis

To prepare protein lysates mouse tissues were dissected and cut in small pieces, frozen in liquid nitrogen and ground with a pestle and mortar. Fragments were suspended in RIPA buffer and homogenized on ice. Cell fragments were spun for 10 min at 20,000 rcf and supernatants were stored at -20°C until usage. Next, the protein concentration was estimated using the BCA protein assay following the manufacturer's instructions.

Separation of proteins was achieved by denaturing, discontinuous, one-dimensional SDS polyacrylamide gel electrophoresis (SDS-PAGE) using pre-cast gels. 2x protein loading buffer was added to 10 μ l cell lysate, boiled for 5 min at 100°C and loaded on the gel. Electrophoresis was performed in protein running buffer at 100 V for stacking and at 130 V for resolving of proteins. Finally the gel was stained with Coomassie Brilliant Blue.

3.2.4. Western Blot

Proteins were electrophoretically transferred from polyacrylamide gels using the semi-dry blotting technique. The transfer was carried out at a current of 0.8 mA/cm² for one hour at RT. Therefore, 6 layers Whatman paper wetted in anode buffer I, 3 layers Whatman paper wetted in anode buffer II, a Polyvinylidene fluoride membrane, the polyacrylamide gel and 6 layers Whatman paper wetted in cathode buffer were stacked in the blotting chamber. After transfer of proteins, the membrane was blocked by incubation in PBS, 5% milk powder over-night at 4°C. The primary antibody was diluted in PBS, 0.1% Tween-20, 1% milk powder. Primary antibody incubation was done for 1 hour at RT. After four washing steps with PBS, 0.2% Tween-20 for 5 min, the membrane was incubated with HRP-coupled secondary antibody in PBS, 0.1% Tween-20, 1% milk powder for 1 hour at RT in the dark. The membrane was washed four times for 5 min; final washing was done in PBS. Bands were detected using ECL Western Blotting Substrate on an ECL hyperfilm.

3.3. Cellular Biology

3.3.1. Preparation of Primary Cell Cultures

For cell culture experiments 6-8 week old wild-type or homozygous transgenic mice were sacrificed by cervical dislocation. Murine kidney fibroblasts (MKF) were obtained from kidneys and smooth muscle cells (SMC) were obtained from bladder. Kidneys and bladder were transferred to a PBS containing dish and cut into small pieces. The pieces were incubated for 30 min at 37°C in DMEM containing 1% Pen/Strep and 2mg/ml collagenase II. The digested tissue was put into a cell culture dish containing DMEM + 10% FCS + 1% Pen/Strep. MKF culture was left for one week until the first change of medium and splitting. For SMC upon media change the following day the cells were ready to use.

For the preparation of astrocytes cultures 2 day old pups were sacrificed. The skull was removed and the brain was dissected. The cortices were separated from the brain and put into HEPES (15 mM) buffered HBSS. The meninges were removed and the cortices were homogenized. Trypsin-EDTA (2mg/ml) was added and incubated for 10 min at 37°C. DMEM containing 10% FCS and 1% Pen/Strep was added and the sample was centrifuged. The pellet was resuspended and filtered through a 70µm cell strainer (BD Falcon) and plated in T75 flasks. The medium was changed every 2-3 days. After 10 days of incubation the flasks were shaken at 300 rpm for 6 hours at 37°C to separate oligodendrocytes from astrocytes. After changing of medium the shaking process was repeated for additional 24 hours.

3.3.2. Dissection of Sinoatrial Node Explants from Adult Mice

Mice of the age of 8-12 weeks were sacrificed. The abdomen was cut open, the diaphragm was carefully removed and the thorax was open by cutting along the lateral side of the ribs. The heart was removed and flipped to the back and pinned in a 10 cm dish filled with silicon. While rinsing the heart with Tyrode Low solution the sinoatrial node (SAN) region was cut out along the superior vena cava and the crista terminalis (Glukhov et al., 2010). The dissected SAN was pinned on a custom built stage equipped with a temperature controlled perfusion system and rinsed with Tyrode III solution.

3.3.3. Preparation of Dispersed SAN Cells

Instead of pinning the dissected SAN region on the stage (see 3.3.2) it was incubated for 5 min at 35°C in Tyrode III. A mixture of Collagenase B (0.12 mg), Elastase (0.4 mg) and BSA (10 mg) was added to the solution and incubated for another 30 min at 35°C for digestion. After digestion the tissues were centrifuged at 700 g the supernatant was discarded and the medium was carefully resuspended in 'Kraft-Brühe'. Centrifugation and the resuspension were repeated for four times to remove the residuals of the proteases. Before usage the dispersed SAN cells kept at 4°C for 30 min to recover.

3.3.4. Preparation of E8.5 Hearts

To obtain embryonic hearts of the desired age of 8.5 days vaginal plug checks were performed the morning after mating with a male mouse with a positive plug check signifying a successful mating event. The progress of pregnancy was calculated from this time point. After 8 more days of pregnancy mice were sacrificed by cervical dislocation (Stieber et al., 2003). The abdomen was opened, the uterus was cut out and put in a dish containing chilled PBS. The embryos were removed and the hearts were dissected under a dissection stereomicroscope and transferred to dishes containing DMEM supplemented with 10% FCS and 1% PenStrep and incubated overnight at 37°C. Experiments were performed the day after dissection.

3.3.5. Transfection of Primary Cultured Cells and Dissociated Neurons

Delivering TN-XXL to primary cell cultures and dissociated Neurons was performed using the lipofectamine approach. For that purpose 2 µg of plasmid DNA were solved in 250 µl of Opti-MEM I. In parallel 10 µl of Lipofectamine 2000 were mixed with 250 µl of Opti-MEM I and incubated for 5 min at room temperature. The DNA- and the Lipofectamine-mix were combined allowed forming vesicles containing DNA and incubated for additional 20 min. The DNA-Lipofectamine-mix was added to cells growing in 30 mm glass bottom dishes and the transfection was allowed to proceed for 3 h incubating at 37°C with 5% CO₂. After 3 h of incubation, cells were washed with 1 ml PBS and 2 ml of DMEM (10% FCS, 1% PenStrep) were added. Cells were allowed to recover from the treatment and to express the TN-XXL over-night and were ready to use the next day.

3.4. Histology and Immunohistochemistry

3.4.1 Cryosections of Fixed Mouse Tissues

Different tissues, the brain, heart, intestines, kidney, liver, skeletal muscle, spleen, stomach and a piece of the mouse tail were dissected from mice sacrificed by cervical dislocation. The mouse tissues were washed in PBS, incubated for 2 hours in 4% PFA solution at room temperature and transferred into PBS containing 30% sucrose for an overnight incubation at 4°C. To prepare for cryosectioning, the tissues were frozen in M-1 Embedding Matrix medium on dry ice and stored at -20°C until usage. The embedded tissues were mounted on a CM 3050 cryostat and cut into 25 µm thin sections. Subsequently, slices were mounted on glass slides, embedded with Roti-Mount Aqua and kept at 4°C until usage.

3.4.2. DAPI Staining of Cryosections of Mouse Tissues

Before embedding the slices in mounting medium DAPI diluted to 1:1000 in PBS was incubated for 10 min before the slides were cover with Roti Aqua Mount medium and a cover slip.

3.4.3 Immunostaining of Sinoatrial Node Tissue

Dispersed SAN cells (see 3.3.3.) stored in a tube were centrifuged and the medium was replaced carefully with PBS and the cells were fixed by incubation with 4% PFA solution for 15-20 minutes at room temperature. The cell suspension was centrifuged again, PFA was exchanged with PBS and the cells were incubated for 20 minutes at room temperature in PBT after another step of centrifugation. The rat monoclonal antibody to HCN4 primary antibody was diluted 1:300 in PBT and the suspension gently shaken either for 1 - 4 hours at room temperature. To avoid background staining, the primary antibody solution was washed with PBS during a minimum of two hours during which the PBS was exchanged every 30 minutes. Afterwards, the Alexa568-conjugated goat anti-rat secondary antibody was diluted 1:400 in PBT and again left for either 4 hours at room temperature or overnight at 4°C. The washing procedure was repeated and the cell suspension was transferred to a

glass slide and covered with Roti Aqua Mount medium. Slides covered in mounting medium were kept refrigerated until imaging analysis.

Fixed SAN explants were treated in the same way apart for the incubation times. Incubation for the first and secondary antibody was extended to 2-3 days at 4°C.

3.4.4 Antibody Staining of Fixed Mouse Brain Sections

Fluorescent protein expression was visualized in fixed 25 µm cryosections of PFA immersed, PCR-positive mouse brains. Immunostaining was done by incubating brain sections overnight at 4°C with polyclonal anti-GFP anti-rat antibodies diluted 1:200 in PBT buffer. The primary antibody solution was removed by washing the slices three times in PBT and PBS for 30 minutes and exchanged by Alexa568-labelled goat anti-rat secondary antibody diluted 1:400 in PBT and incubated again for either 4 hours at room temperature or overnight at 4°C. The first washing procedure was repeated and the slices were finally mounted on glass slides, covered with Roti Aqua Mount medium and a cover glass.

3.5. Imaging Experiments

3.5.1. Imaging of Fixed Tissue Sections and Stained Tissues

Immunostained or unstained frozen sections, stained dispersed single cells, and fixed tissue explants were imaged on a Leica TCS SP5 II laser scanning confocal microscope using direct cpCitrine excitation with an argon ion laser at 514 nm with an output power of 20%. Depending on the tissue preparation and section thickness the acousto-optic tunable filters (AOTF) were adjusted in a range of 5 – 30 %. The emission readout was recorded with a PMT set to 700 V and an emission bandwidth of 525 – 560 nm. Samples labeled with Alexa568 were additionally recorded with a 561nm DPSS (diode pumped solid state) laser at powers of 20-40 % at a PMT value of 700V and an emission bandwidth of 590 – 650 nm. The samples were visualized with oil immersion objectives 20x/0.7NA and 40x/1.25NA and an image resolution of 1024x1024 pixels.

3.5.2. Fluorescence Recovery after Photo Bleaching (FRAP)

FRAP experiments were done with cultured murine kidney fibroblasts (MKF) harvested from homozygous *β-actin* TN-XXL mice (see above). An inverted epifluorescence microscope (DeltaVision RT) equipped with a quantifiable laser module with laser emission at 488nm to apply the bleaching pulse and a CCD camera for image capturing was used. CpCitrine was excited with light that was filtered with a 500/20 nm filter and the emission was read out with 535/25nm filter in front of the CCD camera. Cells were recorded with a 60x/1.4NA oil immersion objective at a resolution of 512x512 pixels and a binning of 2. The experimental procedure was accomplished by taking three images before applying the bleaching pulse to determine the baseline fluorescence followed by a laser pulse of 80 ms with a laser intensity of 50% at defined bleaching area of about 25 μm². After the pulse images were taken at a rate of 220ms over a period of 8 seconds.

3.5.3. Concentration Determination of TN-XXL Expressing Tissue

TN-XXL was purified from *E.coli* BL21 see 3.3.x and concentrated with Amicon Ultra-15 (Millipore, MA, USA) to a concentration of 10 mg/ml (135 μ M). This stock solution was diluted to 1:20, 1:25, 1:40, 1:50, 1:80, 1:100 and 1:160 for experiments.

Organs (hippocampus, cortex, kidney, heart, hind limb muscle) of 6-8 month old homozygous transgenic mice were cut into 400 μ m thin section with a McIlwain tissue chopper and transferred to HBSS containing dishes until usage.

The experiments were performed with a TCS SP5 II laser scanning confocal microscope. Laser light of a 514 nm argon ion laser at 17% output power and AOTF of 15% was used for direct cpCitrine excitation at a pinhole size of 80 μ m. Images were recorded with a water immersion objective of 20x/0.5 NA magnification at a scan speed of 400 Hz with a resolution of 1024x1024 pixels. The emission bandwidth was set to 525 - 600nm with a PMT power of 650 V. These settings were used for all experiments.

3.5.4. Imaging of Primary Cultured Cells

Cells were grown on either Poly-L-lysine coated or untreated glass-bottom dishes. Before the start of the experiments the culture medium was exchanged with HBSS containing calcium and magnesium and the cells were left for 10 min to equilibrate. For the stimulation depending on the cell type either ATP or Carbachol was applied at a final concentration of 10 μ M and 100 μ M, respectively.

Calcium imaging was performed with a 40x objective on a Zeiss Axiovert 35M inverted microscope equipped with a CoolSnapHQ CCD camera. For ratio metric imaging, a 440/20 excitation filter, a 455 dichroic long-pass mirror, and two emission filters (485/35 for CFP, 535/25 for cpCitrine) operated with a filter wheel were used. The imaging parameters, including filter wheels, shutter and acquisition time is controlled by MetaFluor v4.6 software.

3.5.5. Imaging of Embryonic Hearts

To let the hearts recover, the experiments were done one day after dissection. For imaging experiments hearts were transferred into glass bottom dishes with Tyrode III (140mM NaCl, 5.4mM KCl, 1mM MgCl₂, 1.8mM CaCl₂, 5mM HEPES, 5.5mM Glucose). The experiments were performed at 30°C using a custom made heating chamber attached to an inverted fluorescence microscope (iMic, Till Photonics) equipped with a built in 440/20 nm CFP excitation filter and a dual wavelength emission filter of 485/30nm for CFP and 535/30nm for cpCitricine. Split view mode allowed a presentation of the two emission channels to the CCD camera at the same time for simultaneous and faster imaging. Embryonic hearts were recorded with a 10x/0.3NA objective at imaging a frequency of 22 Hz with a CCD chip binning of 2.

3.5.6. Imaging of Sinoatrial Node Explants from Adult Mouse Hearts

After dissection the sinoatrial node (SAN) explant was pinned on a custom built temperature controlled stage and equilibrated with Tyrode III solution to 30°C. Single cell and line scan imaging was performed on a Leica TPS 5 SPII laser scanning confocal microscope using a 458 nm argon ion laser excitation at 20 % output power and AOTF level of 30%. To reduce shot noise generated by the PMTs the gain of the two emission channels was calibrated to a pixel intensity value of 0 for 50 % of an image recorded without laser illumination of the sample. Calcium imaging of single SAN cells was performed with a low magnifying 20x/0.5 NA water immersion objective at a 6x zoom which is coupled to the scanning speed to allow imaging at high speeds of 1400 Hz per line which resulted in acquisition time of 33ms (30Hz) per image consisting of 256x38 pixels or 129.7x19.3 μm per image. The emission was recorded with two PMTs, each collecting photons for the respective emission channel. The bandwidth of the CFP emission channel was set to wavelengths of 465 – 505nm at a PMT level of 750 V, the cpCitricine channel was adjusted to wavelengths of 525 – 600nm at a PMT level of 700 V. For the recording of line scans the same settings as for single cell imaging were used, except the scan speed was adjusted to 400 Hz per line.

3.6. Transgenic Mice

3.6.1. Preparations for the Generation of Transgenic Mouse Lines

3.6.1.1. Subcloning of TN-XXL into the *Thy1.2* Expression Vector

In order to express TNXXL in transgenic mouse lines under control of the *Thy1.2* expression cassette, I followed the protocol published by P. Caroni (Caroni, 1997). To enable cloning of TN-XXL into the pUC18_Thy1.2 vector two *XhoI* sites had to be introduced at the 5' and 3' ends and the *EcoRI* site at the 3' end had to be removed from pRSETB:TN-XXL. Additionally, an *EcoRV* site was introduced between the stop codon (TAA) and the 3' *XhoI* site to check for the right insertion direction. This was performed by PCR amplification with suitable primer pairs. The pRSETB:TN-XXL vector carrying the new restriction sites and the pUC18_Thy1.2 vector were digested with *XhoI*. The digested pUC18_Thy1.2 was dephosphorylated and TN-XXL was inserted, leading to the construct pUC18:Thy1.2_TN-XXL. pUC18:Thy1.2_TN-XXL was linearized by digestion with *EcoRI* and *PvuI*.

3.6.1.2. Subcloning of TN-XXL into the *TLCN3.9* Expression Vector

The cloning vector pRSETB:*SwaI*-mKO2 vector was created carrying the right restriction sites for cloning genes of interest into the transgene expression vector pBstN:*TLCN3.9*. Starting at the 6xHis-Tag which was situated upstream of the multiple cloning site, the vector pRSETB:*SwaI*-mKO2 was composed like the following: pRSETB -6xHisTag_ *NheI*-*SwaI*-*BamHI*_mKO2_ *EcoRI*-*PacI*-*SwaI*. The original insert mKO2 was exchanged with TN-XXL by restriction digest with *BamHI* and *EcoRI*. The resulting pRSETB-*SwaI*-TN-XXL vector and the pBstN:*TLCN3.9* vector were digested with *SwaI*. The opened pBstN:*TLCN3.9* vector was dephosphorylated and TN-XXL was inserted at the *SwaI* site. To linearize the pBstN:*TLCN3.9*_TN-XXL vector a restriction digest with *XbaI* and *AscI* was performed.

3.6.2. Purification of DNA fragments and pronucleus injection

The linearized DNA samples were purified via agarose gel electrophoresis followed by electroelution of the DNA fragment from the agarose into a Spectra/Por dialysis tubing (Sambrook and Russell, 2001a). In order to further free the DNA of all contaminants, an ion exchange chromatography was performed using a small disposable Elutip-D Minicolumn. The column was first equilibrated in Low Salt DNA Purification Buffer, then the DNA obtained from the electroelution procedure applied to the column, washed with Low Salt Buffer and then eluted with High Salt DNA Purification Buffer. The purified DNA fragments were checked for purity by agarose gel electrophoresis and their concentration was adjusted with injection buffer to 100 ng/ μ l.

3.6.3 Creation and Breeding of Transgenic mice

Purified linear DNA fragments were used for injections into pronuclei of mouse oocytes by the DNA microinjection method (Nagy et al., 2003). All injection procedures were performed by the Transgenic Service facility at the MPI for Biochemistry in Martinsried, Germany. The mouse strain used for oocyte injections was C57BL/6N. Founder animals were screened for *Thy1.2/CFP* or *TCLN/CFP* gene sequences by PCR of genomic DNA obtained from tail lysates by the method described above, and PCR-positive founders were crossed with wild type mice. Breeding of the transgenic lines was continued with C57BL/6N mouse strain; all animals used were obtained from the MPI for Biochemistry's animal breeding facilities.

All animal procedures used in this report were in accordance with guidelines of the committee on animals of the Max Planck Institute of Neurobiology and with the license of the Regierung von Oberbayern (Munich, Germany).

3.6.4. Genotyping

Genomic DNA was gained from mouse tail tissue using the Proteinase K/isopropanol precipitate method (Sambrook and Russell, 2001b). Tail tissue samples of about 2-3 mm length were cut off and incubated in 250 µl Mouse Tail Lysis Buffer containing proteinase K over night at 55°C. The dissolved tail lysates were centrifuged at maximum speed for 6 minutes, the supernatant transferred to fresh tubes, and chromosomal DNA precipitated by adding 200 µl isopropanol. After a second step of centrifugation the precipitated DNA formed a white pellet. The supernatant was discarded and the DNA pellet was resuspended in 200 µl TE Buffer and incubated for 30 min to 1 h at 50°C to remove the remains of isopropanol. For a complete resuspension the DNA was incubated at 4°C overnight.

For the genotyping PCR reaction of genomic DNA two primer pairs was used (Table 7). The first primer was chosen to amplify a fraction of the transgene, binding at the end of the promoter region and in the conserved region of the CFP chromophore. The second primer pair, binding a part of the gene Interleukin 2 (IL-2) was used as internal control to verify the success of the PCR reaction.

Table 7: Primer sequences for the genotyping of transgenic mice

Primer Name	Primer Sequence
Mouse-Thy1.2-2_fwd	5'-GGA CCT TAG GCA GTG TCA C-3'
Mouse-TLCN3.9_fwd	5'-GCT GTC TCA TCA TTT TGG CAA AG
Mouse-CFP-Chr_rev	5'-TGC AGC CCC CAG GTC AG-3'
Mouse-IL-2_fwd	5'-CTA GGC CAC AGA ATT GAA AGA TCT-3'
Mouse-IL-2_rev	5'-GTA GGT GGA AAT TCT AGC ATC ATC C-3'

Reaction mixture (Table 8) was prepared on ice and placed into the preheated thermal cycler and the PCR reaction was initiated (Table 9).

MATERIALS AND METHODS

Table 8: PCR reaction mix for genotyping transgenic mice

Reagent	Volume	Unit
mouse tail DNA	1 μ l	100 ng/ μ l
dNTP	0.2 μ l	12.5 mM
Mouse Thy1.2-2_fwd	0.6 μ l	20 μ M
or Mouse TLCN3.9_fwd	0.6 μ l	20 μ M
Mouse CFP-Chr_rev	0.6 μ l	20 μ M
Mouse-LI-2_fwd	0.3 μ l	20 μ M
Mouse-LI-2_rev	0.3 μ l	20 μ M
Taq Polymerase Buffer	1.2 μ l	10x
Taq Polymerase	0.2 μ l	5 U/ μ l
add H ₂ O to a total volume of 12 μ l		

Table 9: PCR protocol for genotyping transgenic mice

Reaction step	Temp.	Time
1. Hot start	94°C	1.5 min
2. Denaturation	94°C	30 s
3. Annealing	60°C	1 min
4. Elongation	72°C	30 s
35x repetition of step 2.-4.		
6. Final hold	10°C	forever

After the PCR reaction the whole sample was used for analysis using agarose gel electrophoresis.

3.6.5 Breeding mouse lines for homozygosis

Breeding pairs of two heterozygous female and one heterozygous male were prepared. The offspring was tested for the TN-XXL transgene by performing PCR from genomic DNA obtained from mouse tail tissue (see above). Defined by Mendelain inheritance, 25 % of offspring should be homozygous for the transgene. To analyze this, the PCR positive offspring (H1) of the breeding pair was backcrossed with a C57BL/6N wild type resulting in the crossed generation (H2). If all H2 animals are positive for the transgene the PCR positive H1 animal can be considered as homozygous for TN-XXL.

3.7. *Microarray assays*

For microarray analysis samples from hippocampus, heart and skeletal muscle from hind limb were used from 3 homozygous and 3 wild-type littermates. The tissue was dissected and shock-frosted in liquid nitrogen. RNA extraction and further analyses were performed by MFT Services (University of Tübingen, Germany). RNA was isolated and 100ng RNA per sample was amplified and marked with the GeneChip WT Terminal Labeling and Controls Kit (Ambion). Amplified and marked the RNA was hybridized on a MoGene 1.1 ST Gene Chip (Affymetrix Inc., Santa Clara, CA), scanned with the GeneChip Scanner 3000 and analyzed with the GeneChip Command Console Software AGCC 3.0 (Affymetrix Inc., Santa Clara, CA). Microarray data collection was normalized with robust multichip average (RMA) (Irizarry et al., 2003). Moreover, transcripts were filtered for non-informative transcripts. For further analysis only transcripts were included which were 'detected above background' (DABG) in all three array samples for at least one tissue.

3.8. Data Generation

3.8.1. Image Processing

To analyze FRET-based calcium recordings the ratio (R) of images from the emission channels of CFP and cpCitrine and subsequently the ratio change $\Delta R/R$ was calculated using the following formula:

$$\frac{\Delta R}{R} = \frac{R - R_0}{R_0}; R = \frac{F_{Citrine}}{F_{CFP}}; F = \text{fluorescence intensity}$$

All recorded images and movies were analyzed using ImageJ software and implemented plugins. In all calcium imaging experiments a background was selected from a region where no calcium signal was present and subtracted from the image sequence, before further quantification were made. Regions of interest (ROI) were manually drawn and saved with the ROI Manager Plugin. The mean fluorescence intensities and ratios of ROIs were calculated using the ROI ratio manager plugin. In all recorded z-stack the maximum projection was used for assembling the individual z layers.

3.8.2. Data Analyses

All data points obtained from imaging processing analyses were generated in Imagej and transferred to OriginLabs 8.1 for further analyses and graphical illustration.

3.9. Materials

3.9.1. Instruments

Table 10: List of instruments

Name	Supplier
Autoflow CO2 Water-Jacketed Incubator	NuAire, Plymouth (USA)
Bench Top Centrifuge 5415D	Eppendorf, (Germany)
Cary 100 Scan UV-Visible Spectrophotometer	Varian, Mulgrave (Australia)
Cary Eclipse fluorescence spectrophotometer	Varian, Mulgrave (Australia)
CCD-Camera Cool Snap HQ	Roper Scientific, Tucson (USA)
Cyrostat CM 3050	Leica, Wetzlar (Germany)
DeltaVision RT inverted microscope	Applied Precision, WA (USA)
Dissecting Microscope	Leitz, Stuttgart (Germany)
Dyad DNA Engine Peltier Thermal Cycler	MJ Research Inc., Waltham (USA)
iMIC Digital Microscope	Till Photonics, Gräfelfing (Germany)
Mcllwain tissue chopper	Mickle Lab. Engineering Comp., Gomshall (UK)
Metafluor 4.6 imaging software	Universal Imaging, Downingtown (USA)
Microscope TCS SP5 II	Leica, Wetzlar (Germany)
Polytron PT 3000	Kinematica, Luzern (Switzerland)
Mighty Small gel chamber	Hoefer, San Francisco (USA)
Amersham Hyperfilm ECL	GE Healthcare, Munich (Germany)
Microscope Axiovert 35M	Zeiss, Oberkochen (Germany)
Shutter Lambda 10-2	Sutter Instruments, Novato (USA)

3.9.2. Consumables

Table 11: List of consumables

Name	Supplier
Calcium Calibration Buffer Kit #1	Invitrogen, Carlsbad (USA)
cannula Neolus 26Gx23 (NN-2623R)	Terumo Medical Corp., Somerset (USA)
Domed Cap Strips for 48 Well Plates	AB-Gene, Epsom (UK)
Eartags for mice, Monel Nr. 1005-1	Nat. Band & Tag Comp., Newport (USA)
ECL Western Blotting Substrate	Thermo Scientific Pierce, Rockford (USA)
Elutip-D Minicolumns	Schleicher & Schüll, Keene (USA)
Falcon Tissue Culture Dishes 100 mm	Becton Dickinson, Franklin Lakes (USA)
Falcon Tissue Culture Plate, 12 Well	Becton Dickinson, Franklin Lakes (USA)
Glass Bottom Culture Dishes 35mm, Nr. P35G-0-14-C	MatTek Corp., Ashland (USA)
Novex 4-12% tris-glycine gels	Invitrogen, Carlsbad (USA)
Polypropylene Columns	Qiagen, Hilden (Germany)
PureYield™ Plasmid Midiprep System	Promega, Madison (USA)
QIAprep Miniprep Kit	Qiagen, Hilden (Germany)
QIAquick Gel Extraction Kit	Qiagen, Hilden (Germany)
QIAquick PCR Purification Kit	Qiagen, Hilden (Germany)
Roti-Mount Aqua	Roth, Karlsruhe (Germany)
Spectra/Por Dialysis Membrane, MWCO 3500, Nr. 132111	Spectrum Labs Inc., Rancho Dominguez (USA)
Syringe (Luer-Lok) 1ml/5ml/50ml	Becton Dickinson, Franklin Lakes (USA)
Thermo-Fast 48 Well Plates for PCR	AB-Gene, Epsom (UK)

3.9.3. Buffers, solutions and media

Table 12: List of buffers, solutions and media

Name	Recipe
Anode Buffer I	300 mM Tris, pH 10.4, 20% methanol
Anode Buffer II	25 mM Tris, pH 10.4, 20% methanol
BAPTA Buffer for dissociation kinetics	10 mM MOPS, pH 7.5 50 mM KCl 20 mM BAPTA
Cathode Buffer	25 mM Tris, pH 9.4, 40 mM 6-aminohexanic acid, 20 % methanol
DMEM/10 % FCS /1% PenStrep	500 ml DMEM 50 ml FCS, heat-inactivated 5 ml Penicillin-Streptomycin
DNA Gel Loading Buffer (10 x)	100 mM Tris/HCl, pH 7.5 10 mM EDTA 50 % Glycerol 1 % Orange G
DNA Purification Buffer: High Salt	20 mM Tris/HCl, pH 7.4 1 M NaCl 1 mM EDTA
DNA Purification Buffer: Low Salt	20 mM Tris/HCl, pH 7.4 200 mM NaCl 1 mM EDTA
HBSS for imaging	25 mM HEPES pH 7.4 140 mM NaCl 5 mM KCl 1 mM CaCl ₂ 1 mM MgCl ₂ 1 mM Glucose 0.25% BSA
Inoue Transformation Buffer for competent cells	10 mM PIPES, pH 6.7 250 mM KCl 15 mM CaCl ₂ 55 mM MnCl ₂

MATERIALS AND METHODS

Kraftbrühe	80 mM L-glutamic acid 25 mM KCl 3 mM MgCl ₂ *6H ₂ O 10 mM KH ₂ PO ₄ 20 mM Taurine 0.5 mM EGTA 10 mM HEPES 10 mM glucose*1H ₂ O pH 7.4 adjusted with 5 M KOH
LB (Luria-Bertani) medium pH 7,0	20 g/l LB broth base in ddH ₂ O
LB Agar	LB Medium 15 g Agar in 1 l ddH ₂ O
MOPS Buffer for fluorescence spectroscopy	10 mM MOPS, pH 7.5 100 mM KCl 25 µM K ₂ EGTA
Mouse Tail Lysis Buffer	100 mM Tris/HCl, pH 8 250 mM NaCl 1 mM EDTA 0.2% SDS 200 µg/ml Proteinase K added freshly
Neurobasal/B27	500 ml Neurobasal medium 10 ml B27 supplement
PBS (10 x)	100 mM Na ₂ HPO ₄ , pH 7.4 20 mM KH ₂ PO ₄ 1.37 M NaCl 27 mM KCl
PBT (1 x)	0.05 % Triton X-100 10 % FBS in 1x PBS
Poly-L-Lysine	0.01 % (w/v) Poly-L-Lysine Hydrobromide in H ₂ O
Protein Buffer for dissociation kinetics	10 mM MOPS, pH 7.5 50 mM KCl 4 mM CaCl ₂ 2 mM MgCl ₂
Protein Elution Buffer	20 mM NaPO ₄ , pH 7.8 300 mM NaCl 250 mM Imidazole
Protein Loading Buffer 2x	250mM Tris pH 6.8 10% SDS 10% glycerol, 10% b-mercaptoethanol bromophenol

MATERIALS AND METHODS

Protein Resuspension Buffer	20 mM NaPO ₄ , pH 7.8 300 mM NaCl 10 mM Imidazole
Protein Running Buffer 10x	250 mM Tris-base, pH 8.8 1% SDS 1.92 M glycine
RIPA Buffer	50 mM Tris-HCl, pH 7.5 150 mM NaCl 1 mM EDTA, 1% Triton-X 100, 0.5% sodium deoxycholate, 0.1% SDS
TAE (1 x)	40 mM Tris-acetate 1 mM EDTA
TAE (10 x)	48.4 g Tris base 11.4 ml glacial acetic acid 20 ml of 0.5 M EDTA, pH 8.0 add H ₂ O to 1 liter
TE (1 x)	10 mM Tris/HCl, pH 8.4 1 mM EDTA,
Tyrode III	140 mM NaCl 5.4 mM KCl 1 mM MgCl ₂ *6H ₂ O 1.8 mM CaCl ₂ *2H ₂ O 5 mM HEPES 5.5 mM Glucose*1H ₂ O pH 7.4 adjusted with 5 M NaOH
Tyrode low	140 mM NaCl 5.4 mM KCl 0.5 mM MgCl ₂ *6H ₂ O 0.2 mM CaCl ₂ *2H ₂ O 1.2 mM KH ₂ PO ₄ 50 mM Taurine 5 mM HEPES 5.5 mM glucose*1H ₂ O pH 6.9 adjusted with 5 M NaOH

3.9.4. Chemicals

Table 13: List of chemicals

Name	Supplier
Agar	Sigma-Aldrich, St. Louis (USA)
Ampicillin, sodium salt	Roth, Karlsruhe (Germany)
anti-GAPDH mouse monoclonal	Sigma-Aldrich, St. Louis (USA)
anti-GFP rabbit monoclonal	Research Diagnostics Inc., Flanders (USA)
anti-HCN4 rat monoclonal	Santa Cruz Biotechnology, Santa Cruz, USA
anti-mouse IgG horse polyclonal	Cell Signaling Technology, Boston (USA)
anti-rabbit IgG goat polyclonal	Cell Signaling Technology, Boston (USA)
BAPTA, tetrapotassium salt	Molecular Probes, Eugene (USA)
BES	Roth, Karlsruhe (Germany)
Bovine Serum Albumin (BSA)	Sigma-Aldrich, St. Louis (USA)
Calcium Chloride, dihydrate	Sigma-Aldrich, St. Louis (USA)
Carbachol	Sigma-Aldrich, St. Louis (USA)
Collagenase II	Worthington, Lakewood (USA)
DAPI	Sigma-Aldrich, St. Louis (USA)
Deoxyribonuclease	Sigma-Aldrich, St. Louis (USA)
Dispase	Gibco, Grand Island (USA)
DMEM w/o Sodium Pyruvate; w/ 4500 mg/ml Glucose; w/ Pyridoxine-HCl	Invitrogen, Carlsbad (USA)
DMEM/F12	Invitrogen, Carlsbad (USA)
DMSO (Dimethylsulfoxide)	Roth, Karlsruhe (Germany)
EGTA (Ethylene glycol bis(beta-amino ethyl ether tetra-acetic acid)	Sigma-Aldrich, St. Louis (USA)
Fetal Bovine Serum (FBS)	Gibco, Grand Island (USA)
Glucose (D-(+)-Glucose anhydrous, min 99%)	Sigma-Aldrich, St. Louis (USA)
Glycine	Merck, Darmstadt (Germany)
HEPES free acid	Sigma-Aldrich, St. Louis (USA)
Herculase II Fusion DNA Polymerase	Stratagene, La Jolla (USA)

MATERIALS AND METHODS

Imidazole	Merck, Darmstadt (Germany)
Ionomycin, calcium salt	Sigma-Aldrich, St. Louis (USA)
Kanamycin, sulfate	Roth, Karlsruhe (Germany)
Leupeptin hydrochloride	Sigma-Aldrich, St. Louis (USA)
L-Glutamic acid	Roth, Karlsruhe (Germany)
Lipofectamine 2000	Invitrogen, Carlsbad (USA)
Lysozyme	Sigma-Aldrich, St. Louis (USA)
M-1 Embedding Matrix	Thermo Fisher Scientific, Waltham (USA)
Magnesium chloride hexahydrate	Merck, Darmstadt (Germany)
MES monohydrate	Sigma-Aldrich, St. Louis (USA)
MOPS	Merck, Darmstadt (Germany)
NeuroBasal medium	Gibco, Grand Island (USA)
Ni-NTA Agarose	Qiagen, Hilden (Germany)
Opti-MEM I	Invitrogen, Carlsbad (USA)
Penicillin-Streptomycin	Gibco, Grand Island (USA)
Pepstatin A	Sigma-Aldrich, St. Louis (USA)
Phenylmethylsulfonylfluoride (PMSF)	Sigma-Aldrich, St. Louis (USA)
Poly-L-lysine hydrobromide	Sigma-Aldrich, St. Louis (USA)
Potassium chloride	Merck, Darmstadt (Germany)
Ribonuclease A	Sigma-Aldrich, St. Louis (USA)
Sepharose CL6B	Sigma-Aldrich, St. Louis (USA)
Sodium bicarbonate	Sigma-Aldrich, St. Louis (USA)
Sodium chloride	Sigma-Aldrich, St. Louis (USA)
Sodium phosphate monobasic, anhydrous	Sigma-Aldrich, St. Louis (USA)
Sucrose	Merck, Darmstadt (Germany)
T4-Ligase	New England Biolabs, Beverly (USA)
Tetracycline, hydro chloride	Roth, Karlsruhe (Germany)
Triton-X-100	Sigma-Aldrich, St. Louis (USA)
Trizma Base	Sigma-Aldrich, St. Louis (USA)
Trypsin	Sigma-Aldrich, St. Louis (USA)
Trypsin-EDTA	Gibco, Grand Island (USA)
Yeast extract	Sigma-Aldrich, St. Louis (USA)

3.9.5. Plasmids, bacterial strains, cell-lines and mice

Table 14: List of plasmid for cloning and the generation of transgenic mice

Plasmid Name	Supplier
pcDNA 3.1	Invitrogen, Carlsbad (USA)
pRSET B	Invitrogen, Carlsbad (USA)
pBstN- <i>TLCN3.9</i>	provided by Yoshihiro Yoshihara, RIKEN Brain Science Institute, Saitama, Japan
pUC 18 <i>Thy1.2</i>	provided by Pico Caroni, Friedrich-Miescher-Institute, Basel, Switzerland

Table 15: List of bacterial strains, cell-lines and transgenic mice

Strain Name	Supplier
BL21(DE3)	Invitrogen, Carlsbad (USA)
XL-1 Blue	Invitrogen, Carlsbad (USA)
HEK 293T	ATCC, Manassas (USA)
<i>β-actin</i> TN-XXL transgenic mouse line	provided by Marsilius Mues, Max-Planck-Inst. for Neurobiology

4. Results

4.1. Transgenic Mice Expressing TN-XXL under the *Thy-1.2* Promoter

It is known that the *Thy1.2* cassette drives expression of transgenes in the nervous system in either a mosaic pattern or generalized manner depending on the insertion site in the founder line. The onset of *Thy-1.2* expression of the transgene is constitutive and detectable from postnatal day 6-10 (Caroni, 1997). A previous study showed the successful transgenic expression of the troponin C-based genetically encoded calcium indicator Cer TN-L15 in the FVB/N mouse strain (Heim et al., 2007). This mouse strain was chosen as oocytes of FVB strains are highly suited for pro-nucleus injections due to their large size and the lack of pigmentation. However, the FVB/N mouse strain carries the retinal degeneration 1 mutation *Pde6b^{rd1}* (phosphodiesterase 6B, cGMP, rod receptor, beta polypeptide) which causes blindness of the animal from the early onset. Despite C57BL/6N oocytes being smaller and pigmented and therefore more difficult to handle the C57BL/6N mice are not displaying a blind phenotype, which is a very important factor as studying the visual system is a large and important field in neuroscience e.g. studying cortical plasticity by monocular deprivation (Frenkel and Bear, 2004; Mrcsic-Flogel et al., 2007). Indeed the scientific value of the visual system cannot be overstated and calcium-based studies have already shown imaging experiments in the primary visual cortex V1 or further downstream compartments of the visual system preferably with synthetic dyes (Andermann et al., 2010; Hofer et al., 2011; Mrcsic-Flogel et al., 2007; Liu et al., 2009).

4.1.1. Generation of Mice Expressing TN-XXL under the *Thy1.2* Promoter

The generation and purification of the construct *Thy1.2:TN-XXL* was performed with the help of Marco Mank who was further involved in the genotyping of the founder lines. Pronucleus injection fertilized eggs of C57BL/6N oocytes carried out by the Transgenic Mouse Facility of the Max-Planck Institute of Biochemistry brought 105 successfully fertilized oocytes serving as vital founder candidates. The founder tails were identified for the insertion of *Thy1.2:TN-XXL* by PCR using a forward primer binding the terminal region of the *Thy1.2* cassette and a reverse primer that binds the chromophore region of CFP. The PCR resulted in 19 positive founders indicated by a 400 bp band determined by gel electrophoresis. All 19 positive founders were mated with C57BL/6N wild type. The animals of the resulting F1 generation were also PCR validated and additionally their brains were

RESULTS

analyzed for TN-XXL expression under a fluorescence stereomicroscope. Out of 16 PCR positive founder lines, 2 lines were not able to produce offspring, 5 lines displayed no detectable expression, 5 lines displayed very little expression and 4 lines (#7952, #7959, #8057 and #8103) showed high TN-XXL fluorescence in *post mortem ex vivo* analyzed brains. These 4 lines were considered for further analysis.

In transgenic animals created by pronucleus injection transgene expression can be lost over the generations due the mosaic manner of insertion. For observing the stable and permanent insertion of TN-XXL, selected PCR positive F1 generation animals of each founder line were mated with C57BL/6N. The PCR positive animals of the resulting F2 generation again were mated with C57BL/6N giving generation F3. Brains analyzed from the F3 generation in general showed a slight decrease of TN-XXL expression compared to the F1 generation. Next, to facilitate the handling with the mouse lines, to remove the requirement of genotyping and to eventually increase the expression of TN-XXL, homozygous animals were generated from all 4 high transgene expressing founder lines. Based on the fact that all PCR positive mice are heterozygous for TN-XXL due to constant breeding with C57BL/6N wild types one can achieve homozygous lines by mating PCR positive littermates of each line among themselves resulting in homozygous generation (H1). To identify potential homozygous animals the H1 positives were crossed with wild type C57BL/6N mice. For each breeding pair at least 20 animals of the offspring were checked for expression by fluorescence microscopy. PCR positive mice of the H1 generation from all 4 founder lines were considered the breeding of homozygous mice and were crossed with C57BL/6N wild type mice. In the H1 generation of the lines *Thy1.2:TN-XXL* #7952, *Thy1.2:TN-XXL* #7959, *Thy1.2:TN-XXL* #8057 and *Thy1.2:TN-XXL* #8103 3 of 20 (2 female and 1 male), 4 of 24 (2 female and 2 male), 6 of 23 (2 female and 4 male) and 7 of 32 (2 female and 5 male) mice were homozygous.

4.1.2. Expression Patterns of *Thy1.2* TN-XXL Mouse Lines

Next the lines were analyzed for expression patterns. First *ex vivo* brains of 6-8 weeks old homozygous offspring were analyzed for global expression of TN-XXL and were imaged from above using a custom built screening setup. In order to compare global TN-XXL expression levels the acceptor fluorophore cpCitrine was directly excited with a 500/20 nm filter with an acquisition time of 150 ms. The emission was read out with a 535/50nm filter. For a better estimation of the expression levels, the fluorescence intensity of the images was illustrated in color code (Figure 9 A). The expression levels of the *Thy1.2:TN-XXL* mouse

RESULTS

lines were compared to a previously generated mouse line (*Thy1.2:TN-L15*) amongst which the line TN-L15C exhibited the highest transgene expression. This mouse line was generated by Nicola Heim. Therefore, the TN-L15C mouse line was recorded with equal imaging settings. For analysis an elliptic region of interest (ROI) was drawn over the left cortical hemisphere of each line (n=4) quantifying the fluorescence distribution of the mouse lines.

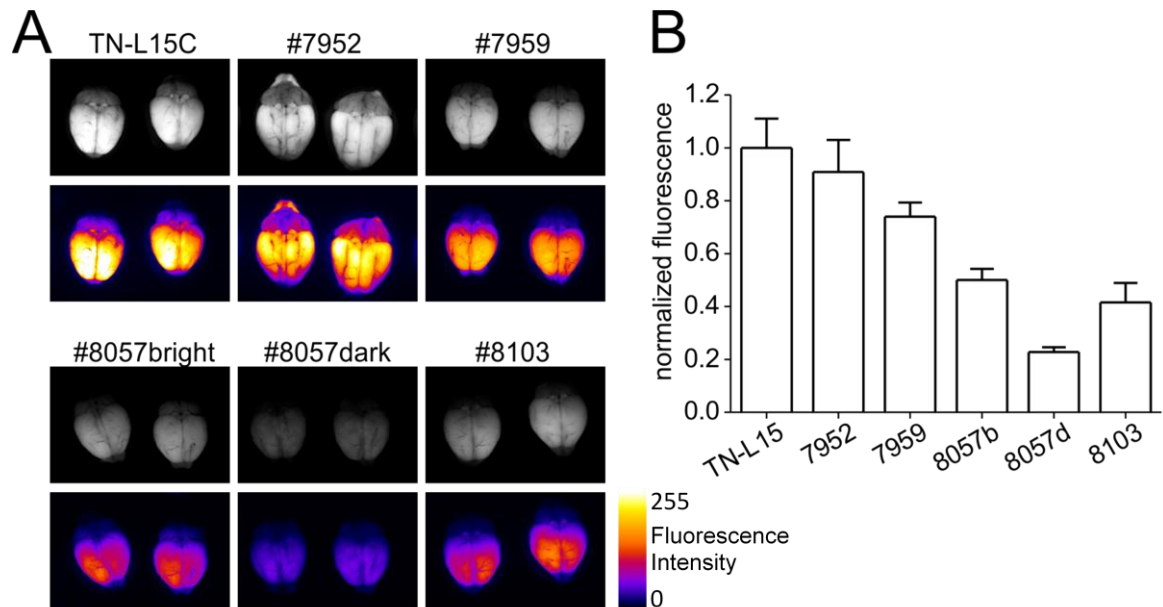


Figure 9: Thy1. TN XXL mouse lines overview. (A) Fluorescence images of the 6 homozygous mouse lines. Color-coded images below each line illustrate the differences in intensity of TN-XXL expression. (B) Statistical analysis of the brightness measured with ROIs of the left cortical hemisphere (n=4; error bar, S.D.)

The highest expression was found in the TN-L15C line, however the line *Thy1.2:TN-XXL#7952* displayed a similar level of intensity. *Thy1.2:TN-XXL#7959* had a decreased intensity compared to #7952 but was the second brightest line analyzed. For *Thy1.2:TN-XXL#8057* the intensity differed from the two analyzed breeding pairs and therefore they were named #8057bright and #8057dark. #8103 displayed similar brightness compared to #8057bright (Figure 9 B). The least expression was found in #8057dark. Whilst it is not abundantly clear why these differences in expression occur one can postulate that the differences in expression level might be due to a different number of tandem repeat insertions in the mouse lines (Jasin et al., 1996; Garrick et al., 1998).

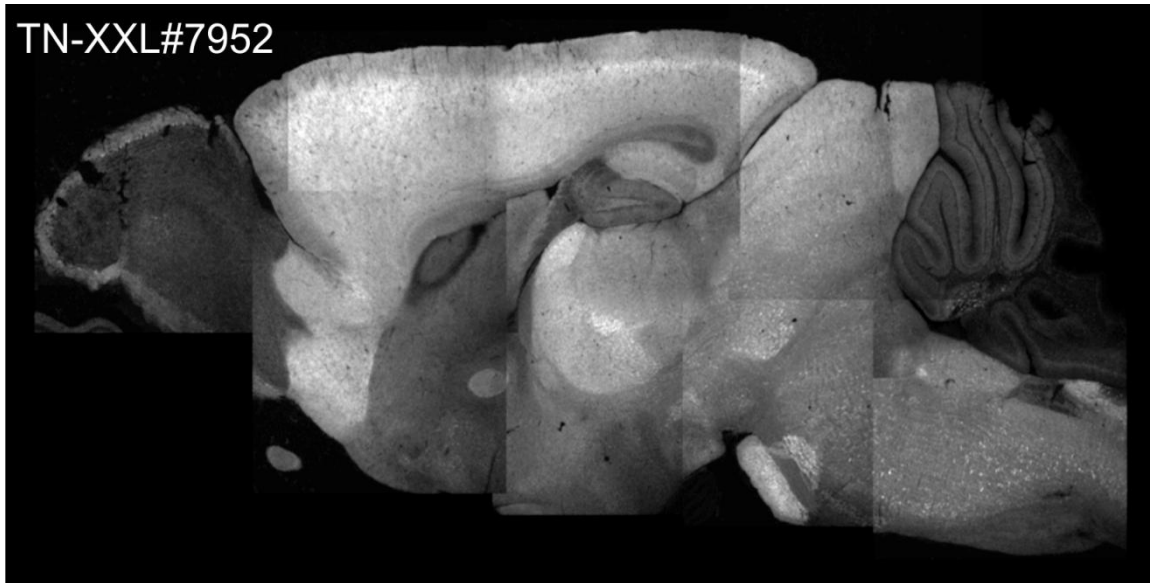


Figure 10 Composite image of a sagittal section of *Thy1.2:TN-XXL#7952*. A sagittal section of a fixed mouse brain showing expression of TN-XXL in the olfactory bulb, cortical, hippocampal, thalamic and brainstem regions.

Furthermore, 20 μm thick sagittal cryosections of PFA fixed brains from all *Thy1.2:TN-XXL* lines were taken from different regions of the brain for fluorescence microscopy using a laser scanning confocal microscope. For all lines the global expression pattern was similar and subsequently for the line #7952 a sagittal section of a whole brain was recorded, that serves as an estimation of expression for all analyzed mouse lines (Figure 10). Expression was present in the olfactory bulb, the cortex (mainly in cortical layer 4 and 5), the CA1 and CA3 region of the hippocampus, and various thalamic and brainstem regions. Apart from the cerebellar nucleus no expression could be found in the cerebellum. Brain sections from homozygous adult mice of the different lines were imaged with identical settings to maintain comparability. Pictures of the cortex, the hippocampus region CA1, the olfactory bulb and the cerebellum were taken and analyzed for brightness and expression pattern. Imaging of the cortex was performed in the visual cortex V1 situated 2.64 mm lateral and -3 to -5 mm of Bregma. In Figure 11 examples of fluorescence pictures of six mouse lines show the expression in the visual cortex and the CA1 region of the hippocampus. As expected from the fluorescence image recorded from whole *ex vivo* brains, the mouse lines showed different fluorescence strength.

RESULTS

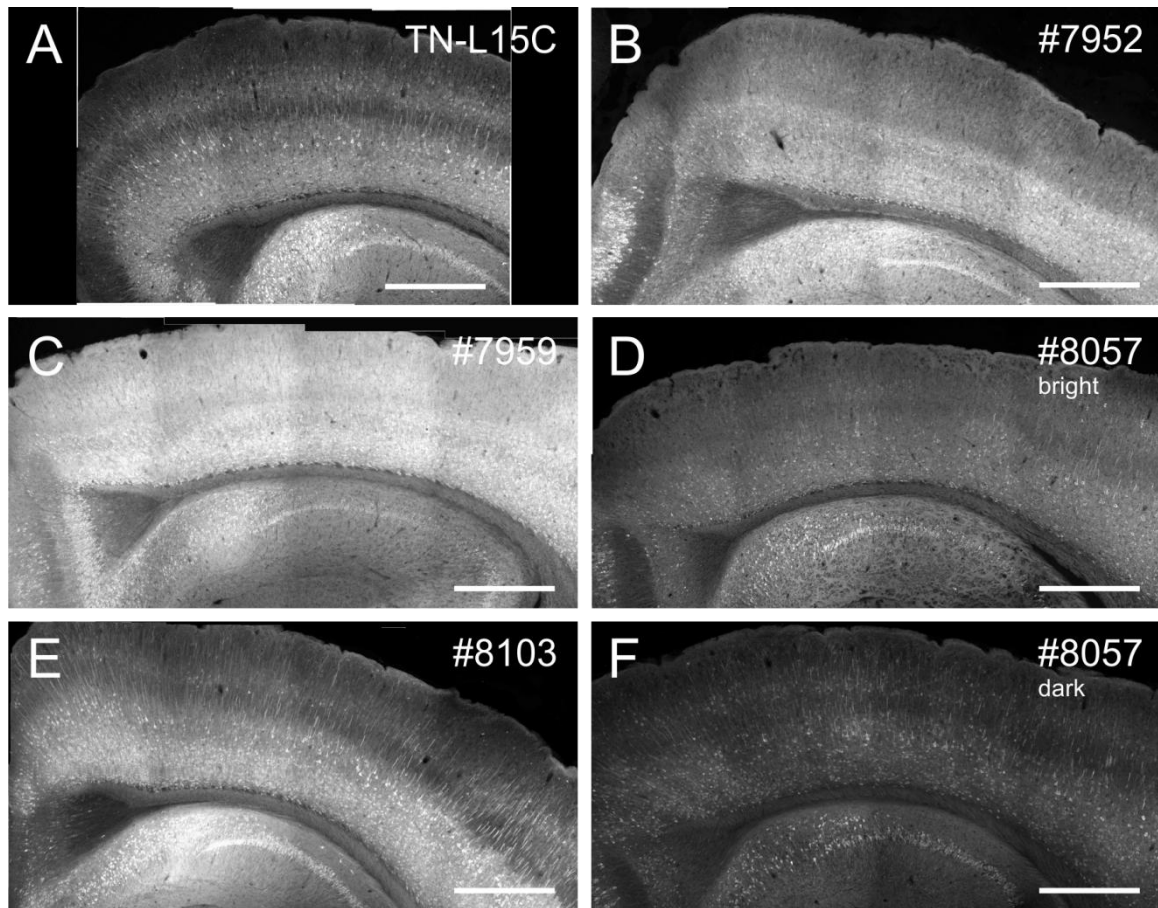


Figure 11 Comparison of expression patterns of the V1 cortex of 6 transgenic mouse lines. Composite images of sagittal cortical sections showing the region -3 to -5 mm of Bregma (V1 cortex) at 2.64 mm lateral. Below the cortex the CA1 region of the hippocampus and transition to the rhinal cortex is visible (scale bars: 500 μ m).

Expression of TN-XXL in cortical sections was present in all lines. Especially in the cortex differences in the background fluorescence mainly caused by the fluorescent neuropil was detected. The lines #7959 and #8057bright showed the highest background fluorescence and therefore the lowest contrast between neuropil and cell bodies (Figure 11 C and D, Figure 12 C and D). A comparable level of background was observed in the lines #7952 and TN-L15C. Here, at least some neuronal projections from deeper situated neurons are visible (Figure 11 A and B, Figure 12 A and B). In the lines #8057dark and #8103 the lowest background level was analyzed, therefore single neuronal somata, apical dendrites of layer 4 and 5 neurons and neurons in layer 2/3 were clearly visible (Figure 11 E and F, Figure 12 E and F) rendering these lines suitable candidates for functional *in vivo* calcium imaging approaches.

RESULTS

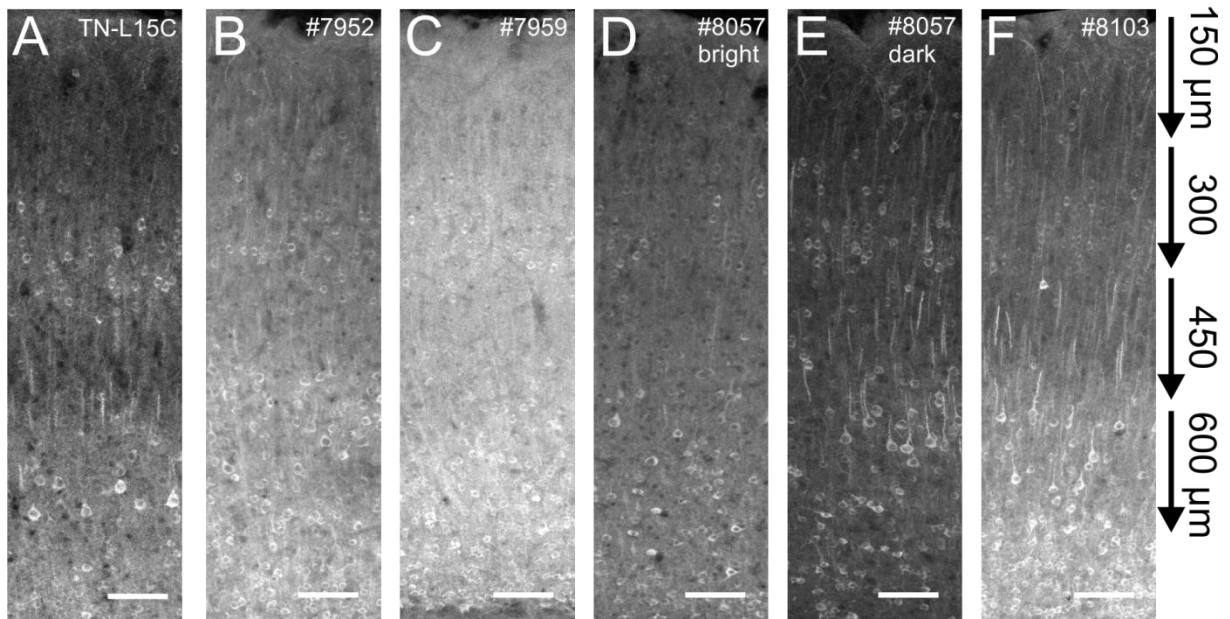


Figure 12. Enlarged images of the visual cortex V1 for six *Thy1.2* mouse lines. (A) The line TN-L15C which expresses the GECI TN-L15 driven by the *Thy1.2* promoter. (B-F) 5 different mouse line expressing TN-XXL under the control of the *Thy1.2* promoter. All pictures display a section of the primary visual cortex V1. The Arrow-heads on the right illustrate the tissue depth in μm from top to bottom (scale bar, $75\mu\text{m}$).

Nevertheless expression in the deeper layer 4 and 5 was higher than in upper layers which impedes imaging in upper layers. Furthermore, fluorescence in the hippocampal formation was present in all lines (Figure 11). Lines #7952 and #8103 showed similar strong expression in the CA1 region as in the lines TN-L15C #8057bright, #8057dark and #7959 the hippocampal expression was lower.

In the following, the fluorescence intensity in olfactory bulb was also determined by cryosections. In all lines examined fluorescence was absent in the granule cell layer and internal plexiform layer, however all lines exhibited TN-XXL expression in the mitral cell layer and in glomeruli of the olfactory bulb. In contrast to the lines #7952, #8057bright, #8057dark which displayed only low expression, the line #7959 showed high fluorescence, the line #8103 displayed the highest fluorescence signal in the mitral cell layer and glomeruli (Figure 13 A and B). Analyzing the cerebellum the only line exhibiting fluorescence was the line #7959, which showed expression of TN-XXL in the purkinje cell layer. Here, purkinje cells and projection of dendrites into the molecular layer were clearly visible (Figure 13 C).

RESULTS

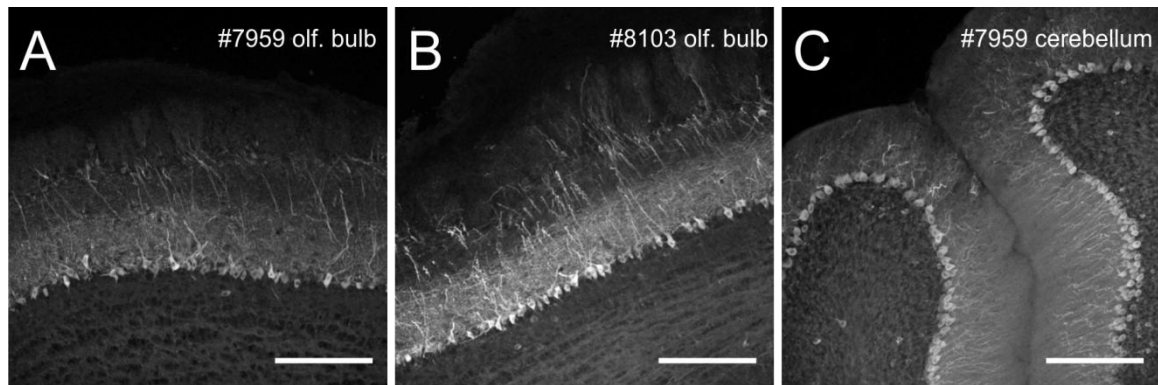


Figure 13: Expression pattern of lines *Thy1.2:TN-XXL*#7959 and #8103. (A) Fluorescence image of a section through the olfactory bulb of line #7959. (B) Fluorescence image of a section through the olfactory bulb of line #8103. (C) Fluorescence image of a section through the cerebellum of line #7959 (scale bars: 200 μ m).

To conclude, one can assume that several lines would be suitable for functional calcium imaging experiments. In contrast to the other lines, the high TN-XXL expression of lines #8103 and #7959 in the olfactory bulb entitles them most for calcium imaging in mitral cells and glomeruli. Additionally, in line #7959 the high expression of TN-XXL in the cerebellum would enable imaging of cerebellar purkinje cells. The low fluorescence background in the line #8057dark showing also the lowest global expression could be a candidate for imaging the somas in upper cortical layers 2/3 neurons with the line #7952. In line #8103 due to the strong expression of deeper cortical neurons, the apical dendrites could be imaged. The large background fluorescence present in the lines #7959 and #8057bright might impede functional *in vivo* calcium imaging experiments in the upper cortical layer 2/3.

4.2. Transgenic Mice Expressing TN-XXL under the Control of the TLCN Promoter

As illustrated above, the transgene expression driven by the *Thy-1.2* promoter is very low in the upper cortical layers, specifically in pyramidal layer 2/3. Many *in vivo* 2-photon studies successfully showed calcium signaling experiments in cortical layer 2/3 pyramidal neurons e.g. in visual cortex V1 (Mrsic-Flogel et al., 2007; Mank et al., 2008) or the barrel cortex (Stosiek et al., 2003), which were carried out either by bolus loading of synthetic calcium dyes (e.g. OGB-1AM), viral injections or by utero electroporation of genetically encoded calcium indicators (Mank et al., 2008). With most of the available standard 2-photon microscopes imaging depth is restricted to 200 to 400 μm depending on laser power, acquisition time, excitation wavelength, brightness of the indicator and refractive index of the tissue producing scattering artifacts.

Therefore, it would be advantageous to create a transgenic animal that displays high expression levels in the upper cortical layers. Telencephalin (TLCN) a member of the ICAM (intracellular adhesion molecule) protein family is expressed exclusively in the telencephalon of mammals (Sugino et al., 1997). A previous study showed the development of transgenic mice expressing GFP under the control of the *TLCN* promoter successfully labeling the upper cortical layer 2/3, the dentate gyrus and the CA3 region of the hippocampus and the olfactory bulb (Mitsui et al., 2007). They further tested different *TLCN* promoter lengths for expression that resulted in the identification of the *TLCN3.9* promoter that gave the best expression and therefore was chosen for this work.

4.2.1. Testing the Functionality of pBstN-TLCN3.9:TN-XXL in Dissociated Neurons

The construct *pTLCN3.9:TN-XXL* was generated with the help of Marco Mank and before creating transgenic animals the functionality of the construct was tested in dissociated hippocampal neuronal cultures isolated from E18 embryonic rats. For this approach neurons that already have been cultured for 10-14 days were chosen due to the high level of spontaneous activity (O'Donovan, 1999). Neurons were transfected with *pTLCN3.9:TN-XXL* by lipofection. Expression of TN-XXL was detected 2-3 days after transfection.

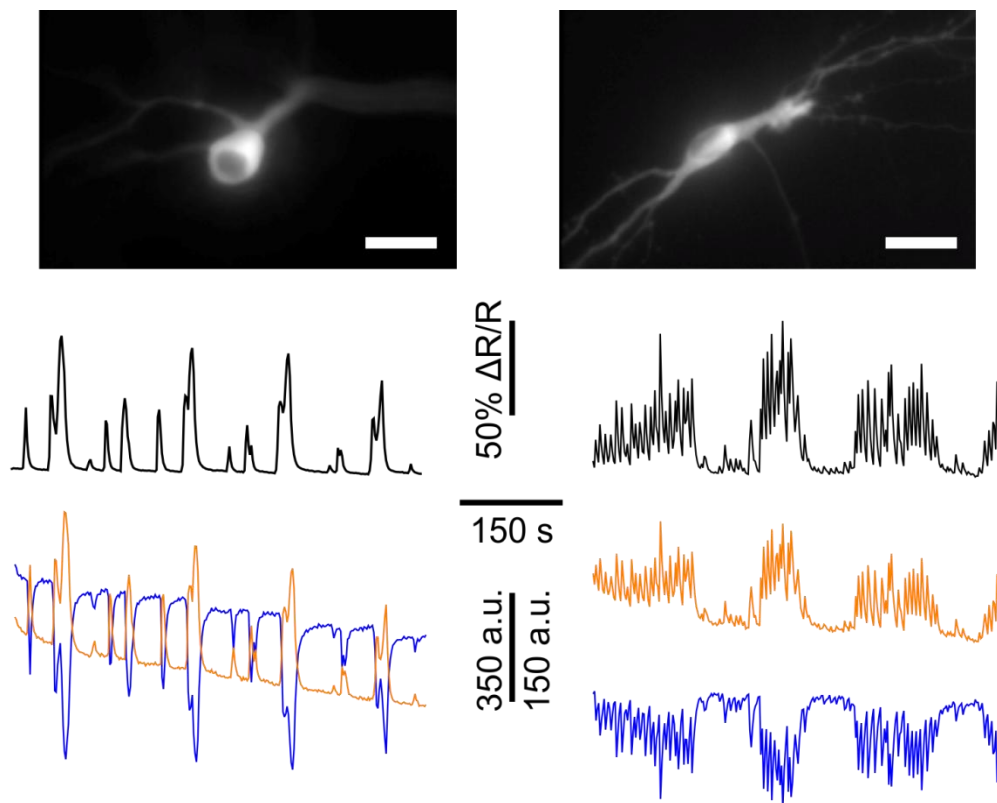


Figure 14: Spontaneous active cultured neurons transfected with *pTLCN3.9:TN-XXL*. To check whether the construct *pTLCN3.9:TN-XXL* is working correctly, the functionality of TN-XXL is tested in cultured rat hippocampal neurons. Two neurons with different spontaneous firing patterns are depicted. Black lines show ratio changes due to calcium influx. The orange and blue lines illustrate the single emission channels for the readout of CFP and cpCitrine fluorescence, respectively (scale bars: 25 μm).

Figure 14 illustrates calcium imaging experiments of two cultured neurons with different spontaneous firing patterns recorded with an inverted epifluorescence microscope. The lower left and right panel showed the signal readout of the donor (CFP, blue) and the acceptor (cpCitricine, orange) fluorophore which demonstrates the functional expression of TN-XXL. Ratio changes of up to 80 % evoked by spontaneous activity could be detected in neuronal culture (Figure 14, black lines).

4.2.2. Expression Pattern of *TLCN3.9* TN-XXL Mouse Lines

After the functionality of *TLCN3.9*:TN-XXL was determined by *in vitro* experiments in neuronal culture, the vector was linearized by restriction digest with *Xba*I and *Asc*I and DNA fragments were prepared for the injection in mouse oocytes. Pronucleus injections in fertilized eggs of C57BL/6N oocytes were carried out by the Transgenic Mouse Facility of the Max-Planck Institute of Biochemistry.

One round of pronucleus injection delivered 19 vital founder candidates. Within the founder candidates PCR analysis of lysed tail tissue resulted in 4 positive founders that were mated with wild type C57BL/6N. All mated founders were fertile and delivered vital offspring, which were again approved by PCR. The PCR positive offspring were checked for the expression of TN-XXL. Unfortunately, comparing PCR positive with negative littermates determined by fluorescence imaging of dissected brains, none of the 4 lines brought fluorescent offspring. Increasing the acquisition time of the microscope to more than 5 seconds yield weak fluorescence identified in one of the four lines. To exclude the possibility that the weak signal in the one line was a result of neuronal tissue autofluorescence immunohistochemistry experiments were performed. Therefore, brains were cut into 20 μ m thick sagittal sections and antibody staining against GFP was performed. The secondary antibody was tagged with Alexa568, a red fluorescence marker, which does not spectrally interfere with cpCitricine fluorescence. Additionally, positive controls with *Thy1.2*:TN-XXL#7952 and negative controls of wild type C57BL/6N were treated in an identical manner.

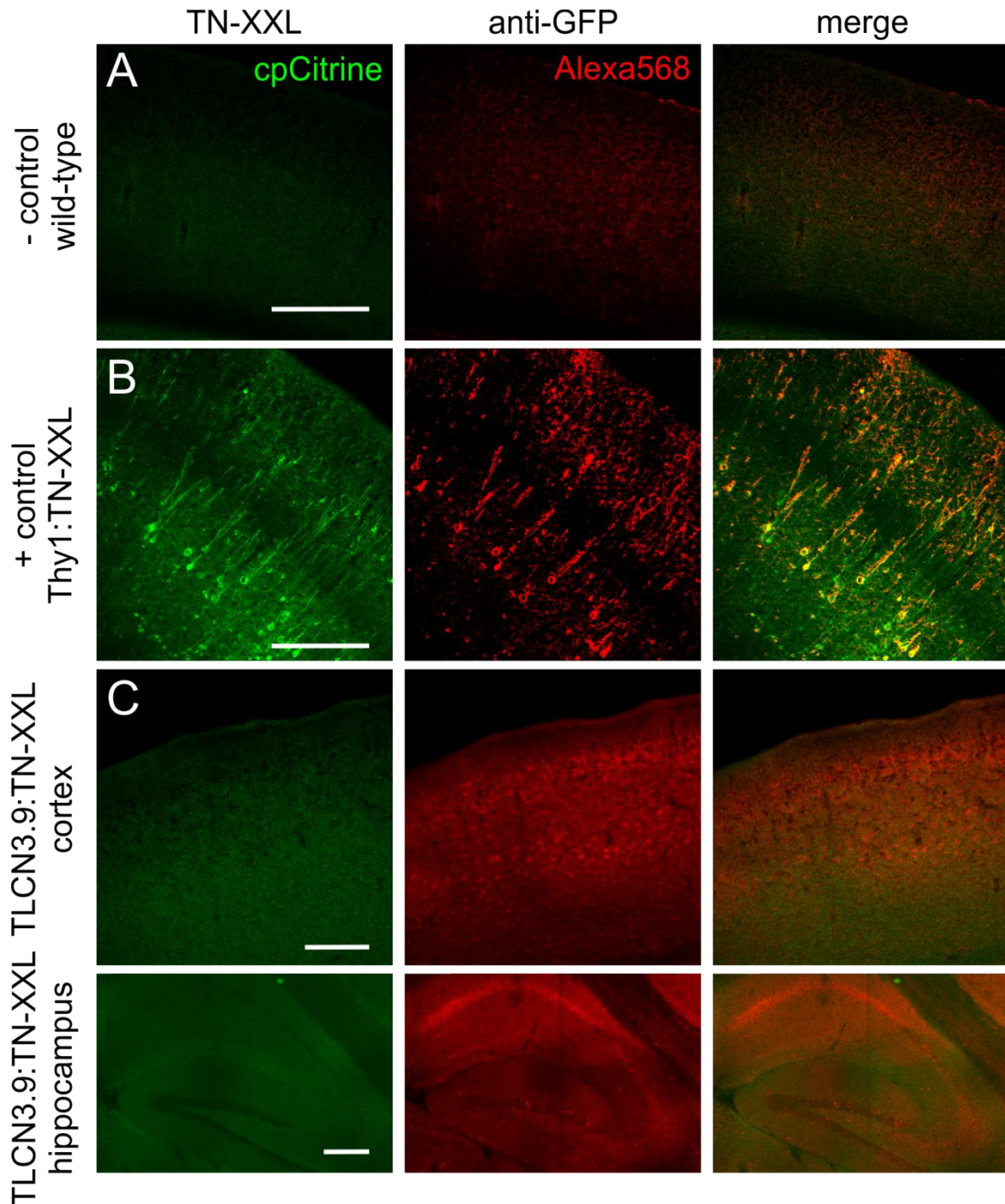


Figure 15: Immunostaining of various mouse lines against GFP. Left column shows the expression level of TN-XXL directly excited with cpCitrine. The column in the middle depicts anti-GFP staining with Alexa568 co-staining. The right column shows the overlay of the cpCitrine and Alexa568 channel. (A) Wild type negative control which as expected shows no expression of TN-XXL in cortex. (B) Positive control of a *Thy1.2:TN-XXL*#7952 shows expression in cortex. Co-staining with Alexa568 shows labelling of cell bodies and neurites. The picture on the right illustrates the overlay of cpCitrine and Alexa568 channel. (C) Cortical and hippocampal section of *TLCN:TN-XXL* mouse line. Fluorescence signal of TN-XXL in the cpCitrine channel is absent due to weak expression (left). Anti-GFP counter-staining with Alexa568 shows expression of TN-XXL (middle) in cortical layers 2/3 and 4/5 (top) and CA1 region of hippocampus (bottom) (scale bars: 200 μ m).

RESULTS

As expected the negative control did not show any fluorescence in the emission channels for cpCitrine and Alexa568 (Figure 15 A). The positive control showed high TN-XXL expression in cortical layer 4 and 5 that overlapped with the antibody staining against GFP illuminated in the Alexa568 channel (Figure 15 B). In the sections of *TLCN3.9:TN-XXL* brain no fluorescence was detectable by the direct excitation of cpCitrine caused by the low expression of TN-XXL in the cortical and hippocampal regions. However, expression was confirmed by the antibody staining against GFP visualized with Alexa568. Here, a strong labeling of the CA1 region of the hippocampus and upper cortical regions most probably layer 2/3 neuron was noticeable (Figure 15 C).

Despite the successful integration of *TLCN3.9:TN-XXL* in the mouse genome, the expression levels were too low to be visualized by fluorescence microscopy and could solely be confirmed by antibody staining against TN-XXL.

4.3. Transgenic Mice Expressing TN-XXL under the Control of the β -actin Promoter

Previously an *in vivo* study showed that TN-XXL is able to resolve signals in orientation-selective neurons in the visual cortex of mice (Mank et al., 2008). As calcium plays a role in many different cellular processes and functions as second messenger several kinds of cellular mechanisms, a mouse expressing TN-XXL ubiquitously would enable to study calcium transients in a large variety of tissues.

Here, a mouse line which expresses TN-XXL under the control of the well-studied β -actin promoter (Okabe et al., 1997) was chosen to characterize the functionality of TN-XXL on a transgenic background. Additionally, a woodchuck hepatitis virus posttranscriptional regulatory element (WPRE) was placed downstream of TN-XXL to enhance the expression of the transgene (Hlavaty et al., 2005; Zufferey et al., 1999) (Figure 16 A). Marsilius Mues (Max-Planck Institute of Neurobiology, Department of Neuroimmunology) generated and provided this mouse line that was created on a C57BL/6N background. Animals from this mouse line exhibited normal lifespan, fertility, body and litter sizes compared to their non-transgenic siblings.

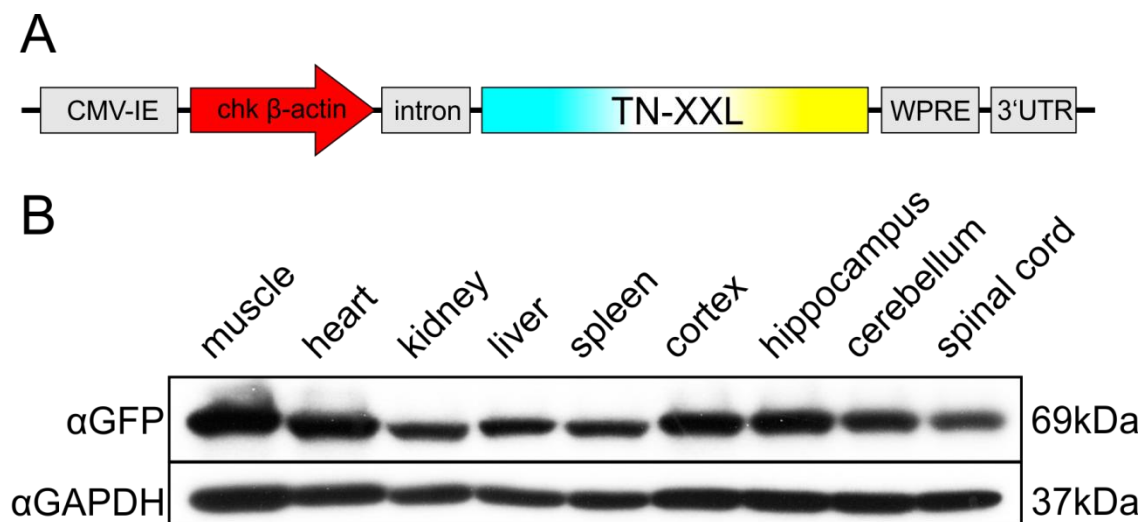


Figure 16: Construction of TN-XXL and Western blot analysis of tissues expressing TN-XXL under the control of the β -actin promoter. (A) Scheme of the construct with the CMV immediate-early enhancer (CMV-IE) and chicken (chk) β -actin promoter upstream and the WPRE downstream of TN-XXL. (B) Western blot analyses of different tissue lysates using an anti-GFP antibody for the TN-XXL expression and an anti-GAP-DH antibody as control performed by Marsilius Mues.

4.3.1. Western Blot Analysis of β -actin TN-XXL mice tissues

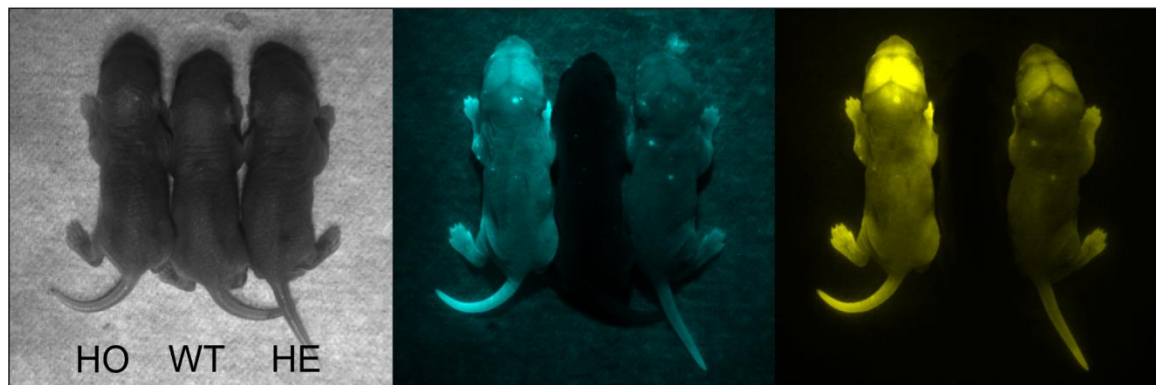
First, to elaborate whether TN-XXL is successfully expressed in different kinds of tissues, samples from hind limb muscle, the heart, kidney, the spleen, the liver, and different regions from the brain (cortex, hippocampus, cerebellum and spinal cord) of 3-4 month old homozygous mice were examined by western blot analysis (Figure 16 B). Together with the help of Marsilius Mues the tissues were homogenized, separated via gel electrophoresis and stained with anti-GFP and anti-GAPDH control antibodies. The anti-GFP staining showed a single band of different intensities at roughly 69kDa demonstrating the expression of TN-XXL in all observed tissue samples. Upon further analysis the bands of muscle, heart, cortical and hippocampal tissue showed higher intensities than bands of kidney, liver, spleen cerebellum and spinal cord indicating higher expression level of TN-XXL in brighter bands compared to the constant intensity of the staining control with anti-GAPDH at 30kDa (Figure 16 B).

4.3.2. Observing Fluorescence Expression pattern of β -actin TN-XXL mice

To further analyze the expression distribution of TN-XXL in this mouse line a series of fluorescence images of whole animals, organs and tissue section were prepared. Images of 3 day old homozygous, heterozygous and wild-type pups were compared demonstrating clear fluorescence of the animals' skin in the transgenic pups (Figure 17 A). A higher expression in homozygous compared to heterozygous mice was found confirming an increase of expression caused by homozygosity. The fluorescence of the pups verified that the onset of TN-XXL expression already takes place during development. To further categorize the expression pattern of the transgenic animals a series of organs were isolated from homozygous adult mice and were compared to wild type C57BL/6N mice of similar age by fluorescence imaging (Figure 17 B). Going along with the western blot results the highest expression was examined in brain, skeletal muscle and heart. Lower expression was found in liver and kidney. However, in contrast to the results from western blot fluorescence in spleen was almost undetectable (Figure 17 B).

To investigate if the expression derived either from a ubiquitous equal expression in all cells or from partial expression in subsets of cells, frozen sections of organs from homozygous adult mice were performed.

A



B

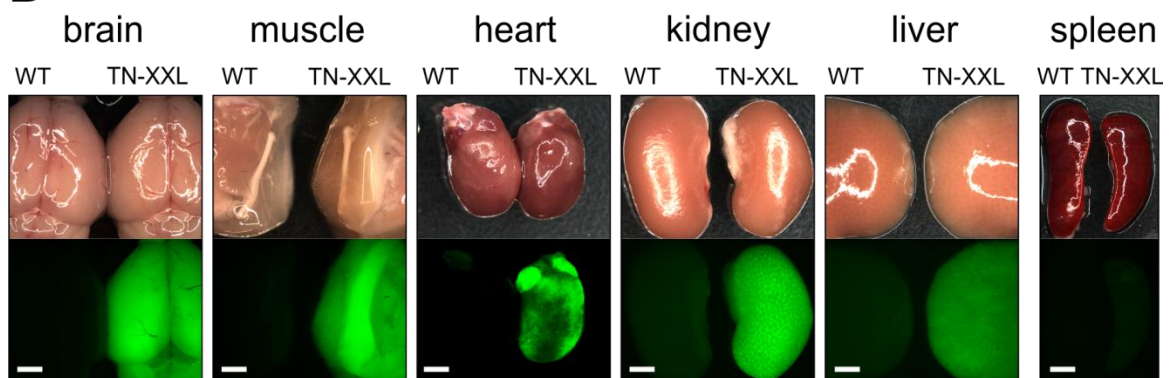


Figure 17: Fluorescence Images of pups and organs. (A) Images of 3 newborn mice (HO, homozygous; HE, heterozygous; WT, wild type) illuminated with bright field (monochrome), CFP (blue) and citrine (yellow) fluorescence. (D) Bright field and fluorescence images of isolated organs of homozygous transgenic compared to wild type controls (Scale bars, 2 mm).

A counter staining with DAPI visualized the DNA located in the nuclei of the cells. In sagittal and coronal section from the brain a fluorescence distribution from high expression in cortex, hippocampus and cerebellum to low expression in brainstem and midbrain regions was detectable (Figure 18 A and B). At higher magnification an increased fluorescence in blood vessels compared to cells is visible (Figure 19 A, B and C). In cross sections from kidney the fluorescence is more prominent in the outer regions especially in subsets of nephrons (Figure 18 C, Figure 19 E). In sections from muscle and heart a spread in different types of fluorescence levels could be seen (Figure 19 D and E). Low but detectable punctuated fluorescence was measured in tissue from liver (Figure 19 F). In Figure 18 I a section through the tail showed the fluorescence in the dermis, in muscles that surround the bone and in blood vessels that proceed along the longitudinal axis. In sections of the spleen fluorescence was only present in connective tissue no expression could be detected in the lymph follicles of the spleen (Figure 18 G).

RESULTS

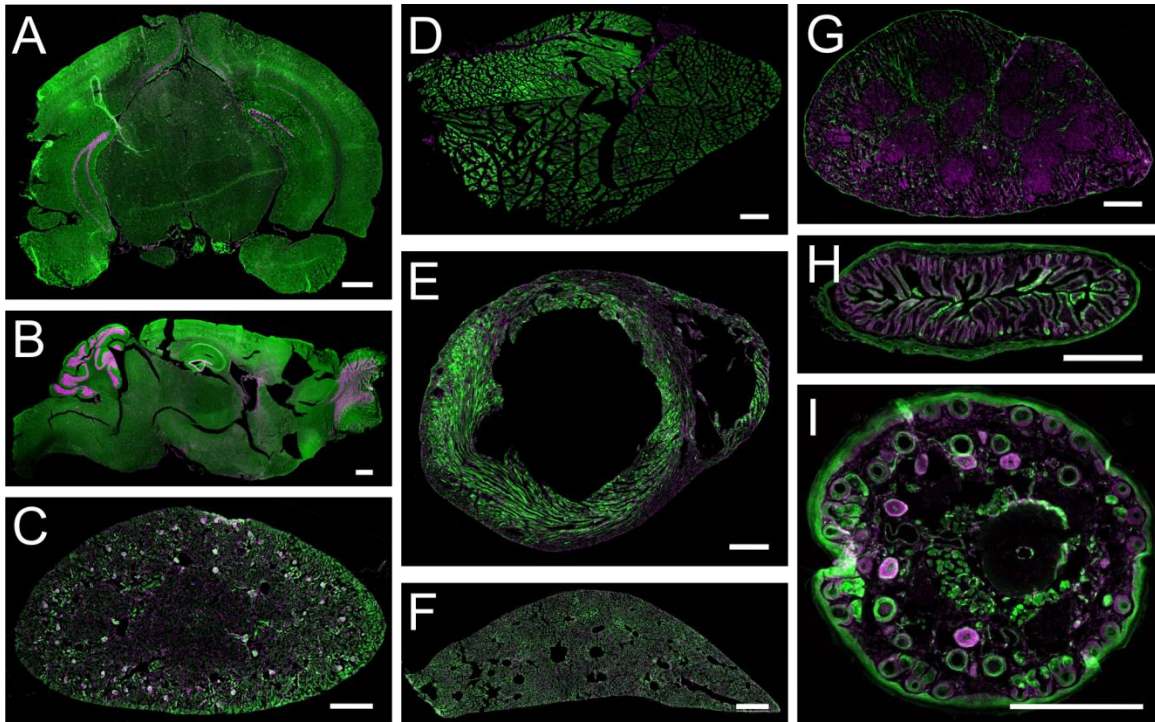


Figure 18: Overview of TN-XXL fluorescence (green) in frozen sections of several tissues counter-stained with DAPI (magenta). (A) Coronal brain section. (B) Sagittal brain section. (C) Kidney. (D) Skeletal muscle. (E) Heart. (F) Liver. (G) Spleen. (H) Intestine. (I) Section through the tail). (Scale bars, 500 µm).

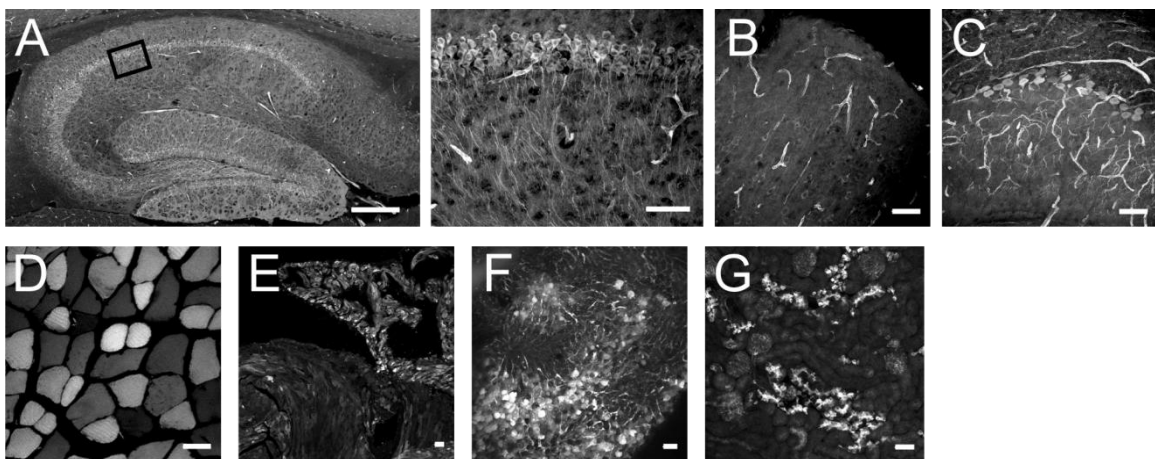


Figure 19: Fluorescence of frozen section of higher magnification. (A) Section of the hippocampus. Black square shows an enlargement for the region depicted on the right. (B) Section of the cortex showing weak labeling of cortical neurons and strong labeling of vessels. (C) Section of the cerebellum showing labeled neurons of the purkinje layer and vessels. (D) Section of the hind limb muscle illustrating muscle fibers of different expression. (E) Heart section showing a part of atrium (top) and ventricle (bottom). (F) Section through the liver. (G) Section of the kidney (Scale bars, 150 µm).

4.3.3. Indicator Concentration, Mobility and Durability Inside Cells

4.3.3.1. Determining the TN-XXL Concentration

The distribution of fluorescence in frozen sections of organs indicated differences in TN-XXL expression levels (Figure 18). To determine whether this observation is valid one can empirically determine the actual concentration by which TN-XXL is expressed and thusly quantify any variations in expression levels. To calculate the TN-XXL concentration in specific tissues, a calibration standard using TN-XXL purified from *E. coli* of known concentration (Figure 20 A) was generated and the resulting fluorescence intensities were compared with acute sections from skeletal muscle, heart, hippocampus, kidney and liver of homozygous transgenic mice.

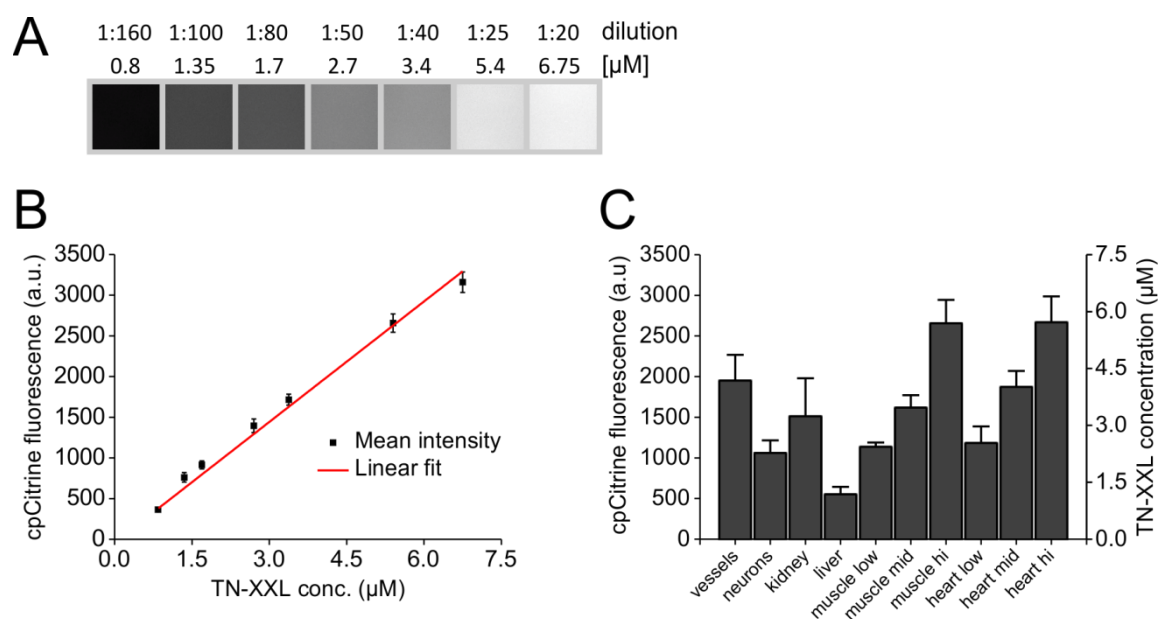


Figure 20: Concentration determination of TN-XXL in transgenic mice. (A) Dilution of purified TN-XXL and corresponding fluorescence images showing the brightness recorded with a laser scanning confocal microscope. (B) Calibration standard (red) of purified TN-XXL. TN-XXL dilution of 1:20, 1:25, 1:40, 1:50, 1:80, 1:100, 1:160 from a stock solution of 10mg/ml (135 μM) imaged with 514 nm excitation and corresponding fluorescence emission of citrine (error bars, standard deviation; n=4). (C) Estimation of TN-XXL protein concentration of acute slices (400 μm) from brain, kidney, liver, muscle and heart. The citrine fluorescence is measured and the resulting protein concentration is concluded from the calibration standard in D (error bars, standard deviation).

RESULTS

Therefore, a TN-XXL stock solution (135 μM) was diluted to 1:20 (6.75 μM), 1:25 (5.4 μM), 1:40 (3.375 μM), 1:50 (2.7 μM), 1:80 (1.69 μM), 1:100 (1.35 μM) and 1:160 (0.84 μM) and subsequent fluorescence images were taken, from which the signal intensity was determined (Figure 20 B). Acute slices were imaged with the same imaging settings to evaluate TN-XXL concentration using the calcium insensitive directly excited acceptor fluorescence intensity as measure (Figure 20 C and Figure 21). To minimize tissue scattering artifacts z-stacks of images were taken from the first two cell layers of the sample (20 μm in z). The mean values of the actual measured brightness for chosen regions of interest (ROI) were converted to concentrations determined by the calibration standard.

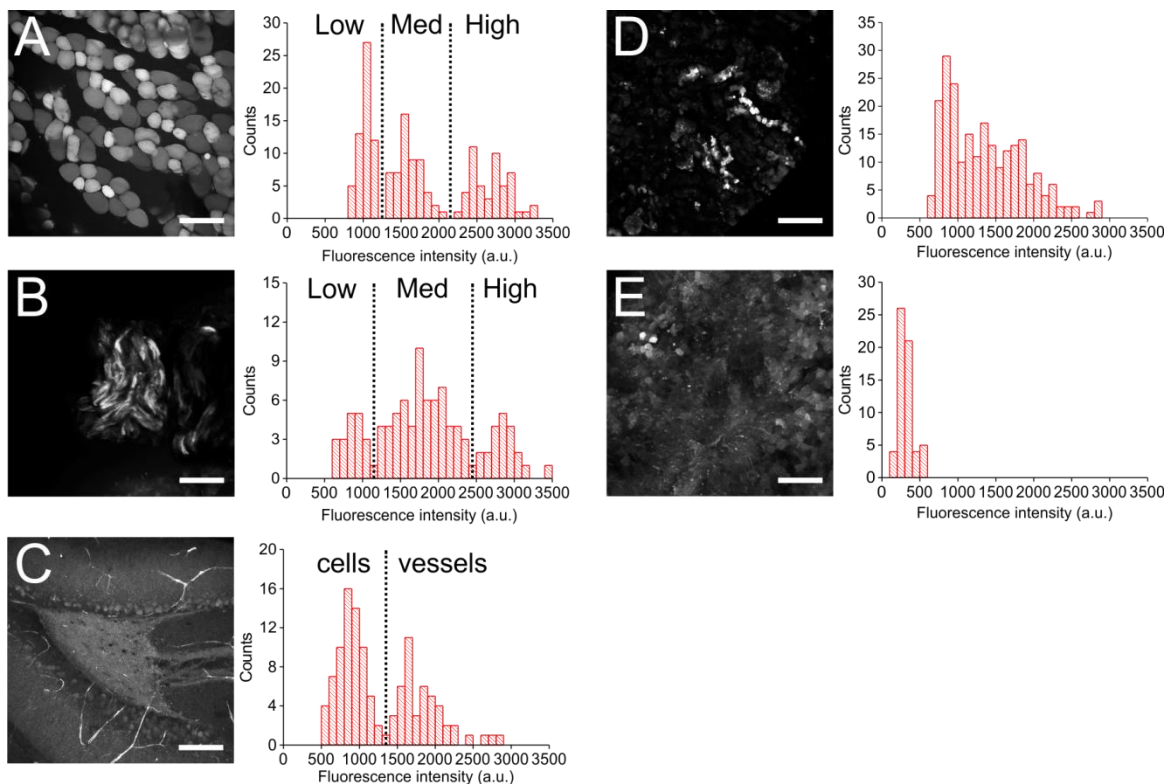


Figure 21: Expression distribution in various tissues. Fluorescence images of various acute organ slices (400 μm thickness) from homozygous transgenic mice and histograms illustrating the distribution of TN-XXL expression within the given organ. A, muscle; B, heart; C, hippocampus; D, kidney; E, liver. (scale bars, 150 μm)

RESULTS

Calculated TN-XXL concentrations were determined in hippocampal blood vessels ($4.2 \mu\text{M} \pm 0.7$), hippocampal neurons ($2.3 \mu\text{M} \pm 0.3$), kidney ($3.2 \mu\text{M} \pm 1.0$) and in liver ($1.2 \mu\text{M} \pm 0.2$) (Figure 20 C). The generation of histograms helped to categorize the expression distribution of TN-XXL in the different tissues (Figure 21). The high standard deviation in kidney derived from the large variety of expression in different cell types that were not further identified (Figure 21 D). In muscle and heart tissue three subsets of expressing fibers (low, medium and high) were observed (Figure 21 A and B). In muscle tissue a concentration of TN-XXL from $2.4 \mu\text{M}$ to $5.7 \mu\text{M}$ and in heart tissue a similar expression pattern from $2.5 \mu\text{M}$ to $5.7 \mu\text{M}$ was calculated (Figure 20 C).

4.3.3.2. Determining TN-XXL Motility in Cells with FRAP

As previous studies showed biosensors or fluorescent protein expressed in the cytosol might aggregate or fuse in cellular compartments. Thereby, the sensor's mobility, diffusion or even signal range could be impaired. As already mentioned above, the calmodulin-based calcium sensor YC3.12 expressed in a transgenic mouse tended to aggregate in cortical neurons causing a decrease in signal strength (Hasan et al., 2004). To test for free diffusion and mobility of TN-XXL fluorescence recovery after photo bleaching (FRAP) experiments were carried out in cultured murine kidney fibroblasts (MKF) prepared from homozygous transgenic mice. The bleaching spot was set close to the cell membrane so that diffusion could have been considered only 2 dimensional (Figure 22 A, arrow). The recovery rate ($t_{1/2}$) of 0.2 s after the bleaching pulse was comparable to rates obtained for GFP (Swaminathan et al., 1997) and suggested free mobility and diffusion of TN-XXL (Figure 22 B).

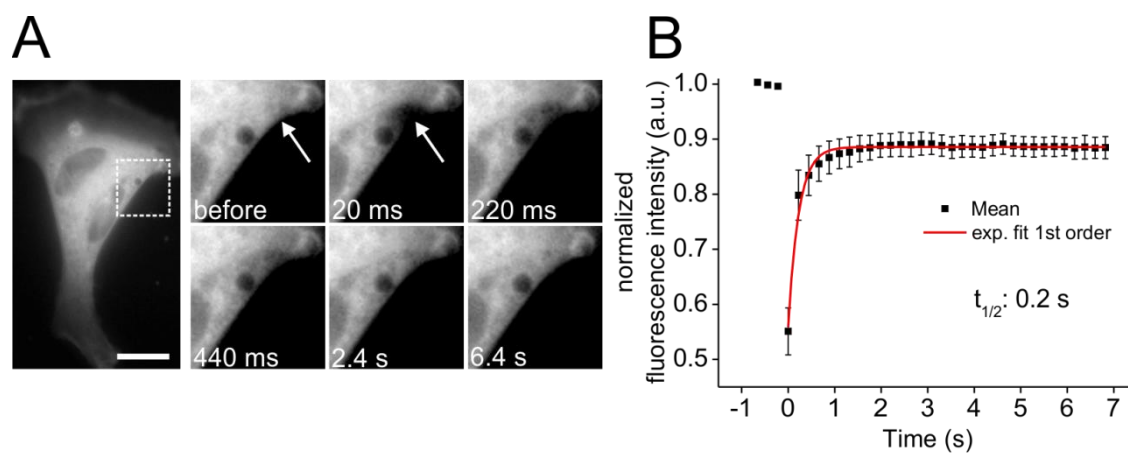


Figure 22: Fast fluorescence recovery after fluorescence recovery after photo bleaching (FRAP) experiments in cultured murine kidney fibroblasts (MKF) of homozygous transgenic mice. (A) Fluorescence images of a MKF. The images on the right show a blow-up of the region marked with a white rectangle in the left picture. Arrows indicate the impact of the bleaching laser pulse. The time course follows the recovery from the bleaching pulse (Scale bar, 15 μ m). (B) Graphical illustration of the bleached area plotted against time. Fluorescence intensities are normalized to the mean of three images taken before the bleaching event. The exponential fit 1st order gave a time constant ($t_{1/2}$) of 0.2 s. The fast recovery rate indicates the distinct cytosolic expression of TN-XXL (error bars, standard deviation).

4.3.3.3. The Effect of Long-term TN-XXL Expression on Cellular Morphology

In addition, I investigated whether long-term expression of TN-XXL could cause changes in cell morphology. In a previous study an aggregation of calmodulin-based calcium indicators in the nucleus and a resulting decrease of the calcium signal was determined in a small amount of cortical neurons (Tian et al., 2009). Here, I looked at 13 days, 36 days, 2 month and 6 month old brains from homozygous TN-XXL expressing mice and generated images of frozen sections of the CA1 and CA3 region of the hippocampus on a laser scanning confocal microscope (Figure 23 A). The cytosolic and nuclear fluorescence distribution was examined by drawing a line through the soma of neurons (Figure 23 B). Even though the expression in CA3 neurons is lower than in CA1 cells, in both regions the fluorescence is restricted to the cytosol (cyto) and is not visible in the nuclear region (nucl.). Statistical analysis revealed no significant difference in hippocampal sections of CA1 and CA3 region comparing the different ages (Figure 23 C).

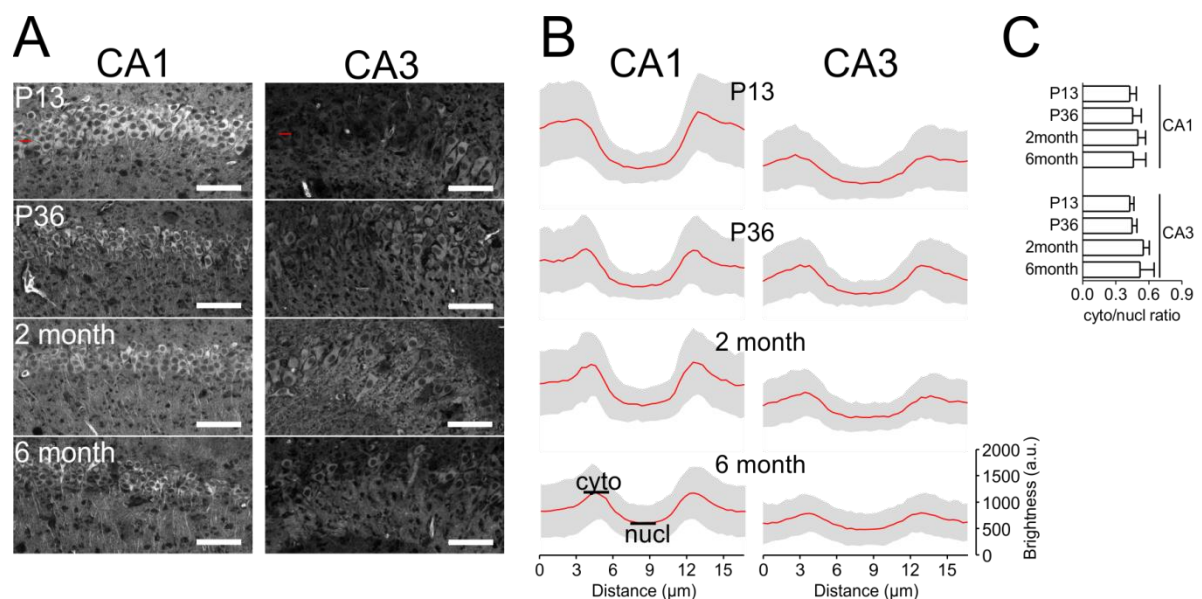


Figure 23: Long-term expression of TN-XXL in transgenic mice under the control of the β -actin promoter. (A) Laser scanning confocal imaging sections through the CA1 and CA3 region of the hippocampus of P13, P36, 2 month and 6 month old homozygous mice (scale bar, 150 μ m). (B) Fluorescence distribution through a cross section of the cell soma (mean value in red and standard deviation in grey). (C) Statistical analyses show that even expression over 6 month does not change the cytosol to nucleus ratio significantly (error bars, standard deviation).

4.3.3.4. Functionality of TN-XXL in Murine Kidney Fibroblasts (MKF)

Furthermore, I tested whether long-term expression of TN-XXL would influence functionality and signal strength of TN-XXL. Therefore, the performance of cultured murine kidney fibroblasts (MKF) isolated from homozygous transgenic mice was compared to wild-type MKF from C57BL/6N mice. Wild-type MKF were transfected overnight with pcDNA3.1:TN-XXL coding for cytosolic expression of TN-XXL. The culturing medium for calcium imaging was exchanged by HBSS and the baseline ratio (R_0) was determined. To analyze the maximal ratio change ($R_{Ca^{2+}}$) MKFs were treated with CCCP ($10 \mu\text{M}$) and sodium-azide NaN_3 ($10 \mu\text{M}$) to inhibit cellular metabolism. Subsequently, $8 \mu\text{M}$ Ionomycin and 10mM extracellular CaCl_2 was added to the medium and the maximal ratio change was determined.

Transfected wild-type and transgenic cells displayed similar base line ratios (R_0) of approximately 1 ± 0.1 . Values obtained for $R_{Ca^{2+}}$ were similar for the two expression conditions from 2.9 ± 0.3 and 2.7 ± 0.2 for transfected and transgenic MKFs, respectively (Figure 24 A). Furthermore, agonist-induced calcium responses evoked by application of $10 \mu\text{M}$ ATP gave comparable ratio changes of $\sim 50\%$ $\Delta R/R$ in MKF of transgenic and wild-type mice acutely expressing TN-XXL (Figure 24 B).

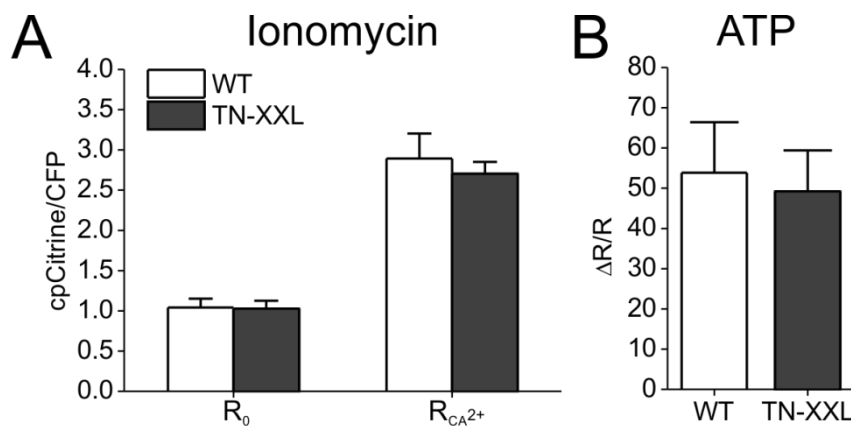


Figure 24: Functionality of TN-XXL in cultured transgenic murine kidney fibroblasts (MKF) compared to transfected wild type MKFs. (A) MKFs were imaged in two conditions: baseline ratio (R_0 ; no Ca^{2+}) and high calcium ratio ($R_{Ca^{2+}}$; 10mM Ca^{2+}). The ratio (YFP/CFP) of the two conditions is plotted in a histogram (WT, wild type MKF; TN-XXL, homozygous transgenic MKF). (B) Ratio change ($\Delta R/R$) of transgenic and wild type MKF upon application of ATP ($10 \mu\text{M}$).

4.3.4. Calcium Responses in Primary Cells Derived from Transgenic Mice

Transgenic mice stably expressing TN-XXL could be a useful source of primary cell types ready for various calcium imaging or drug screening applications. Therefore the functionality of TN-XXL was tested in three primary cell types. Smooth muscle cells from bladder (SMC), fibroblasts from kidney (MKF) and astrocytes from cortical tissue of homozygous transgenic mice were isolated and cultured (Figure 25 A). All cell types exhibited fluorescence for at least 8 weeks in culture (data not shown). Smooth muscle cells responded to application of carbachol (100 μ M) with an average peak response of \sim 30 % Δ R/R and on-going calcium oscillations for several minutes (Figure 25 B, top).

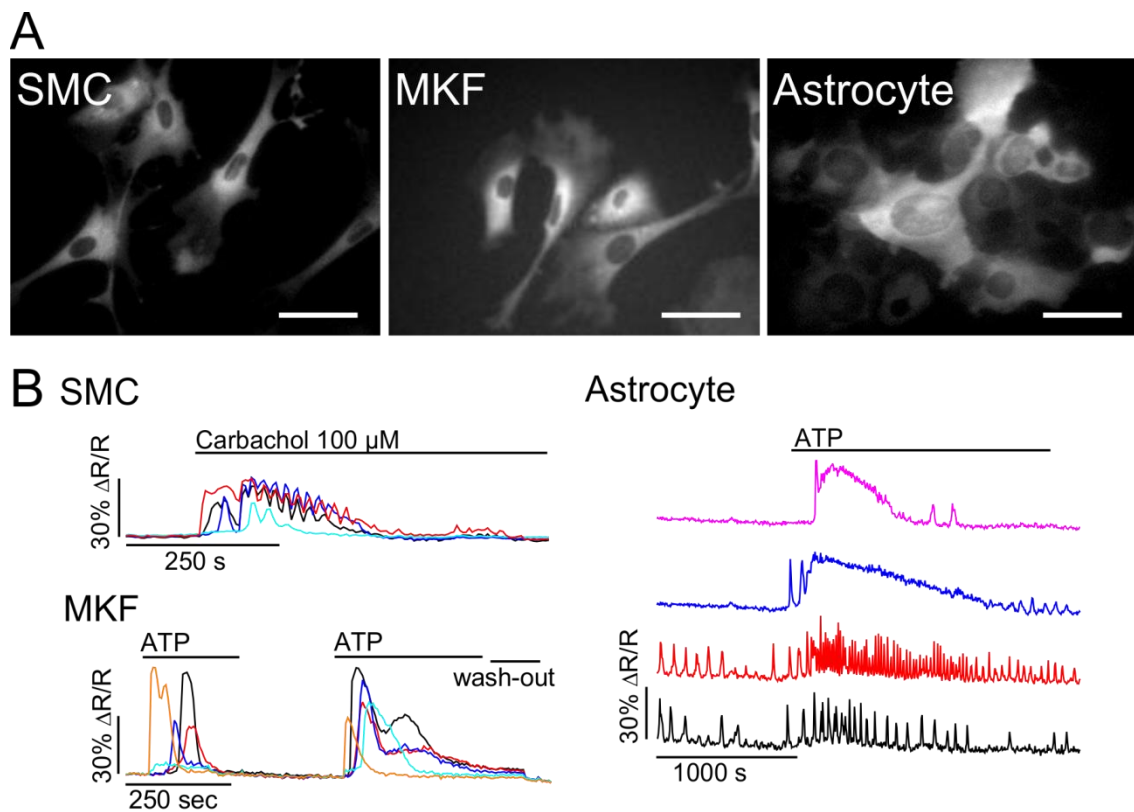


Figure 25: *In vitro* Ca^{2+} imaging of transgenically expressed TN-XXL in different cultured cell types. (A) Fluorescence images of aortic smooth muscle cells (SMC), murine kidney fibroblasts (MKF) and astrocytes (Scale bar, 25 μ m). (B) The upper left graph displays the response of four SMC to carbachol (100 μ M) treatment. The lower left graph shows the response of five murine kidney fibroblasts to ATP (10 μ M). The four graphs on the right depict the response of astrocytes to ATP (10 μ M) either with (lower two graphs) or without (upper two graphs) foregone spontaneous activity.

Calcium responses with ratio changes of up to 60 % $\Delta R/R$ were elicited in kidney fibroblasts after bath application of 10 μM ATP (Figure 25 B, bottom). When 10 μM ATP was applied to cultured astrocytes calcium oscillations were also detected. Older, denser astrocyte culture showed a high rate of spontaneous oscillations. ATP increased the oscillation frequency over the time of application (Figure 25B, right).

4.3.5. Calcium Responses of TN-XXL in Cardiac Tissues

As shown before, functional TN-XXL expression in mice under the β -actin promoter was confirmed by calcium imaging experiments in a variety of different cultured primary cell-types. Motion artifacts elicited by moving or contractile tissues are critical factors which can cause distortion of the imaging data. To overcome artifacts produced by tissue movements or contractions one can use ratiometric GECIs which cancel out such artifacts due to the ratio calculation determined from the two recorded emission wavelengths.

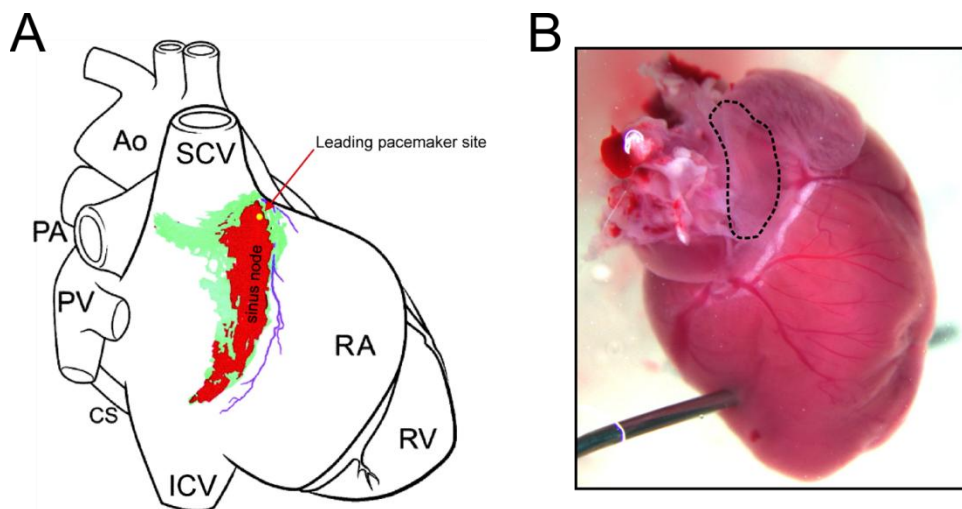


Figure 26: Position of the SAN region in the mouse heart. (A) A schematic diagram of the adult mouse with the SAN region depicted in red. Ao, aorta; CS coronary sinus; ICV, inferior vena cava; PA, pulmonary artery; PV pulmonary vein; RV, right ventricle; SCV, superior vena cava. Adapted from Dobrzynski et al., 2007. (B) Picture of the backside of the dissected heart. The SAN region is marked with black dots.

RESULTS

To determine the benefits of the ratiometric imaging readout of TN-XXL, the heart was chosen as it is a fast beating, highly contractile and challenging tissue for studying calcium transients. Hence, the following experiments were focused on a special region of the heart, the sinoatrial node (SAN), located posterior of the left atrium (Figure 26). The SAN is known to be the pacemaker region of the mammalian heart and is also cause for many heart diseases e.g. sinoatrial blocks or atrial arrhythmia (Monfredi et al., 2010).

First, the correct dissection of the SAN was verified by immunostainings of dissociated SAN cells and SAN explants which was achieved by using antibodies against the hyperpolarization activated ion channel HCN4, a specific marker for pace making sinoatrial node cells (Liu et al., 2007)(Figure 27).

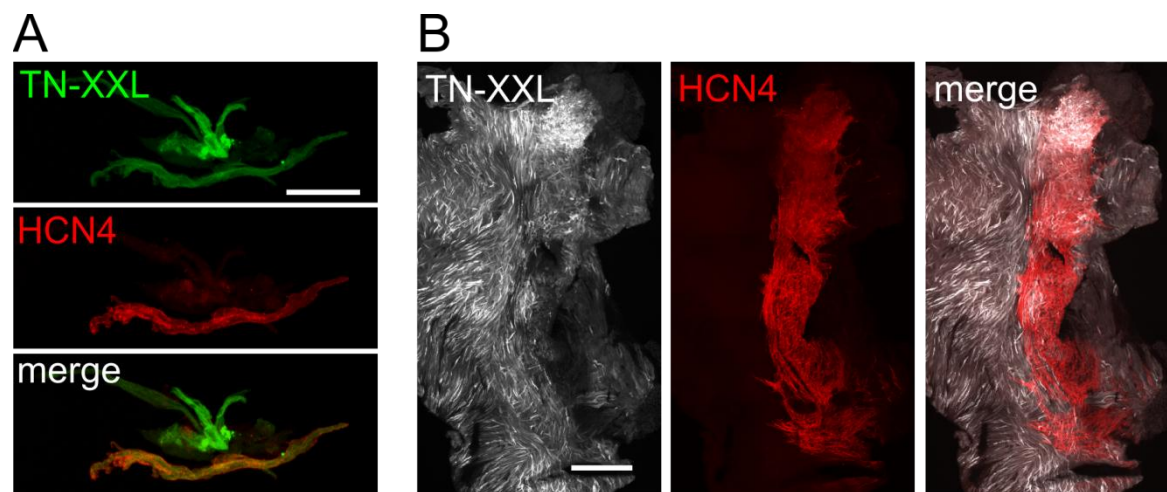


Figure 27: Immunostainings against HCN4 channels of sinoatrial node (SAN) tissue. (A) Dissociated cells from a SAN preparation of transgenically expressing TN-XXL (green) and Alexa568 staining of HCN4 (red) show significant overlap of the lower cell (scale bar: 50 μ m). (B) Immunolabeling of SAN tissue explants. The left image illustrates the fluorescence of TN-XXL, the image in the middle highlights the staining of HCN4 channels with anti-HCN4 antibody (red). On the right image the co-localization of TN-XXL and HCN4 is clearly visible (scale bar: 500 μ m).

4.3.5.1. Calcium Imaging in Dissociated SAN Cells and Tissue Explants

Furthermore, to analyze calcium signaling in dissociated SAN cells imaging experiments were performed using a laser scanning confocal microscope (Figure 28 A). Imaging was carried out at room temperature and at an imaging frequency of 5 Hz. The calcium transients elicited by spontaneous contraction events in single cells were recorded. Single channel emissions of CFP and cpCitrine were measured and the ratio $\Delta R/R$ was calculated. TN-XXL was able to resolve calcium transients shown by the fluorescence intensities of CFP and cpCitrine and resulted in ratio changes of up to 40 % $\Delta R/R$ (Figure 28 B). Due to the low temperature the imaged SAN cells showed a slow contraction frequency of 40 to 80 bpm. Depicting ROIs at different locations of the cell illustrated an onset of the calcium wave at random regions (Figure 28 B). These findings could be confirmed by performing line scans over the horizontal axis of a cell. The onset of the calcium wave could be resolved in high resolution and was in a random manner (Figure 28 C).

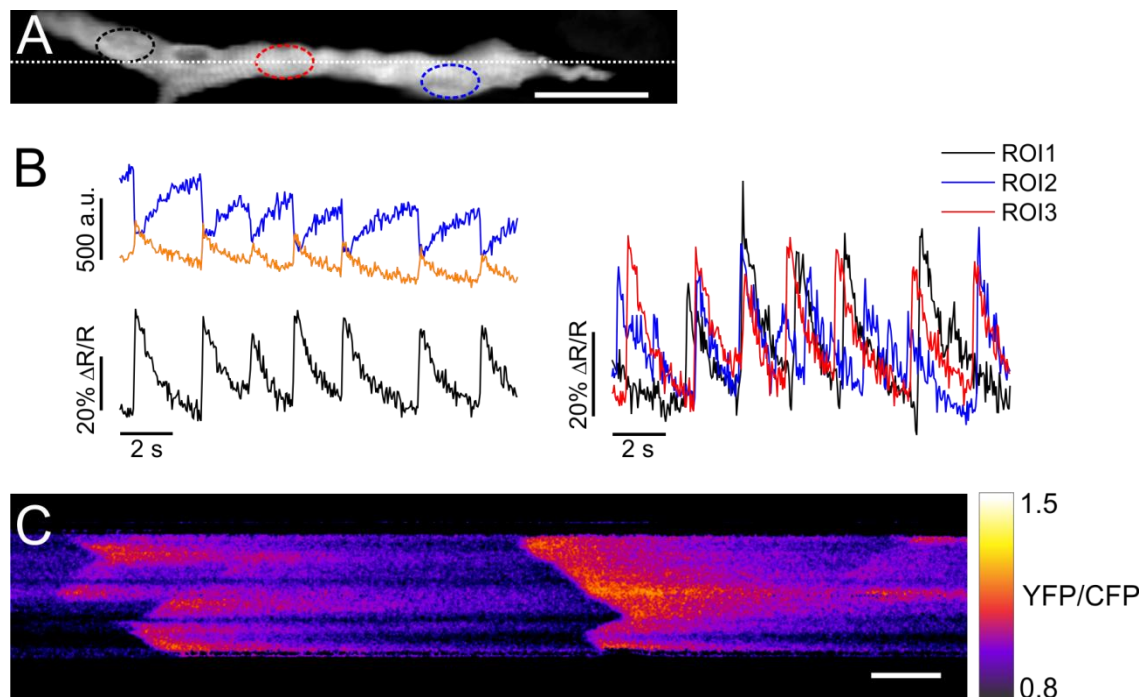


Figure 28: Calcium imaging of dissociated cells gained from SAN preparations. (A) Fluorescence image of a SAN cell (scale bar: 30 μm). (B) Calcium transients of a spontaneous active SAN cell. The emission channels CFP (blue) and cpCitrine (orange) and the resulting ratio changes (black) are depicted in the left graph. The graph on the right shows calcium response of 3 ROIs chosen in A (black, red and blue) with various onsets of the calcium signal. (C) Confocal line scan through the cell in A (white dotted line) demonstrated the onset of the calcium response in different locations (time bar: 250 ms).

RESULTS

Organ explants offer ease of pharmaceutical manipulation for research and drug screening applications, retain tissue context and thus are a first approximation to *in vivo* work. Consequently SAN preparations from the adult TN-XXL mouse heart were used for further confocal calcium imaging experiments. First, living SAN explants were analyzed on a single cell based resolution with an imaging frequency of 30 Hz (Figure 29 A). Keeping the explants at a temperature of 30°C, beating frequencies of up to 4 Hz were recorded. In Figure 29 B calcium imaging experiments of three cells are illustrated and ratio changes of 8 – 16 % $\Delta R/R$ were observed depending of the preparation. Motion artifacts owing to the high beating frequencies were cancelled due to the ratiometric readout of TN-XXL (Figure 29 B).

Second, long-term studies on SAN explants were achieved. SAN explants were cultured for up to three days post preparation. Imaging experiments were performed on day 0 (d0), the day of the preparation and two days afterwards (d1, d2). Additionally, SANs were treated with triiodothyronine (T3) the active form of thyroid hormone. Thyroid hormone is an important regulator of cardiac function and its active form T3 is known to act on ion channels especially in the SAN which influences the heart rate (Danzi and Klein, 2004; Dillmann, 2002). Therefore, increasing of T3 concentrations over a longer period are causing tachycardia, a chronic increase of the resting heart rate. Single cells from SAN explants were imaged at three consecutive days (d0, d1, d2). Due to the preparation and the culturing in untreated SAN explants the beating frequency dropped from ~240 bpm at d0 to ~100 bpm at d2 (Figure 29 C). Application of T3 (150nM) over three days should increase the heart rate (Iordanidou et al., 2010). Unfortunately, no increase in the heart rate could be observed between the control group and T3 treated group (Figure 29 D).

RESULTS

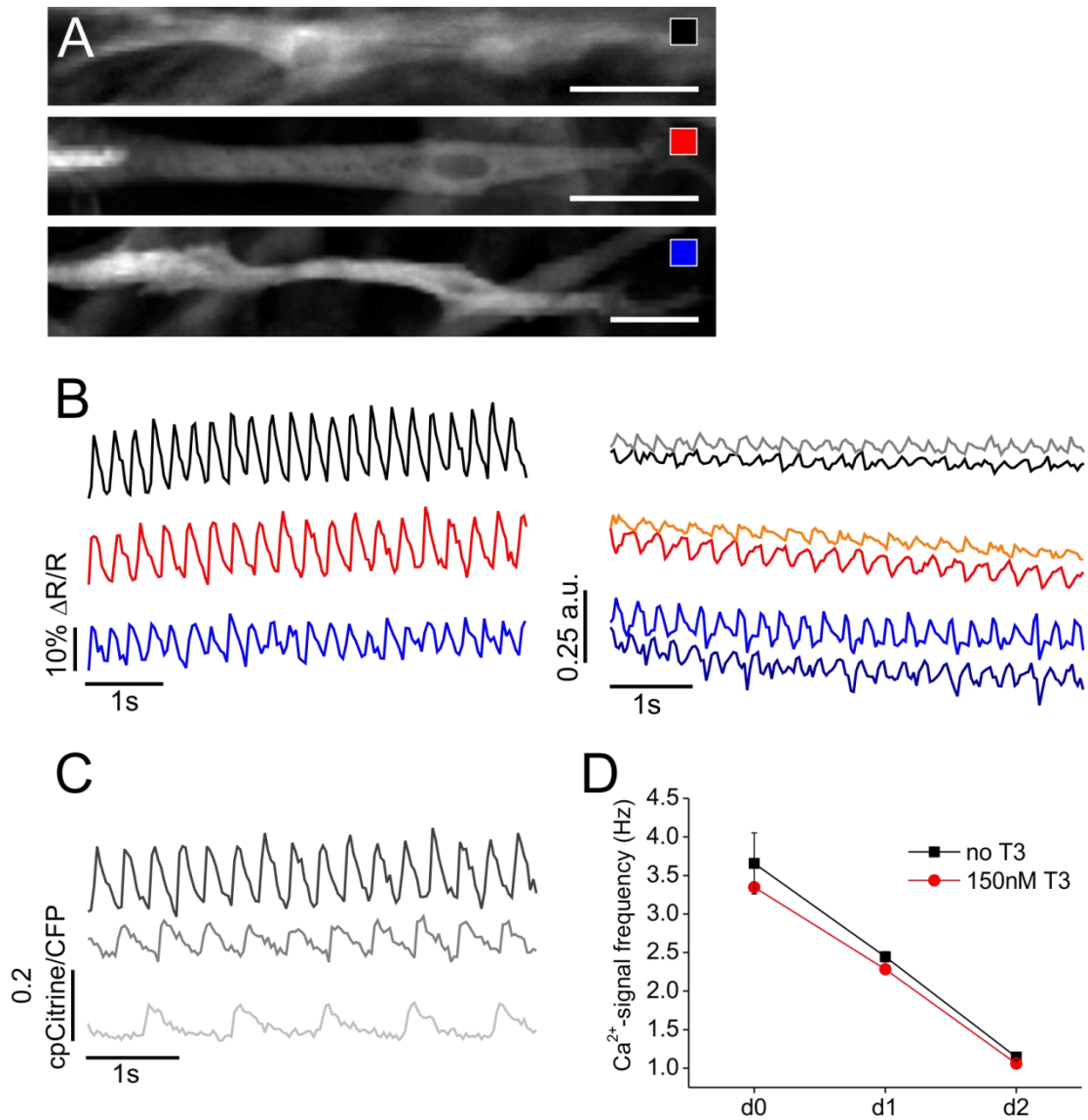


Figure 29: Calcium imaging of cells of an SAN explant. 30 Hz high speed imaging of three cells (blue, red, and black square) from three different spontaneous beating SAN explants recorded at 30°C. (A) Images from 3 cells of an SAN explants. (B, left) Single traces show beating rates up to 4 Hz with $\Delta R/R$ of 10-15%. Colors of the traces refer to the colored squares in A. (right) The single emission channels for CFP (black, red, navy) and cpCitrine (gray, orange, blue). (C-D) Long-term imaging of single cells in SAN explants. (C) Calcium signal decrease in a SAN cell imaged over three consecutive days. (D) Application of T3 (Thyroid hormone) over 3 days to SAN explants.

4.3.5.2. Calcium Imaging in the Developing Heart

The heart is one of the first functional organs in developing organisms. Studying defects already occurring during the development of organs could help getting insight to the cure of further cardiovascular diseases. The β -actin promoter in this transgenic mouse line is switched on during fetal development; therefore, expression of TN-XXL is already present in this embryonic stage. Here, I managed to isolate fetal hearts at embryonic day 8.5 (E8.5) and performed calcium imaging experiments on the whole beating heart.

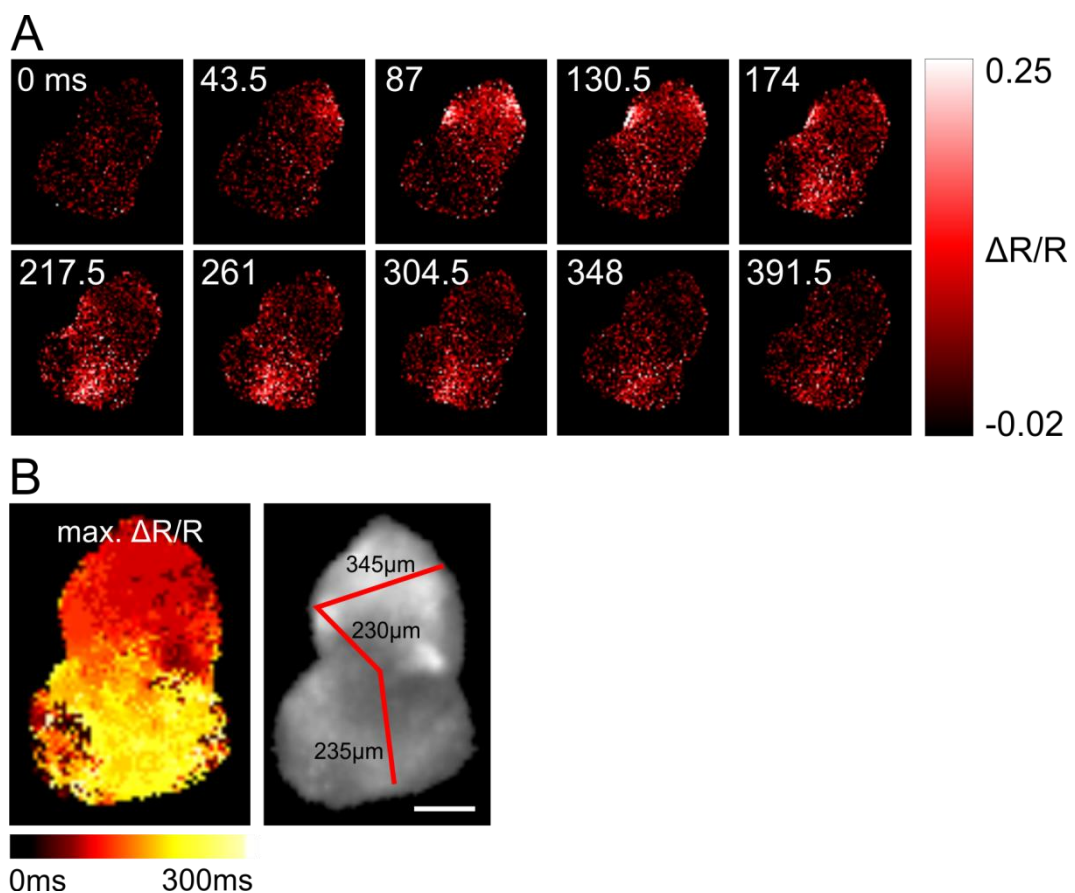


Figure 30: Calcium imaging of a cardiac cycle in the developing heart. (A) The Ca^{2+} dependent changes in $\Delta R/R$ are plotted from black (no ratio change) to white (25 % ratio change). (B) A heat map illustrating the progression of the calcium signal over one heart beat cycle. The color code indicates the maximal $\Delta R/R$ at a given pixel and time (left). The distance the calcium wave travels over time is shown (right) (scale bar: 150 μm).

RESULTS

For this purpose, wide-field fluorescence imaging was preferred, which allows investigating large scale imaging with a suitable temporal resolution. Whole E8.5 embryonic hearts were dissected and cultured for up to 2 days (An et al., 1996; Stieber et al., 2003). Using wide field calcium imaging, calcium waves travelling through the heart were recorded at a temporal resolution of 22 Hz and single heart beat cycles could be resolved (Figure 30 A). The propagation of the calcium wave across the atrial and ventricular region in roughly 300 ms over a distance of about 800 μm with every heart beat were determined (Figure 30 B). The ratiometric nature of TN-XXL facilitated imaging in this moving organ preparation and produced ratio changes of up to 20 % $\Delta R/R$. The curve progression of ROIs picked in the atrial and ventricular region (Figure 31 A) demonstrated the temporal delay of the conduction of the calcium signal from the atria to the ventricles (Figure 31 B, lower graph).

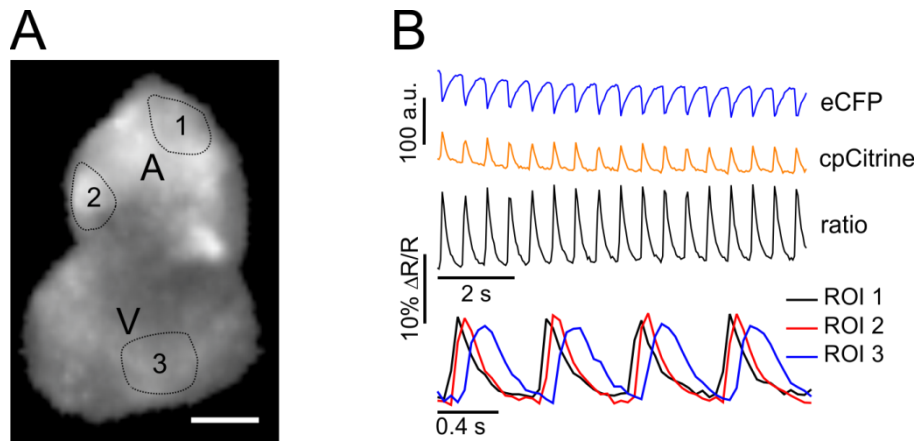


Figure 31: Signal transduction in the embryonic heart. (A) Fluorescence image of an E8.5 embryonic heart. Dotted circles refer to the regions of interest (ROI) shown in B (A, atrium; V, ventricle). (B) Ca^{2+} transients of spontaneous heart beat recorded from the heart in A. The upper graphs show single traces of CFP (blue) and cpCitrine (orange) emission channels of ROI 1. The FRET ratio is plotted in the trace below (black). The lower graph shows four beating cycles for the three ROIs marked in A. The temporal delay from ROI 1 to ROI 3 represents the progression of the calcium wave. Note the short time delay between ROI1 and ROI2 within the atrial region and large delay between ROI2 and ROI3 transmission from the atrium to the ventricle (scale bar: 150 μm).

4.3.6. Transcription Profiling of TN-XXL Expression in Transgenic Mice

After the functional expression of TN-XXL in transgenic mice was confirmed, genomic effects of TN-XXL were analyzed by genome wide transcription profiling using microarrays.

In the past decades transcription analysis became a more and more sophisticated tool to investigate alteration in gene regulation. Microarrays enable studying gene knock downs and resulting effects on influenced signaling pathways or cascades on mRNA level as well as behavioral induced alterations in gene regulation. The effect of long-term expression of fluorescent proteins and predominantly genetically encoded biosensors in host cells or organisms has always been a highly discussed topic in life science since disruption of endogenous genes due to the integration itself cannot be excluded (Okabe et al., 1997; Huang et al., 2000). Furthermore, the binding unit of biosensors, in particular the calcium binding domains are speculated to affect endogenous calcium buffering, may interfere with signaling processes or modify the regulation of gene expression involved in these processes. Studies by which either calmodulin alone or the calmodulin-based calcium indicators were expressed in hearts of mice indeed caused a severe increase of the heart size due to the interference with endogenous signaling pathways (Colomer et al., 2004; Tallini et al., 2006).

Here, the influence of ubiquitous expression of TN-XXL in a mouse model was observed by large scale transcriptional profiling of global mRNA levels in tissues where the highest level of TN-XXL expression was determined. Therefore, tissue samples from skeletal muscle, heart and hippocampus of homozygous *β -actin* TN-XXL mice were compared to wild type control mice (n = 3). The mRNAs were extracted from tissue samples, analyzed with Affimetrix MoGene ST1.1 arrays and processed by the company MTF Services (Tübingen, Germany).

First, the data of the 18 arrays was compiled with principal component analysis (PCA) to display the grade of variability of a single array. A 3 dimensional scatter plot displays the similarity distribution of the analyzed arrays (Figure 32 A). Each data point describes one array.

RESULTS

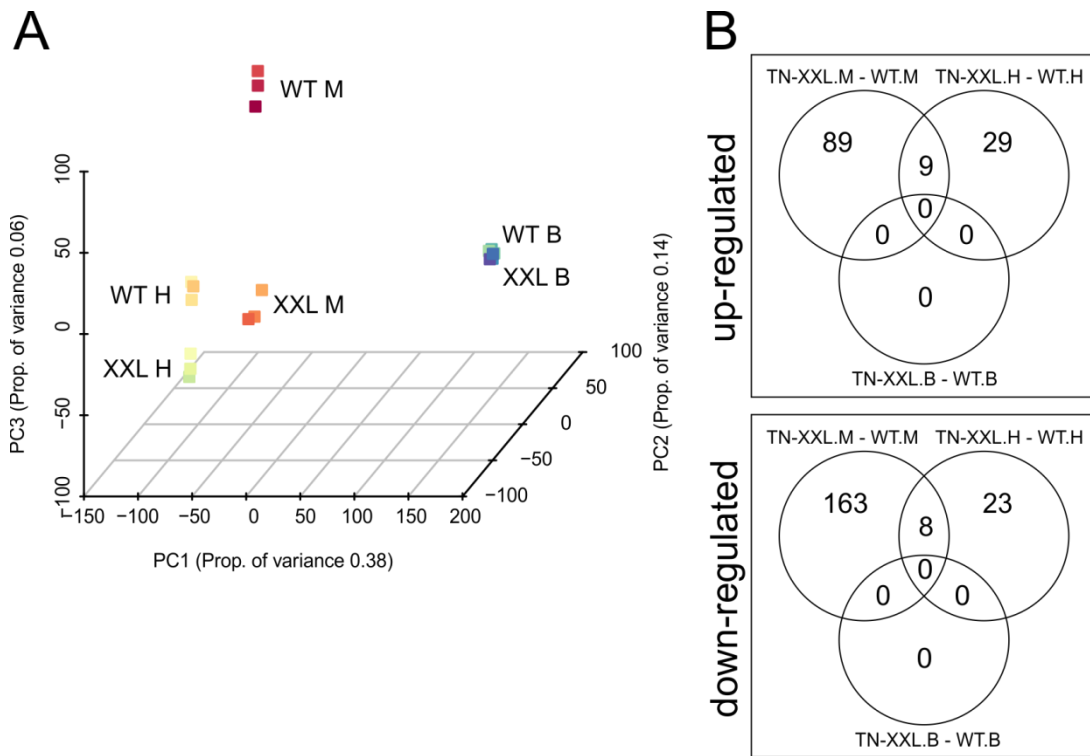


Figure 32: Microarrays analysis of TN-XXL expressing mice. Gene expression in hippocampus, heart and skeletal muscle for homozygous transgenic (TN-XXL) and wild type control mice (WT) were compared. (A) 3D scatter plot of a principal component analysis (PCA) illustrates the variance in gene regulation of the different samples. The further two points are apart, the larger the variance (XXL, transgenic; WT, wild type; B, hippocampus; H, heart; M, muscle). (B) Venn diagram showing the intersection of up- and down-regulated genes of TN-XXL compared to WT of the three tissues.

Table 16: Overview of the number of regulated genes.

comparison of tissues	sum of up-and down-regulated genes	up-regulated genes	down-regulated genes
TN-XXL.muscle - WT.muscle	269	98	171
TN-XXL.heart - WT.heart	69	38	31
TN-XXL.hippo. - WT.hippo.	0	0	0

RESULTS

Table 17: Intersection of up-regulated genes of muscle and heart from the Venn diagram.

Gene Name	Fold change		Biological Function
	muscle	heart	
Mt2	8.23	2.68	cellular zinc ion homeostasis; nitric oxide mediated signal transduction; copper ion binding
Lrrc51	4.00	2.13	unknown
Itgb1bp3	3.95	3.39	integrin-mediated signaling pathway; myoblast differentiation
Coq10b	3.52	2.24	unknown
Fbxo36	3.09	3.13	modification-dependent protein catabolic process
Hyal3	2.42	3.09	no proved function eventually degradation of hyaluronan
Slc10a6	2.16	2.12	sodium ion transport
Usp2	2.13	2.03	ubiquitin-dependent protein catabolic processes
Tef	2.10	2.67	DNA-dependent regulation of transcription

Table 18: Intersection of down-regulated genes of muscle and heart from the Venn diagram.

Gene Name	Fold change		Biological Function
	muscle	heart	
Adhfe1	-3.98	-2.34	oxidation of 4-hydroxybutyrate
AI317395	-3.41	-2.72	sodium ion and carbohydrate transport
Mlycd	-2.82	-2.26	fatty acid biosynthetic process; carboxy-lyase activity
Ddah1	-2.63	-2.22	nitric oxide biosynthetic process; hydrolase activity; zinc ion binding
Nfil3	-2.51	-3.70	DNA-dependent regulation of transcription
Ypel2	-2.42	-2.32	unknown
Mecr	-2.13	-2.10	mitochondria fatty acid biosynthetic process
Mcat	-2.08	-2.01	mitochondria fatty acid biosynthetic process

RESULTS

Arrays which are in close proximity imply similar gene expression like it is the case for wild type (WT) and transgenic (XXL) probes of the hippocampus (B). A high variation was detected for the arrays of muscle and heart tissue, where WT arrays and XXL arrays were found to lay further apart (Figure 32 A).

This preliminary approximation is additionally confirmed by the concrete number of genes which showed differences in regulation. A large number of genes were found showing just marginally altered regulation in all three tissues. To narrow down the amount of genes, transcript levels differences between TN-XXL and WT mice lower than 2-fold were considered as not relevant. Additionally, genes which are involved in circadian rhythm and control of molecular clocks (Dbp, Per1, Per2 and Per3 (Sakamoto and Ishida, 2000), Arntl (Preitner et al., 2002) and Npas2 (Hogenesch et al., 1998)) change expression and transcription levels on a scale of hours and were therefore excluded from the analysis. With a cut-off value of 2, an up-regulation of 98, 38 and 0 genes and a down-regulation of 171, 31 and 0 genes was observed for muscle, heart and hippocampus, respectively (Table 16). Furthermore, a Venn diagram for the cut-off value of 2-fold illustrates an overlap of only 9 up-regulated genes and 8 down-regulated genes in muscle and heart tissue (Figure 32 B). The low number of correspondence between the tissues already indicates that the expression of TN-XXL does not cause severe global effects to the host organism. Looking at these shared regulated genes also did not bring any further conclusions of the hypothesis that FP formation or interaction of the TN-XXL calcium binding site could administer cellular stress induced by production of reactive oxygen species, interference with signaling pathways, metabolic processes, changes in calcium homeostasis and buffering systems (Table 17, Table 18).

Most notable is the significant 8.2 and 2.7 fold induction of transcripts coding for metallothionein-2 in muscle and heart, respectively. Metallothionein-2 is a zinc and copper binding protein that has been suggested to play a role in protection against oxidative damage (Kumari et al., 1998), but its detailed cellular role is to date unknown. One can speculate that the gene is induced in response to reactive oxygen species generated during FP chromophore formation (Tsien, 1998).

4.3.7. Behavioral Testing of TN-XXL Mice

Behavior is the result of an array of physiological and cognitive processes that have to be coordinated and fine-tuned within the organism. The preceding experiments performed with this mouse line clearly demonstrate the functional expression of TN-XXL. In addition, no perturbation of the cellular morphology during long-term expression and no obvious effects of the transgene TN-XXL were detected since the animals exhibited normal lifespan, fertility, litter and body size compared to the wild-type siblings. Furthermore, the evaluation of gene transcription profiling showed only minor differences in gene regulation between transgenic and wild-type mice. To further investigate whether the cellular up- and down-regulation of genes in response to TN-XXL expression has a global effect on the organism, a collaboration with the Max-Planck-Institute for Psychiatry was undertaken with the aim of assessing animal responses to behavioral tasks in order to evaluate the influence of TN-XXL expression on behavior. The experiments were carried out at the MPI for Psychiatry under the direction of Carsten Wotjak and were implemented by Vincenzo Micale.

A battery of seven behavioral tasks for motor-coordination, motor-learning behavior, emotionality and depression-related behavior was performed and behavior of homozygous transgenic mice (TN-XXL) and wild-type littermates (WT) was compared. All animals (n = 12 – 15 per group) were singly housed under an inverse 12 h light/dark cycle to ensure the execution of experiments during the activity phase of the animals. A detailed description of the experimental procedures is given in the appendix.

Tests monitoring exploratory, motor behavior and skilled movements were performed, taken into consideration the pronounced expression of TN-XXL in muscle, motor neurons and all cortical cerebral areas. To evaluate general motor activity mice were transferred to a hole-board where the animals' behavior for the covered distance, the time animals were moving or resting, the number of jumps, nose pokes into holes and rearing was observed for a period of 30 min. Animals' movements were recorded with infrared sensors. The exploratory hole-board test revealed no differences between TN-XXL mice and wild type mice in any of the explored parameters (Figure 33 A).

RESULTS

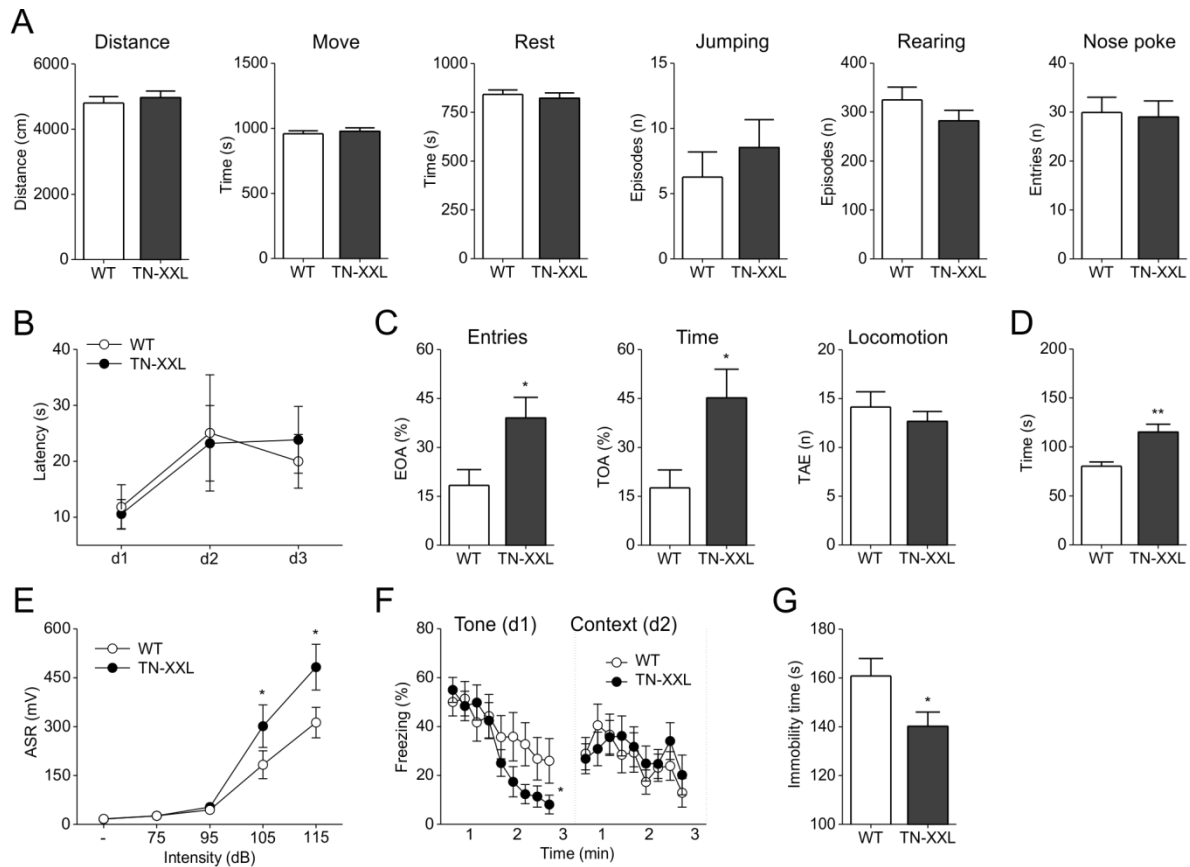


Figure 33: Homozygous TN-XXL transgenic mice and wild-type controls (WT) were compared in a battery of behavioral experiments. (A) Hole board. Distance covered, distance in time, resting, jumping, rearing behavior and number of nose pokes were analyzed. **(B) Rotarod.** Mice were placed on accelerating drums. The time at which an animal fell from the drum was measured. Motor learning behavior was assessed by consecutive trials over a period of 3 days (d1, d2, d3). **(C) Elevated plus maze (EPM).** Time spent in open arm (TOA), entries in open arm (EOA) and locomotion as motility control was analyzed. **(D) Social interaction (SI).** Pairs of unfamiliar mice (n=7 pairs each) were placed into neutral environment. The time of active interacting contacts (sniffing, licking, close following, grooming) was recorded. **(E) Acoustic startle response (ASR).** To test for hyperarousal, startle stimuli consisted of white noise bursts of 75, 90, 105 and 115 dB were applied. **(F) Fear conditioning.** Mice were placed into a shock chamber and a tone was presented followed by an electric foot shock. After conditioning, mice were exposed either to the tone in neutral environment (d1) or to the shock chamber without applying an electric shock (d2). Freezing behavior served as a measure of fear memory. **(G) Tail-suspension test.** Mice were suspended by the tail from a metal rod and the immobility times during the last 4 min of the 6 min trial period was recorded. Data provided by Carsten Wotjak and Vincenzo Micale.

RESULTS

In addition, the 'rotarod test' was carried out as task for motor coordination, skilled movement and motor learning. Animals of both groups were placed on accelerating rotating drums and the time until the animal fell from the drum was measured. To assess motor learning behavior animals received three trails per day for three consecutive days (d1, d2 and d3). No significant differences in behavior for motor coordination (latency d1: TN-XXL: 10.6 s \pm 2.6; WT 11.8 s \pm 4.0; standard deviation) and motor learning (latency d3: TN-XXL: 23.8 s \pm 6.0; WT: 20 s \pm 4.8; standard deviation) could be detected (Figure 33 B).

When exposing the test animals to tasks that are assigned to trigger anxiety like behavior differences became apparent. The 'elevated plus maze' (EPM) exploits the animal's natural aversion against open spaces and conflicts with the natural instinct to explore new environments. Animals were placed in the center of the maze and the number of entries and the time spent in open and closed arms was analyzed for a period of 5 min. TN-XXL mice showed an increased percentage of both entries (EOA) and time (TOA) in open arms, which suggested a reduced anxiety-like behavior ($t=2.556$; $p<0.05$) (Figure 33 C). No difference was found in the total arm entries as an index of locomotion or any movement defects. Observing the social interaction also correlates to the level of anxiety of animals. In this task two animals (TN-XXL with TN-XXL, or WT with WT) were placed in a neutral environment and the interaction was monitored. The TN-XXL group spent more time interacting compared to WT ($t=3.800$; $p<0.01$) which indicates a less anxious condition of TN-XXL mice (Figure 33 D). Furthermore we examined the level of arousal with the startle response test. Acoustic bursts provoke a brainstem reflex to protect the back of the neck. Analysis showed a slightly higher response of TN-XXL at the noise of 105 and 115 dB ($p<0.001$) which indicates a higher degree of arousal or hyperactivity (Figure 33E).

A further test to address induced anxiety like behavior was the 'fear conditioning task'. In this test the animals were conditioned by putting them into a shock chamber applying a tone and an electric foot shock. The day after conditioning the animals were exposed to the two contexts: a neutral environment where they were solely exposed to a tone (d1) or the shock context without applying an electric shock (d2). This test revealed a faster decline of freezing in response to tone (d1) indicating an accelerated acute fear relief to the presented tone in TN-XXL mice (2-way ANOVA; f1: genotype, f2: intervals; $p<0.001$). In contrast, contextual conditioning (d2) showed no significant differences (Figure 33 F). Finally, TN-XXL mice were less immobile in the tails suspension test which measures depression-like behavior (Figure 33G; $t=2.184$; $p<0.05$). A summary of the behavioral tasks is given by Table 19.

RESULTS

Table 19: Behavioral experiments. Summary of tasks for motor behavior, emotionality and depression-related behavior of transgenic mice expressing TN-XXL compared to wild-type controls. Data provided by Carsten Wotjak and Vincenzo Micale.

Test	Behavior	Phenotype
Hole board	↔	↔ Locomotion
Rotarod	↔	↔ Motor learning
EPM	↑TOA ↑EOA	↓ Anxiety
SI	↑ Interaction time	↓ Anxiety, ↑Social behavior
ASR	↑ Response	↑ Arousal
Fear condition	↓ Freezing	↓ Anxiety
TST	↓ Immobility	↓ Depression-like phenotype

EPM, elevated plus maze; LD, light-dark avoidance test; ASR, acoustic startle response; TOA, time in open arm; EOA, entries in open arm. ↓, ↑, ↔ indicating a decreased, increased or unchanged behavior of TN-XXL compared to WT mice, respectively.

All in all, TN-XXL mice showed normal locomotion, motor co-ordination, spatial navigation and were unhindered in motor learning elaborated by the ‘hole board’ and the ‘rotarod’ paradigm. Furthermore, the hippocampus- and amygdala-dependent learning behavior determined by the ‘fear conditioning test’ remained unaffected. However, TN-XXL mice were less anxious and more disposed to develop active coping strategies in stressful situations. This implies beneficial consequences of the transgene in tests related to neuropsychiatric disorders.

5. Discussion

The generation of transgenic animals expressing a genetically encoded calcium indicator becomes more and more important in the research field of life science. Despite the successful generation of transgenic animals expressing GECIs, the majority of calcium imaging experiments still rely on approaches based on either synthetic calcium dyes like OGB-1 AM, Fura-2 and Fluo-4 or on virus mediated gene transfer of GECIs. In contrast to transgenic approaches loading synthetic dyes or injecting GECIs in form of viruses requires a preceding invasive step that can cause tissue damage resulting in a corruption of the experimental outcome. However, several previous studies reported that transgenic long-term expression of calmodulin-based GECIs resulted in numerous problems causing pathological defects of the animal or a loss of indicator function (Tallini et al., 2006; Hasan et al., 2004). It is thought that these effects are caused by the interference of the sensors' calcium binding unit calmodulin (CaM) with endogenous CaM or further regulatory mechanisms. These facts have to be taken into account when the long-term expression of a GECI is required e.g. for the accomplishment of chronic imaging experiments.

A more appropriate class of GECIs – troponin C-based GECIs – may be used for transgenic approaches as troponin C (TnC) is more biologically autonomous than CaM since it is not involved in further regulatory processes except muscle contraction. Preceding studies already reported the successful generation of transgenic mice with the TnC-based GECI TN-L15 in the nervous system and furthermore the *in utero* electroporation of TN-XXL enabled chronic *in vivo* calcium 2-photon imaging in the mouse primary visual cortex V1 (Heim et al., 2007; Mank et al., 2008). Thereby calcium transients of orientation selective cortical layer 2/3 neurons could be recorded over days and weeks. Moreover, no morphological defects or loss of function caused by TN-XXL expression was reported in neither of the sensors in the work published. As a consequence TN-XXL was selected as the GECI of choice for this work.

The primary aim of this thesis was the investigation and characterization of transgenic animals expressing the GECI TN-XXL under the control of several promoter cassettes. The generated transgenic mouse lines which expressed TN-XXL in the nervous system under the *Thy1.2* and the *TLCN* promoter were tested for expression pattern using fluorescence microscopy.

Furthermore, I performed detailed analyses of expression patterns, the functionality and the biocompatibility of TN-XXL expressed under the control of the ubiquitous β -*actin* promoter in an already existing mouse model. The functionality of TN-XXL was examined by *in vitro* and *ex vivo* experiments in a variety of cell types and in tissue explants from the developing and the adult heart. Moreover, the biocompatibility of long-term expression of TN-XXL was

determined by investigating morphological changes, elaborating genome-wide mRNA transcriptional analysis and finally by the exploration of behavioral experiments which were conducted in a collaboration with Carsten Wotjak and Vincenzo Micale from the Max-Planck-Institute of Psychiatry.

5.1. Expression of TN-XXL under the *Thy1.2* Promoter

The *Thy1.2* promoter is a widely used and well characterized model for the generation of transgenic mice. It has already been used in several studies to investigate morphology of the brain by expressing fluorescent proteins or to study neuronal activity by expressing genetically encoded calcium indicators. Furthermore, the *Thy1.2* expression cassette showed remarkable expression levels and neuron specific labeling in a sub-regional manner (Feng et al., 2000).

Expression of TN-XXL under the control of the *Thy1.2* promoter on a C57BL/6N background gave rise to a total number of 5 founder lines which displayed high expression in the central nervous system. Line #8057 was separated into #8057bright and #8057dark after several rounds of breeding due to a large difference in expression levels. Founder lines that were void of expression or were not able to produce offspring might have been affected by insertions of the transgene at sites where genomic loci responsible for fertility were disrupted. Analyzing the expression of TN-XXL examined by fluorescence imaging of whole brains brought clear differences in intensities from bright lines #7952 to dim lines such as #8057dark and #8103. The differences in TN-XXL expression intensity most likely derived from different numbers of tandem repeat insertions in the genome during the injection procedure (Jasin et al., 1996; Garrick et al., 1998). Surprisingly, generating homozygous mice did not increase the expression level which was still beneficial since no more laborious genotyping of the lines was necessary. Furthermore, homozygous mouse lines did not exhibit impairments concerning litter size, body size, fertility or conspicuous behavior. All examined lines displayed a similar TN-XXL expression pattern examined by fluorescence microscopy of fixed sagittal sections of the brain but differed in expression levels. TN-XXL expression was found mainly in the hippocampus, the olfactory bulb and several thalamic and brainstem regions. The expression explored in cortical regions was predominantly found in deeper cortical layers (layer 4 and 5). Additionally, all lines displayed a weaker TN-XXL expression of neurons situated in upper cortical regions (layer 2/3). The intensity by which layer 2/3 neurons were detectable strongly depended on the intensity of background fluorescence. The background fluorescence is believed to derive from TN-XXL expression of

DISCUSSION

the neuropil mainly from neuronal protrusions of deeper cortical layers. The highest background fluorescence was observed in the lines #7959 and #8057bright whereby due to the high background labeling detection of cell bodies in upper cortical layers turned out to be difficult. Further, the line #7952 showed a moderate level of background fluorescence and the lines #8103 and #8057dark displayed the lowest degree of background which enabled the visualization of neuronal protrusions in upper cortical layers in fixed sections. Due to the low background fluorescence, the lines #7952, #8057dark and #8103 are potential candidates for the application of *in vivo* 2-photon imaging experiments in upper cortical neurons.

In addition, the lines #7959 and #8103 displayed strong expression in the mitral cell layer and the glomeruli of the olfactory bulb. TN-XXL expression was absent in neurons of the cerebellum, except the line #7959 showed strong labeling of cell bodies and dendrites in the purkinje cell layer. Therefore, this mouse line could also be applicable for *in vivo* imaging experiments in purkinje cells of the cerebellum (Sullivan et al., 2005) or the investigation of imaging of mitral cells in the olfactory bulb (Charpak et al., 2001; Kapoor and Urban, 2006).

5.2. *In vivo* Recordings in the Visual Cortex of *Thy1.2* Mice Expressing TN-XXL

Despite the preferred *Thy1.2* driven expression of TN-XXL in deeper cortical layers the line #7952 was taken into account for the accomplishment of *in vivo* calcium imaging experiments of neurons from the layer 2/3 in the primary visual cortex V1.

Previously it has been shown that TN-XXL expressed via virus mediated gene transfer or *in utero* electroporation is able to resolve calcium signals of direction selective neurons in the visual cortex V1 over days with *in vivo* 2-photon imaging (Mank et al., 2008). Hence, the suitability of the *Thy1.2* TN-XXL mouse line #7952 for *in vivo* 2-photon calcium imaging in neurons of the primary visual cortex V1 was observed. To determine whether the expression pattern and the level of TN-XXL expression are suitable for long-term *in vivo* 2-photon calcium imaging experiments Alexandre Ferraro Santos from the Max-Planck-Institute for Neurobiology prepared and completed all *in vivo* imaging experiments with this mouse line.

The visual system enables organisms to process visual light and construe information to build a representation of the surrounding environment. In general, in rodents visual information is transduced from sensory afferents of the retina of the eyes via the optic chiasm and the optic tract to project to the LGN (lateral geniculate nucleus) from where information is projected to the primary visual cortex V1. The primary visual cortex V1 receives and computes spatial information mainly from the contralateral eye (Hübener, 2003). For the investigation of long-term function and plasticity of primary visual cortical neurons expressing TN-XXL A. Ferraro Santos selected the monocular deprivation paradigm whereby one eye remains closed for a given period of time to manipulate the optical signaling pathway. To facilitate the experimental procedure animals were anesthetized and a permanent cranial window was inserted by stereotactic surgery. The cranial window was located at the primary visual cortex V1 to enable chronic calcium imaging without repeating surgical interventions. After animals recovered from the surgery they were transferred to the imaging setup and moving bars of different orientations were presented at random to inhibit stimulus adaptation. Simultaneously the calcium response of orientation selective neurons in layer 2/3 of the V1 cortex was recorded with a laser scanning 2-photon microscope.

DISCUSSION

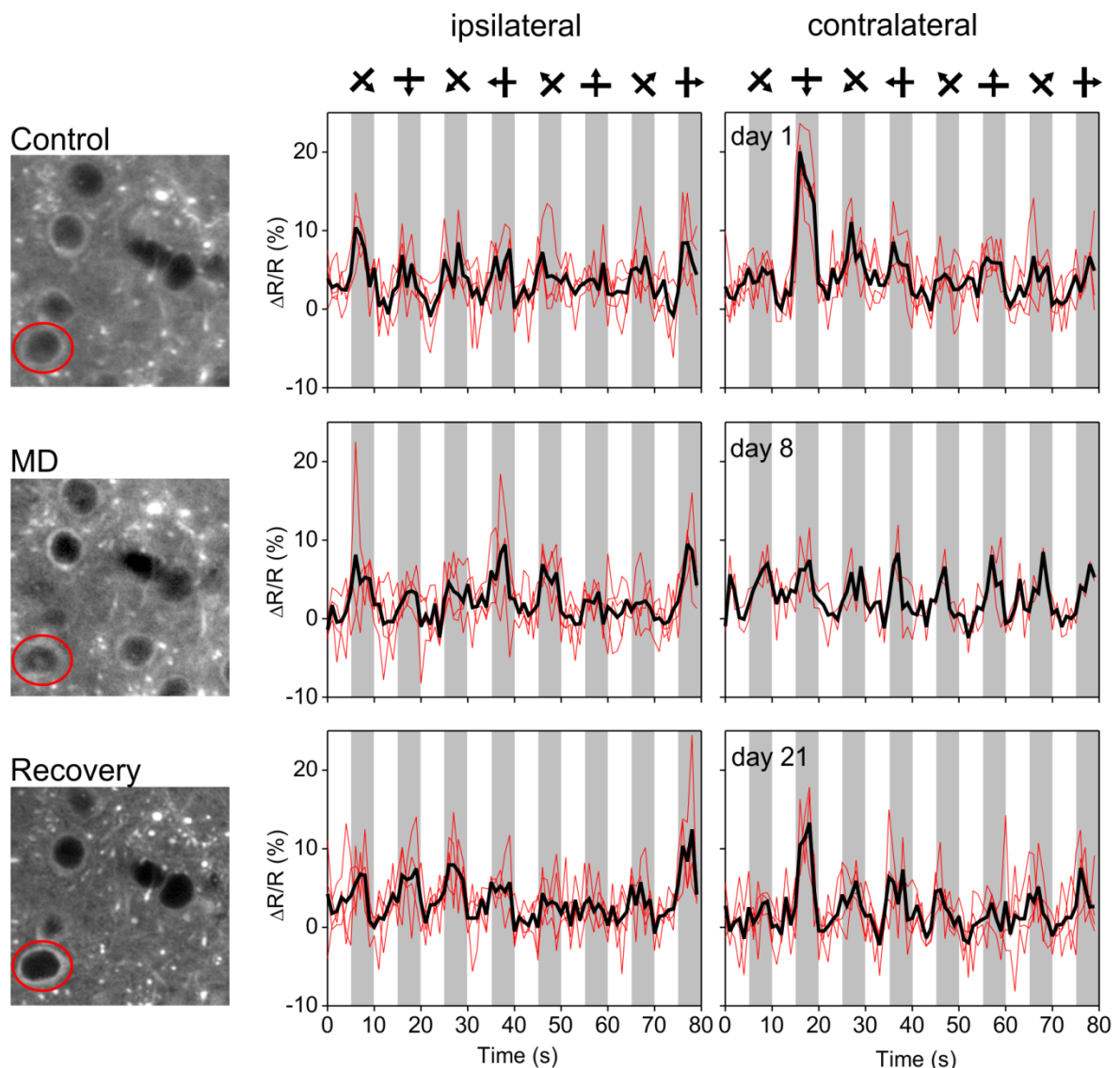


Figure 34: Chronic *in vivo* imaging of sensory evoked calcium transients during monocular deprivation (MD) in the primary visual cortex V1 of the *Thy1.2* TN-XXL mouse line #7952. Images on the left display the cortical region which was recorded before MD (control), shortly after MD (MD) and after a 2 week recovery phase (recovery). The panels illustrate the calcium response properties of TN-XXL to the presentation of moving bars of different orientations (indicated by arrows above) to the ipsilateral (left) and contralateral eye (right). The traces are recorded from the depicted on the left (red circle). Data from Alexandre Ferraro Santos (unpublished observations).

DISCUSSION

The stimulus was always presented to contralateral eye and additionally as a control the same stimulus protocol was provided to the ipsilateral eye. With the termination of the experiment the contralateral eye was sutured shut to inhibit visual input. During the phase of monocular deprivation (MD) the animals were kept under normal housing conditions. After one week the deprived eye was re-opened and the animals underwent the same stimulation protocol as in the previous experiment. This was again repeated after a two week recovery phase whereby the animal was kept under regular condition again. The effect of MD was monitored by consecutive recordings of the same neuron during a 21 day trial period.

The closure of an eye elicits a disruption of information flow due to the loss of sensory input which in turn leads to a modification in synaptic processing and an altered computation of signal inputs. After a phase of recovery the orientation selectivity can be recaptured. Figure 34 shows chronic recordings of sensory evoked calcium responses of a neuron expressing TN-XXL which are elicited by the presentation of moving bars in different directions. In a test trial before MD the neuron showed an orientation selective response with ratio changes of 20% to downward motion presented to the contralateral eye (Figure 34, right panel, day 1). Furthermore, no orientation selective response was detected when the ipsilateral eye was stimulated (Figure 34, left panel). Recordings which were performed shortly after eye opening after the 7 day period of MD of the same neuron clearly demonstrate that the orientation selectivity disappeared (Figure 34, right panel, day 8). Moreover, the neuron responded to all presented stimuli in a similar manner. After a 2 week recovery phase the neuron regained orientation selection which is illustrated since the neuron showed the identical tuning to the presented stimuli than before MD (Figure 34, right panel, day 21).

This first preliminary experiment clearly demonstrated the usefulness of transgenic mice expressing TN-XXL under the control of the *Thy1.2* promoter. The long-term expression of TN-XXL enabled the recording and observation of changing response properties of single neurons over weeks and therefore confirmed the applicability of TN-XXL for chronic *in vivo* imaging in transgenic mice. Furthermore, this underlines the importance of the generation of transgenic animals expressing a GECI like TN-XXL, which will allow monitoring of single neurons and small neuronal networks changing their response properties during development, learning and memory consolidation or during the development of neurodegenerative diseases.

5.3. Transgenic Mice Expressing TN-XXL under the *TLCN3.9* Promoter

The functional expression of TN-XXL under the *Thy1.2* promoter has been proven by chronic *in vivo* 2-photon calcium imaging experiments in the mouse visual cortex performed by A. Ferraro Santos. Nevertheless TN-XXL expression of neurons in upper cortical layers (layer 2/3) was reduced by high background fluorescence. Especially the labeling of the neuropil which most likely derived from dendritic projections of neurons from deeper cortical layers disturbed the imaging quality and lowered the signal to noise ratio (SNR) which plays a role when imaging at faster acquisition rates is performed. To overcome the disturbing background fluorescence the *TLCN3.9* promoter was chosen which reported to exhibit higher transgene expression in upper cortical neurons (Mitsui et al., 2007).

Unfortunately, the generation of transgenic mice under the control of the *TLCN3.9* did not reveal any founder lines that displayed expression of TN-XXL above the detection limit of fluorescence microscopy. However, pre-testing of the construct in neuronal culture and immunofluorescence labeling against TN-XXL of fixed frozen sections of brains confirmed the expression of TN-XXL and consequently excluded incorrect cloning of the construct or technical problems during the injection process. The reason why the expression of TN-XXL was almost absent remains unclear. Possible explanations could be very low expression of the *TLCN* promoter in general, insufficient amounts of DNA during the pronucleus injection procedure leading or the insertion of the TN-XXL transgene at genomic loci which already were silenced during development.

Supplementary attempts to produce transgenic animals with the same construct could be accomplished and hopefully will result in better expression levels. Furthermore the insertion of the woodchuck hepatitis virus posttranscriptional regulatory element (WPRE) downstream of TN-XXL could be included which is known to enhance transgene expression (Zufferey et al., 1999). If the *TLCN3.9* promoter in general exhibit low expression levels other promoters with similar expression pattern must be evaluated. A recent study reported the generation of a toolbox of 'Mini promoters' with different expression in the central nervous system which display promising expression pattern for the study neuronal research (Portales-Casamar et al 2010). However, further investigations have to be accomplished to determine the suitability of these promoters for the generation of transgenic animals expressing GECIs like TN-XXL.

5.4. TN-XXL in Mice under the β -actin Promoter

As shown before TN-XXL has proven to monitor calcium signals of neurons and neuronal networks. GECIs nowadays are able to compete with synthetic calcium dyes in terms of brightness, dynamic range and calcium affinity. In contrast to synthetic dyes GECIs have the advantages of labeling specificity, the ability to obtain long-term imaging and further the production of transgenic animals. Moreover, the importance of calcium imaging exceeds the central nervous system since calcium is involved in signaling processes in every cell of an organism and researchers would benefit from the application of GECIs in other approaches. To achieve this goal a transgenic mouse line was generated that globally expresses the GECI TN-XXL driven by the β -actin promoter. Generated by Marsilius Mues, this mouse line shows transgene expression in a multiple cell types and organs. In following sections the functionality and biocompatibility of TN-XXL is discussed.

5.4.1 Ubiquitous TN-XXL Expression

Initial expression analysis performed by fluorescence imaging of whole animals, organ and tissue section of various organs demonstrated the expression of TN-XXL in the majority of tissue types including brain, skeletal muscle, heart, kidney, liver and intestines. The highest expression levels were found in skeletal and cardiac muscle tissue which was expected promoted by the high endogenous expression of β -actin in these tissues. Additionally, high expression was found in the brain of which the highest expression was detected in blood vessels. Due to the cell type unspecific transgene expression of the β -actin promoter the identification of neurons was disturbed by glia cell fluorescence in the cortex. Nevertheless, regions of low glia cell density like the cerebellum or the hippocampal formation enabled the detection of neurons with low levels of background fluorescence. Surprisingly, no TN-XXL expression was found in lymph follicles of the spleen and other organs of the hematopoietic system. Marsilius Mues performed flow cytometric and mRNA level analysis which showed a significant down-regulation of mRNA levels and TN-XXL expression in cells of hematopoietic system compared to cell derived from kidney. The mechanisms behind the shutdown of the transgene remain unsolved. However, it has been reported that the WPRE element which was integrated downstream of TN-XXL acting as expression enhancer in rare cases causes a down-regulation of transgenes especially in cells of the hematopoietic system (Werner et al., 2004).

Already illustrated with fluorescence microscopy the levels of TN-XXL expression clearly differed between tissues. By comparing fluorescence intensities from bacterial purified TN-XXL solution with TN-XXL expressing tissues, concentrations of TN-XXL at concentrations in the low micromolar range (1.2 – 5.7 μM) were identified. The lowest TN-XXL expression analyzed was found in liver whereas as expected the highest expression levels were determined in skeletal muscle and cardiac tissues. Furthermore, in skeletal and cardiac tissue a distribution of expression into 3 cellular subsets was observed. One can speculate that subdivided TN-XXL expression in skeletal muscle subsidizes with the muscle type distribution (Type I, Type II A, type II B). This hypothesis, however, needs to be further investigated. The sub-division of TN-XXL expression in cardiac remains unstated.

5.4.2. Long-term Expression and Performance of TN-XXL in Cultured Cells

So far GECI research has focused on the improvement and extension of sensors dynamic range, calcium affinity, kinetics and sensor brightness that together form the fundamental direction for GECI development. However, the biocompatibility of GECIs played either a minor role or was often disregarded when engineering calcium biosensors. Nowadays, through the augmented complexity of experiments GECIs have become more and more valuable for research and the generation of transgenic animals expressing GECIs especially for long-term *in vivo* studies is essential. Therefore analyzing the biocompatibility of GECIs in such systems becomes of unprecedented importance.

Previous studies already reported that the long-term expression of GECIs in some cases – exclusively observed with CaM-based GECIs – causes punctuated aggregation, a shuttling of the indicator into nucleus or morphological defects (Hasan et al., 2004; Tallini et al., 2006; Tian et al., 2009). This is speculated to occur due to the interaction of indicator molecules with endogenous proteins or their interference with signaling processes which can inhibit indicator function and can elicit cytotoxic effect on the cell and the organism. In contrast to CaM-based GECIs, expression of TN-XXL did not reveal any morphological difference when comparing acutely transfected wild-type murine kidney fibroblasts (MKF) with MKF isolated from transgenic mice. Investigating the performance of TN-XXL at basal calcium concentrations showed indistinguishable baseline ratios which in addition demonstrated that endogenous calcium levels are not affected by the long-term expression of TN-XXL. Furthermore, examining ATP induced calcium responses in MKF between acutely and long-term expressed TN-XXL did not reveal any differences in signal strength which indicates

DISCUSSION

that long-term expression does not impair the dynamic range and therefore does not alter TN-XXL function.

Additionally, the functionality of transgenically expressed TN-XXL was tested in a variety of primary cultured cells. In MKF, smooth muscle cells (SMC) gained from bladder, cortical astrocytes and cardiomyocytes TN-XXL clearly followed spontaneous and agonist induced calcium responses. TN-XXL was able to monitor calcium transients with ratio changes up to 60% $\Delta R/R$ in MKF. Even in astrocytes and MKF maintained in culture for up to 6 month no decrease or loss of TN-XXL function and only a slight reduction of expression was noticeable.

Furthermore, long-term expression of TN-XXL did not show morphological changes on cellular and organism level. The investigation of diffusion rates in MKF of transgenically expressing TN-XXL with fluorescence recovery after photobleaching (FRAP) experiments confirmed the free-diffusible cytosolic expression of TN-XXL. In contrast to previous studies with CaM-based sensors (Hasan et al., 2004) neither punctuated expression due to aggregation nor the formation of indicator precipitates in inclusion bodies was detected in TN-XXL expressing MFK. Additionally, elaborated with fixed hippocampal sections in transgenic mice from postnatal day 13 to the age of 6 month no nuclear localization of TN-XXL could be detected. Other than in a study where the virus mediated long-term expression of the CaM-based GECI G-CaMP 3 yielded a pathologic nuclear translocation and subsequently a reduction of indicator function determined in cortical neurons (Tian et al 2009).

The given results clearly demonstrate the viable and functional long-term expression of TN-XXL. Purchasing functional primary cell cultures, mouse embryonic fibroblasts or even pluripotent stem cells from homozygous transgenic TN-XXL mice could be of great interest for research and pharmaceutical industry e.g. for the application of calcium based *in vitro* drugs screenings.

5.4.3. Calcium Imaging of TN-XXL in Tissues of the Developing and Adult Heart

The functional expression of TN-XXL was already shown by the detection of calcium responses in various cultured cell-types. Furthermore, transgenic expression of TN-XXL facilitates tissue handling in rather complex experiments as no further preparations to enable the accomplishment of calcium imaging such as dye loading or transfection of a GECI were required. Apart from investigating calcium signaling in cell culture the study of tissue complexes and whole organs represents a superior way to gain knowledge on calcium dynamics as cyto-architecture tissue connectivity remains conserved. The early onset of the *β-actin* promoter moreover allowed the study of calcium signaling even in developing tissues. The high expression of TN-XXL in the developing heart enabled the detection of calcium transients spreading over the whole heart using wide-field fluorescence microscopy. Calcium waves initialized at the atrial region and their propagation to ventricles during cardiac cycles were readily recorded with TN-XXL.

The study of calcium dynamics is not only essential during animal development but also in matured organisms whereby the regulation of calcium homeostasis is important to maintain tissue function. The rapidly beating mouse heart is probably the most challenging tissue for the use of GECIs. In explants of sinoatrial node (SAN), the pacemaker region of the adult heart, TN-XXL was able to follow calcium signals even on a single cell basis. Motion artifacts deriving from the fast beating SAN were cancelled out due to the ratiometric readout of TN-XXL which simplified and assured correct signal detection and sustained robust data analysis. Furthermore, TN-XXL allowed tracing of calcium signals of fast beating cells in SAN explants whereby signals of up to 240 bpm beating frequency were readily reported. The transgenic expression further permitted chronic imaging of cells in the SAN preparation over three consecutive days.

The successful signal evaluation in SAN explants underlined the stable and reliable signal detection of TN-XXL even in tissues with fast calcium dynamics and a high degree of motion artifacts and favored chronic imaging due to the advantages of transgenic long-term expression. This striking example reveals possibilities of this mouse line to investigate calcium dynamics on chronic basis in other clinically relevant tissues such as kidney or liver. Ongoing advances in fiber-optics and endoscopic imaging techniques could further extrapolate the use of such a mouse line for the study of calcium homeostasis and disease related dysregulations in a variety of visceral organs *in vivo*.

5.4.4. Effects of TN-XXL Expression on Gene Regulation and Animal Behavior

The effects of long-term expression of GECIs on host cells and organism have been a platform for discussion over a long period of time. Regardless, most efforts to improve GECIs were motivated by optimizing signal intensity, kinetics or dynamic range; the effects of chronic GECI expression usually remained disregarded and have not been studied in detail, yet. Analyzing the effects of TN-XXL expression on cellular level by investigating genomic transcription levels and on global level by studying animal behavior was necessary to establish a benchmark of TN-XXL biocompatibility.

Investigating transcriptional effects of TN-XXL expression was important for two reasons. Firstly, global and long-term expression of TN-XXL could exhibit effects on the level of calcium homeostasis since cellular calcium buffering may be affected by the GECI's calcium binding domain. This additional calcium buffering could elicit changes in the intrinsic mechanisms regulating genes coding for endogenous proteins that are involved in the modulation of calcium homeostasis. Secondly, during the formation of the FP fluorophore reactive oxygen species (ROS) are produced (Tsien, 1998) which can induce oxidative stress in cells. Hence both effects, the modulation of calcium buffering on the one hand and mechanisms coping against oxidative stress on the other should be detectable on the transcriptional level of genes which are involved in calcium homeostasis and oxidative stress prevention.

The genome wide investigation of transcription levels of mRNAs with microarrays of tissues from muscle, cardiac tissue and from the hippocampal region of the brain which exhibited the highest expression level of TN-XXL resulted in a vast number of differently regulated genes. However, the majority of mRNA transcripts of genes analyzed exhibited only a mild up- or down-regulation which was considered insignificant (cut-off value >2-fold). Despite the high TN-XXL expression level in the brain, no genes were observed that exhibited a significantly up-/down-regulation. A reason for that might be that cerebral cells are unaffected by TN-XXL expression. However, TN-XXL forfeits some of its advantages in muscle tissue where the calcium binding domain TnC is derived from. Therefore, the main focus was drawn on the analysis of genes which showed significant up-or down-regulation in both, skeletal muscle and heart. Looking at transcription levels 9 genes were found showing an up-regulation and 8 a down-regulation in both, muscle and heart tissue. Interestingly, the transcriptional changes of the listed genes do not imply to be evidently TN-XXL expression related since none of them is directly involved in calcium regulation or cellular stress prevention. Therefore, these genes were considered physiologically

DISCUSSION

irrelevant. The only exception is metallothionein-2 which showed an up-regulation of 8.2 and 2.7-fold in muscle and heart tissue, respectively. Metallothionein-2 is a zinc- and copper-binding protein that further is suggested to play a role in oxidative stress prevention by scavenging ROS, but its detailed physiological role is unknown. Although it is conceivable that the up-regulation is related to ROS generated during FP fluorophore formation. The protection against oxidative stress typically is maintained by antioxidants such as peroxidases, catalases or superoxide dismutases (Han et al., 2008; Stadtman, 2001) but no significant up-regulation of antioxidant genes was detected. A recent study, however, showed that exceptionally high expression of YFP, which is found in neurons of a *Thy1.2*-YFP reporter mouse line, provoked a significant up-regulation in more than 40 genes involved in cellular stress prevention, inflammation and apoptosis (Comley et al., 2011). Therefore, the long-term expression of TN-XXL in this mouse line appears to be well accepted.

Foregoing observations regarding animals' daily routine did not reveal any obvious effects of TN-XXL expression since the animals exhibited a normal life span, fertility, or mating behavior and showed regular litter and body sizes. Therefore, a detailed study of TN-XXL effects on animal behavior was performed in collaboration with Carsten Wotjak and Vincenzo Micale from the Max-Planck-Institute of Psychiatry. Tests covering motor behavior, locomotion and motor learning were selected due to the high TN-XXL expression in muscle and cerebral tissues. Furthermore, the animal behavior regarding anxiety and neuropsychiatric disorders was analyzed. No evidence for expressional effects of TN-XXL could be determined in tests regarding motor behavior, locomotion and motor learning which were covered by the 'hole board' and the 'rotarod' tasks. However, in behavioral experiments covering anxiety related neuropsychiatric disorders such as 'elevated plus maze', 'fear conditioning' and 'social interaction' a less anxious phenotype became apparent in TN-XXL mice. Furthermore, the faster fear relieve of TN-XXL mice explored in the 'fear conditioning' task indicates that these animals perform better in developing coping strategies to handle stressful situation. A similar phenotype was found in a recent study observing calcium-mediated plasticity changes in the thalamus-amygdala pathway whereby blocking of L-type voltage-gated calcium channels impaired the acquisition of conditioned fear (Langwieser et al., 2010). In this regard one can speculate that the less anxious phenotype is a consequence of buffering effects of TN-XXL interfering with calcium homeostasis which were not covered by transcriptional profiling investigations. The general observations of the animals' daily routine and the detailed behavioral analysis highlighted that TN-XXL does not exhibit a negative effect to the animals. The unaffected motor behavior and the reduced anxiety and better handling of stressful situations moreover tempt to

DISCUSSION

speculate even beneficial effects of TN-XXL expression. These effects, however, can also be due to positional effects of transgene integration which have to be taken into account.

To briefly summarize, ubiquitous TN-XXL expression exhibited only minor effects on the transcriptional and behavioral level which underlines the biocompatibility of TN-XXL and viability of this mouse model which again emphasizes the biocompatibility in contrast to calmodulin-based sensor studies.

5.5. Conclusion

This study shows a solid foundation for the characterization of viable and functional mouse lines expressing the GECI TN-XXL on different transgenic backgrounds. The expression of TN-XXL under the *Thy1.2* promoter enabled chronic *in vivo* imaging of sensory evoked calcium transients in the visual cortex despite predominant expression in deeper cortical layers. Using the palette of applicable promoters one could guide transgene expression to further desired regions.

The main focus of this work was a detailed global analysis of function and biocompatibility of long-term ubiquitous TN-XXL expression in the *β -actin* mouse line, which to this extent has not been previously performed. This study establishes a fundamental experimental platform by which future transgenic mice expressing GECIs can be tested. Moreover, this work not only assesses the current features of TN-XXL expression and functionality but also displays important discoveries of effects that GECI expression exhibit on physiological systems. TN-XXL function was confirmed in various cultured cell types and in tissues explants of the developing and adult heart. Additionally, no defects or impairments of cellular function or morphology were identified in the examined TN-XXL expressing tissues and only minor effects were detectable in investigations on transcriptional and behavioral levels. Considering these minor effects the further optimization of TN-XXL, especially the calcium binding domain, must endeavor to assess the biocompatibility aspects of GECI expression at the earliest possible opportunity. A reduction of the calcium buffering capacity of GECIs by lowering the number of EF-hands of the sensor's calcium binding domain is an approach that our group is currently undertaking. Furthermore, the implementation of new brighter FP variants such as mCerulean 3 (Markwardt et al., 2011) or mTurquoise (Goedhart et al., 2010) to substitute ECFP as a donor fluorophore, will enable imaging with lower intensities to reduce photo-toxic effects and lowering expression levels without losing imaging quality.

As a promising tool for further investigations this 'ready-to-image' mouse could pioneer new applications in research by the facilitated harvesting and handling of cells for pharmaceutical drug screenings and the usage of motion retaining tissues for chronic calcium imaging approaches supported by the ratiometric TN-XXL imaging readout. Moreover, the crossing of the TN-XXL mouse line with available disease models can open a significant avenue of *in vitro* and *in vivo* research for the investigation of diseases exhibiting aberrant calcium functions.

Appendix

Behavioral Experiments of β -actin TN-XXL Mice

To investigate a phenotype of *β -actin* TN-XXL mice assessed by several behavioral task regarding motor behavior, emotionality and depression-related behavior a collaboration was established with Carsten Wotjak and Vincenzo Micale from the Max-Planck-Institute of Psychiatry who planned and performed all behavioral experiments. Homozygous transgenic *β -actin* TN-XXL (TG) mice and wild-type (WT) control litter mates (n = 12-15 per group) were transported to their new facility at the MPI of Psychiatry and were allowed to acclimatize to the new environment. Animals were singularly housed with food and water *ad libidum* under an inverse 12 hour light/dark cycle to enable performing the experimental tasks during the activity phase of the mice between 9:30 a.m. and 5 p.m. All behavioral experiments were carried out by Vincenzo Micale.

Hole Board Task

To assess general motor activity, TG and WT mice were tested in an hole-board (40×40cm) contained 16 equidistant holes (5.5 cm apart, 2.5cm diameter, 3 cm depth) placed in the central zone of the apparatus equipped with infrared beams (TrueScan; Coulbourn Instruments, Allentown, PA) at 300 lux for 30 min. Three infrared sensor rings (sensor spacing, 1.52 cm) around the boxes allowed the measurement of horizontal and vertical (up or down) activity. All sensor rings were connected via interface to a computer equipped with TruScan Software Version 99 (Coulbourn Instruments). Boxes and sensor rings were surrounded by an additional box made of opaque Plexiglas side walls (47 x 47 x 38 cm) without roof and floor. Horizontal locomotion (total distance moved), vertical movements (exploratory rearing), and time spent at rest, frequency of head dipping (the mouse introduced its nose in a hole) were analyzed during the 30 min monitoring period. After each session, the apparatus was cleaned with a solution containing neutral soap.

Rotarod Test

The rotarod test, using an accelerating rotarod, was performed by placing mice on rotating drums (3 cm diameter), which is accelerated from 4 to 20 rpm over the course of 5 min. The time at which each animal fell from the drum was recorded automatically when it contacted a plate which stopped the timer. Each animal received three consecutive trials for three consecutive days. Data of the three trials per day were averaged to obtain a single score.

Elevated Plus Maze (EPM)

The apparatus consisted of two opposite open arms, (30 x 5 cm) and two arms with walls (30 x 5 x 14 cm) that were attached to a central platform (5 x 5 cm) to form a cross. The maze was elevated 50 cm from the floor (Pellow et al., 1985). Illumination measured at the center of the maze was 300 lux. The animal was placed at the center of the maze with its nose in the direction of one of the closed arms, and observed for 5 min, according to the following parameters: number of entries in the open and closed arms, and time of permanence in each of them (i.e., the time spent by the animal in the open and closed arms). An entry was defined as all four paws having crossed the line between an arm and the central area. It is accepted that the anxiolytic effect of a drug treatment is illustrated by increased parameters in open arms (time and/or number of entries). The augmented percentage of entries in open arms over the total number of entries in both arms is a good indicator of anxiolytic-like behavior as well, although entries in closed arms and total entries reflect the motor component of the exploratory activity. On removal of each mouse, the maze floor was carefully wiped with a wet towel. The behavior of all animals was recorded on a tape using a video-camera and then scored in monitor display by an experienced observer by means of a video/computer system.

Tail Suspension Test

Mice were individually suspended by the tail from a metal rod (35 cm above the floor) using adhesive tape. Mice demonstrated several escape-oriented behaviors interspersed with temporally increasing bouts of immobility. The duration of immobility was recorded during the last 4-min of the 6-min testing period, after a 2-min habituation period from videotapes.

Fear Conditioning Test

The setup has been described and displayed in detail before (Kamprath and Wotjak, 2004). Briefly, the experiments were performed in two contexts: (1) the neutral test context which was cylindrically shaped and made of transparent Plexiglas with wood shavings as bedding and (2) the shock context was a cubic-shaped box with a metal grid for shock application. All two contexts were cleaned thoroughly after each trial with differently smelling detergents, and bedding was changed. For conditioning (d0), mice were placed into the shock chamber. After 180 s a tone was presented (9kHz, 80dB, 20s) which co-terminated with a single scrambled electric foot shock (2 s, 0.7 mA). Animals remained in the shock chamber for another 60s before they were returned to their home cages. On day 1 and day 2 after conditioning, mice were exposed either to the tone (200s) in the neutral test context (d1) or to the conditioning context (180s). The behavioral performance was videotaped by small CCD cameras (Conrad Electronics, Hirschau, Germany). Animals' behavior was rated off-line by a trained observer who was blind to the experimental condition (EVENTLOG, Robert Henderson, 1986). Freezing behavior was defined as immobility except for respiration movements and served as a measure of fear memory.

Social Interaction Test

Experiments were performed in a novel environment (new cage) at 300 lux that was placed into a soundproof isolation cubicle. The lid of the new cage was removed and the walls elongated by 12.5 cm of semi-transparent plastic. Pairs of unfamiliar mice (n=7 pairs of TG or WT) were placed into the cage per 5 min. The time spent in social interaction (active contact such as sniffing, licking, close following, grooming) was recorded for each pair of mice.

Startle Response

To test for hyper arousal, acoustic startle responses were measured in the following way: mice were placed into one out of seven identical startle set-ups, consisting of a non-restrictive Plexiglas cylinder (inner diameter 4 cm, length 8 cm) mounted onto a plastic platform, each housed in a sound attenuated chamber (SRLAB, San Diego Instruments SDI, San Diego, CA, USA). The cylinder movement was detected by a piezoelectric element

mounted under each platform and the voltage output of the piezo was amplified and then digitized (sampling rate 1 kHz) by a computer interface (I/O-board provided by SDI). The startle amplitude was defined as the peak voltage output within the first 50 ms after stimulus onset and quantified by means of SRLAB software. Before startle measurements, we calibrated response sensitivities for each chamber in order to assure identical output levels. Startle stimuli and background noise were delivered through a high-frequency speaker placed 20 cm above each cage. The 3 different startle stimuli consisted of white noise bursts of 20 ms duration and 75, 90, 105 and 115 dB(A), respectively, and were presented in a constant background noise of 50 dB(A) provided by the fan. Noise intensity was measured using an audiometer (Radio Shack, 33-2055, RadioShack, Fort Worth, TX, USA). On control trials only background noise was present. After an acclimation period of 5 min duration, 10 control trials and 20 startle stimuli of each intensity were presented in pseudorandom order in each test session. The interstimulus interval was 15 s averaged (13-17 s, pseudo randomized). The startle set-ups were localized in a different building and startle measurements were performed by a scientist unfamiliar to the animals in order to avoid context reminders, thus minimizing confounding influences by context generalization. Plexiglas cylinders were cleaned thoroughly soap water after each trial.

References

- An, R. H., Davies, M. P., Doevendans, P. A., Kubalak, S. W., Bangalore, R., Chien, K. R., and Kass, R. S. (1996). Developmental changes in beta-adrenergic modulation of L-type Ca²⁺ channels in embryonic mouse heart. *Circ. Res* 78, 371-378.
- Andermann, M. L., Kerlin, A. M., and Reid, R. C. (2010). Chronic cellular imaging of mouse visual cortex during operant behavior and passive viewing. *Front. Cell. Neurosci.* 4, 3.
- Axelrod, D., Koppel, D. E., Schlessinger, J., Elson, E., and Webb, W. W. (1976). Mobility measurement by analysis of fluorescence photobleaching recovery kinetics. *Biophys J* 16, 1055-1069.
- Baird, G. S., Zacharias, D. A., and Tsien, R. Y. (1999). Circular permutation and receptor insertion within green fluorescent proteins. *Proc Natl Acad Sci U S A* 96, 11241-6.
- Berridge, M. J., Bootman, M. D., and Roderick, H. L. (2003). Calcium signalling: dynamics, homeostasis and remodelling. *Nat Rev Mol Cell Biol* 4, 517-529.
- Berridge, M. J., Lipp, P., and Bootman, M. D. (2000). The versatility and universality of calcium signalling. *Nat Rev Mol Cell Biol* 1, 11-21.
- Cancela, J. M., Churchill, G. C., and Galione, A. (1999). Coordination of agonist-induced Ca²⁺-signalling patterns by NAADP in pancreatic acinar cells. *Nature* 398, 74-76.
- Caroni, P. (1997). Overexpression of growth-associated proteins in the neurons of adult transgenic mice. *Journal of Neuroscience Methods* 71, 3-9.
- Chalfie, M., Tu, Y., Euskirchen, G., Ward, W. W., and Prasher, D. C. (1994). Green fluorescent protein as a marker for gene expression. *Science* 263, 802-805.
- Charpak, S., Mertz, J., Beaupaire, E., Moreaux, L., and Delaney, K. (2001). Odor-evoked calcium signals in dendrites of rat mitral cells. *Proceedings of the National Academy of Sciences* 98, 1230 -1234.
- Chueh, S. H., and Gill, D. L. (1986). Inositol 1,4,5-trisphosphate and guanine nucleotides activate calcium release from endoplasmic reticulum via distinct mechanisms. *Journal of Biological Chemistry* 261, 13883 -13886.
- Colomer, J. M., Terasawa, M., and Means, A. R. (2004). Targeted Expression of Calmodulin Increases Ventricular Cardiomyocyte Proliferation and Deoxyribonucleic Acid Synthesis during Mouse Development. *Endocrinology* 145, 1356-1366.
- Comley, L. H., Wishart, T. M., Baxter, B., Murray, L. M., Nimmo, A., Thomson, D., Parson, S. H., and Gillingwater, T. H. (2011). Induction of Cell Stress in Neurons from Transgenic Mice Expressing Yellow Fluorescent Protein: Implications for Neurodegeneration Research. *PLoS ONE* 6, e17639.

REFERENCES

- Cormack, B. P., Valdivia, R. H., and Falkow, S. (1996). FACS-optimized mutants of the green fluorescent protein (GFP). *Gene* 173, 33-38.
- Cramer, A., Whitehorn, E. A., Tate, E., and Stemmer, W. P. (1996). Improved green fluorescent protein by molecular evolution using DNA shuffling. *Nat. Biotechnol* 14, 315-319.
- Cubitt, A. B., Heim, R., Adams, S. R., Boyd, A. E., Gross, L. A., and Tsien, R. Y. (1995). Understanding, improving and using green fluorescent proteins. *Trends in Biochemical Sciences* 20, 448-455.
- Danzi, S., and Klein, I. (2004). Thyroid hormone and the cardiovascular system. *Minerva Endocrinol* 29, 139-150.
- Denk, W., Strickler, J. H., and Webb, W. W. (1990). Two-photon laser scanning fluorescence microscopy. *Science* 248, 73-76.
- DiFranco, M., Novo, D., and Vergara, J. (2002). Characterization of the calcium release domains during excitation-contraction coupling in skeletal muscle fibres. *Pflügers Archiv European Journal of Physiology* 443, 508-519.
- Dillmann, W. H. (2002). Cellular action of thyroid hormone on the heart. *Thyroid* 12, 447-452.
- Dimitrov, D., He, Y., Mutoh, H., Baker, B. J., Cohen, L., Akemann, W., and Knöpfel, T. (2007). Engineering and Characterization of an Enhanced Fluorescent Protein Voltage Sensor. *PLoS ONE* 2, e440.
- Dobrzynski, H., Boyett, M. R., and Anderson, R. H. (2007). New Insights Into Pacemaker Activity. *Circulation* 115, 1921 -1932.
- Dombeck, D. A., Khabbaz, A. N., Collman, F., Adelman, T. L., and Tank, D. W. (2007). Imaging large scale neural activity with cellular resolution in awake mobile mice. *Neuron* 56, 43-57.
- Eftink, M. R., and Ghiron, C. A. (1981). Fluorescence quenching studies with proteins. *Analytical Biochemistry* 114, 199-227.
- Fan, J.-S., and Palade, P. (1999). One calcium ion may suffice to open the tetrameric cardiac ryanodine receptor in rat ventricular myocytes. *The Journal of Physiology* 516, 769 - 780.
- Feng, G., Mellor, R. H., Bernstein, M., Keller-Peck, C., Nguyen, Q. T., Wallace, M., Nerbonne, J. M., Lichtman, J. W., and Sanes, J. R. (2000). Imaging Neuronal Subsets in Transgenic Mice Expressing Multiple Spectral Variants of GFP. *Neuron* 28, 41-51.
- Forster, T. (1946). Energiewanderung und Fluoreszenz. *Die Naturwissenschaften* 33, 166-175.

REFERENCES

- Frenkel, M. Y., and Bear, M. F. (2004). How monocular deprivation shifts ocular dominance in visual cortex of young mice. *Neuron* 44, 917-923.
- Friedrich, M. W., Aramuni, G., Mank, M., Mackinnon, J. A. G., and Griesbeck, O. (2010). Imaging CREB activation in living cells. *J. Biol. Chem.* 285, 23285-23295.
- Garrick, D., Fiering, S., Martin, D. I. K., and Whitelaw, E. (1998). Repeat-induced gene silencing in mammals. *Nat Genet* 18, 56-59.
- Gaspers, L. D., and Thomas, A. P. (2005). Calcium signaling in liver. *Cell Calcium* 38, 329-342.
- Glukhov, A. V., Fedorov, V. V., Anderson, M. E., Mohler, P. J., and Efimov, I. R. (2010). Functional anatomy of the murine sinus node: high-resolution optical mapping of ankyrin-B heterozygous mice. *American Journal of Physiology - Heart and Circulatory Physiology* 299, H482 -H491.
- Goedhart, J., van Weeren, L., Hink, M. A., Vischer, N. O. E., Jalink, K., and Gadella, T. W. J. (2010). Bright cyan fluorescent protein variants identified by fluorescence lifetime screening. *Nat Meth* 7, 137-139.
- Gommans, I. M. P., Vlak, M. H. M., de Haan, A., and van Engelen, B. G. M. (2002). Calcium regulation and muscle disease. *J. Muscle Res. Cell. Motil.* 23, 59-63.
- Griesbeck, O., Baird, G. S., Campbell, R. E., Zacharias, D. A., and Tsien, R. Y. (2001). Reducing the environmental sensitivity of yellow fluorescent protein. Mechanism and applications. *J Biol Chem* 276, 29188-94.
- Han, E.-S., Muller, F. L., Pérez, V. I., Qi, W., Liang, H., Xi, L., Fu, C., Doyle, E., Hickey, M., Cornell, J., et al. (2008). The in vivo gene expression signature of oxidative stress. *Physiological Genomics* 34, 112 -126.
- Hara, M., Bindokas, V., Lopez, J. P., Kaihara, K., Landa, L. R., Harbeck, M., and Roe, M. W. (2004). Imaging endoplasmic reticulum calcium with a fluorescent biosensor in transgenic mice. *American Journal of Physiology - Cell Physiology* 287, C932 -C938.
- Hasan, M. T., Friedrich, R. W., Euler, T., Larkum, M. E., Giese, G., Both, M., Duebel, J., Waters, J., Bujard, H., Griesbeck, O., et al. (2004). Functional Fluorescent Ca²⁺ Indicator Proteins in Transgenic Mice under TET Control. *PLoS Biology* 2, e163 EP -.
- Hasenfuss, G., Mulieri, L., Leavitt, B., Allen, P., Haeberle, J., and Alpert, N. (1992). Alteration of contractile function and excitation-contraction coupling in dilated cardiomyopathy. *Circulation Research* 70, 1225 -1232.
- Heim, N., and Griesbeck, O. (2004). Genetically Encoded Indicators of Cellular Calcium Dynamics Based on Troponin C and Green Fluorescent Protein. *Journal of Biological Chemistry* 279, 14280 -14286.

REFERENCES

- Heim, N., Garaschuk, O., Friedrich, M. W., Mank, M., Milos, R. I., Kovalchuk, Y., Konnerth, A., and Griesbeck, O. (2007). Improved calcium imaging in transgenic mice expressing a troponin C-based biosensor. *Nat Meth* 4, 127-129.
- Heim, R., Prasher, D. C., and Tsien, R. Y. (1994). Wavelength mutations and posttranslational autoxidation of green fluorescent protein. Available at: <http://www.pnas.org/content/91/26/12501> [Accessed August 25, 2008].
- Helmchen, F. (2011). Calibration of fluorescent calcium indicators. *Cold Spring Harb Protoc* 2011, 923-930.
- Helmchen, F., Fee, M. S., Tank, D. W., and Denk, W. (2001). A Miniature Head-Mounted Two-Photon Microscope: High-Resolution Brain Imaging in Freely Moving Animals. *Neuron* 31, 903-912.
- Hink, M. A., Visser, N. V., Borst, J. W., Hoek, A. V., and Visser, A. J. W. G. (2003). Practical Use of Corrected Fluorescence Excitation and Emission Spectra of Fluorescent Proteins in Förster Resonance Energy Transfer (FRET) Studies. *Journal of Fluorescence* 13, 1-4.
- Hires, S. A., Zhu, Y., and Tsien, R. Y. (2008). Optical measurement of synaptic glutamate spillover and reuptake by linker optimized glutamate-sensitive fluorescent reporters. Available at: <http://www.pnas.org/content/105/11/4411.full> [Accessed October 18, 2008].
- Hlavaty, J., Schittmayer, M., Stracke, A., Jandl, G., Knapp, E., Felber, B. K., Salmons, B., Günzburg, W. H., and Renner, M. (2005). Effect of posttranscriptional regulatory elements on transgene expression and virus production in the context of retrovirus vectors. *Virology* 341, 1-11.
- Hofer, S. B., Ko, H., Pichler, B., Vogelstein, J., Ros, H., Zeng, H., Lein, E., Lesica, N. A., and Mrsic-Flogel, T. D. (2011). Differential connectivity and response dynamics of excitatory and inhibitory neurons in visual cortex. *Nat Neurosci* 14, 1045-1052.
- Hogenesch, J. B., Gu, Y.-Z., Jain, S., and Bradfield, C. A. (1998). The basic-helix-loop-helix-PAS orphan MOP3 forms transcriptionally active complexes with circadian and hypoxia factors. *Proceedings of the National Academy of Sciences* 95, 5474 -5479.
- Houtsmuller, A. B. (2005). Fluorescence recovery after photobleaching: application to nuclear proteins. *Adv. Biochem. Eng. Biotechnol* 95, 177-199.
- Huang, W.-Y., Aramburu, J., Douglas, P. S., and Izumo, S. (2000). Transgenic expression of green fluorescence protein can cause dilated cardiomyopathy. *Nat Med* 6, 482-483.
- Hübener, M. (2003). Mouse visual cortex. *Current Opinion in Neurobiology* 13, 413-420.
- Inoue, H., Nojima, H., and Okayama, H. (1990). High efficiency transformation of *Escherichia coli* with plasmids. *Gene* 96, 23-28.

REFERENCES

- Iordanidou, A., Hadzopoulou-Cladaras, M., and Lazou, A. (2010). Non-genomic effects of thyroid hormone in adult cardiac myocytes: relevance to gene expression and cell growth. *Mol Cell Biochem* 340, 291-300.
- Irizarry, R. A., Bolstad, B. M., Collin, F., Cope, L. M., Hobbs, B., and Speed, T. P. (2003). Summaries of Affymetrix GeneChip probe level data. *Nucleic Acids Research* 31, e15.
- Jasin, M., Moynahan, M. E., and Richardson, C. (1996). Targeted transgenesis. *Proceedings of the National Academy of Sciences* 93, 8804 -8808.
- Kamprath, K., and Wotjak, C. T. (2004). Nonassociative learning processes determine expression and extinction of conditioned fear in mice. *Learn. Mem.* 11, 770-786.
- Kapoor, V., and Urban, N. N. (2006). Glomerulus-Specific, Long-Latency Activity in the Olfactory Bulb Granule Cell Network. *The Journal of Neuroscience* 26, 11709 -11719.
- Kumari, M. V., Hiramatsu, M., and Ebadi, M. (1998). Free radical scavenging actions of metallothionein isoforms I and II. *Free Radic. Res* 29, 93-101.
- Langwieser, N., Christel, C. J., Kleppisch, T., Hofmann, F., Wotjak, C. T., and Moosmang, S. (2010). Homeostatic Switch in Hebbian Plasticity and Fear Learning after Sustained Loss of Cav1.2 Calcium Channels. *The Journal of Neuroscience* 30, 8367 -8375.
- Lansley, A. B., and Sanderson, M. J. (1999). Regulation of airway ciliary activity by Ca²⁺: simultaneous measurement of beat frequency and intracellular Ca²⁺. *Biophys. J.* 77, 629-638.
- Levene, M. J., Dombeck, D. A., Kasischke, K. A., Molloy, R. P., and Webb, W. W. (2004). In Vivo Multiphoton Microscopy of Deep Brain Tissue. *Journal of Neurophysiology* 91, 1908 -1912.
- Limbäck-Stokin, K., Korzus, E., Nagaoka-Yasuda, R., and Mayford, M. (2004). Nuclear Calcium/Calmodulin Regulates Memory Consolidation. *The Journal of Neuroscience* 24, 10858 -10867.
- Liu, B.-hua, Li, P., Li, Y.-tang, Sun, Y. J., Yanagawa, Y., Obata, K., Zhang, L. I., and Tao, H. W. (2009). Visual Receptive Field Structure of Cortical Inhibitory Neurons Revealed by Two-Photon Imaging Guided Recording. *The Journal of Neuroscience* 29, 10520 -10532.
- Liu, J., Dobrzynski, H., Yanni, J., Boyett, M. R., and Lei, M. (2007). Organisation of the mouse sinoatrial node: structure and expression of HCN channels. *Cardiovascular Research* 73, 729 -738.
- Lytton, J., Westlin, M., Burk, S. E., Shull, G. E., and MacLennan, D. H. (1992). Functional comparisons between isoforms of the sarcoplasmic or endoplasmic reticulum family of calcium pumps. *Journal of Biological Chemistry* 267, 14483 -14489.

REFERENCES

- Mank, M., Reiff, D. F., Heim, N., Friedrich, M. W., Borst, A., and Griesbeck, O. (2006). A FRET-Based Calcium Biosensor with Fast Signal Kinetics and High Fluorescence Change. *Biophys. J.* *90*, 1790-1796.
- Mank, M., Santos, A. F., Drenth, S., Mrcic-Flogel, T. D., Hofer, S. B., Stein, V., Hendel, T., Reiff, D. F., Levelt, C., Borst, A., et al. (2008). A genetically encoded calcium indicator for chronic in vivo two-photon imaging. *Nat Meth advanced online publication*. Available at: <http://dx.doi.org/10.1038/nmeth.1243> [Accessed August 12, 2008].
- Markwardt, M. L., Kremers, G.-J., Kraft, C. A., Ray, K., Cranfill, P. J. C., Wilson, K. A., Day, R. N., Wachter, R. M., Davidson, M. W., and Rizzo, M. A. (2011). An Improved Cerulean Fluorescent Protein with Enhanced Brightness and Reduced Reversible Photoswitching. *PLoS ONE* *6*, e17896.
- McCombs, J. E., and Palmer, A. E. (2008). Measuring calcium dynamics in living cells with genetically encodable calcium indicators. *Methods* *46*, 152-159.
- Mitsui, S., Saito, M., Mori, K., and Yoshihara, Y. (2007). A Transcriptional Enhancer That Directs Telencephalon-Specific Transgene Expression in Mouse Brain. *Cerebral Cortex* *17*, 522 -530.
- Mittmann, W., Wallace, D. J., Czubayko, U., Herb, J. T., Schaefer, A. T., Looger, L. L., Denk, W., and Kerr, J. N. D. (2011). Two-photon calcium imaging of evoked activity from L5 somatosensory neurons in vivo. *Nat Neurosci* *14*, 1089-1093.
- Monfredi, O., Dobrzynski, H., Mondal, T., Boyett, M. R., and Morris, G. M. (2010). The Anatomy and Physiology of the Sinoatrial Node-A Contemporary Review. *Pacing and Clinical Electrophysiology* *33*, 1392-1406.
- Mrcic-Flogel, T. D., Hofer, S. B., Ohki, K., Reid, R. C., Bonhoeffer, T., and Hübener, M. (2007). Homeostatic regulation of eye-specific responses in visual cortex during ocular dominance plasticity. *Neuron* *54*, 961-972.
- Mullis, K., Faloona, F., Scharf, S., Saiki, R., Horn, G., and Erlich, H. (1986). Specific enzymatic amplification of DNA in vitro: the polymerase chain reaction. *Cold Spring Harb. Symp. Quant. Biol.* *51 Pt 1*, 263-273.
- Murayama, M., Perez-Garci, E., Luscher, H.-R., and Larkum, M. E. (2007). Fiberoptic System for Recording Dendritic Calcium Signals in Layer 5 Neocortical Pyramidal Cells in Freely Moving Rats. *J Neurophysiol* *98*, 1791-1805.
- Nagai, T., Ibata, K., Park, E. S., Kubota, M., Mikoshiba, K., and Miyawaki, A. (2002). A variant of yellow fluorescent protein with fast and efficient maturation for cell-biological applications. *Nat Biotech* *20*, 87-90.
- Nagai, T., Sawano, A., Park, E. S., and Miyawaki, A. (2001). Circularly permuted green fluorescent proteins engineered to sense Ca²⁺. *Proceedings of the National Academy of Sciences of the United States of America* *98*, 3197-3202.

REFERENCES

- Nagai, T., Yamada, S., Tominaga, T., Ichikawa, M., and Miyawaki, A. (2004). Expanded dynamic range of fluorescent indicators for Ca²⁺ by circularly permuted yellow fluorescent proteins. *Proceedings of the National Academy of Sciences of the United States of America* *101*, 10554 -10559.
- Nagayama, S., Zeng, S., Xiong, W., Fletcher, M. L., Masurkar, A. V., Davis, D. J., Pieribone, V. A., and Chen, W. R. (2007). In vivo simultaneous tracing and Ca(2+) imaging of local neuronal circuits. *Neuron* *53*, 789-803.
- Nagy, A., Gertsenstein, M., Vintersten, K., and Behringer, R. (2003). Production of transgenic mice. In *Manipulating the Mouse Embryo: A Laboratory Manual* (Cold Spring Harbor: CSHL Press).
- Nakai, J., Ohkura, M., and Imoto, K. (2001). A high signal-to-noise Ca²⁺ probe composed of a single green fluorescent protein. *Nat Biotech* *19*, 137-141.
- Newman, E. A. (2001). Propagation of Intercellular Calcium Waves in Retinal Astrocytes and Müller Cells. *J Neurosci* *21*, 2215-2223.
- O'Donovan, M. J. (1999). The origin of spontaneous activity in developing networks of the vertebrate nervous system. *Curr. Opin. Neurobiol.* *9*, 94-104.
- Ohki, K., Chung, S., Kara, P., Hubener, M., Bonhoeffer, T., and Reid, R. C. (2006). Highly ordered arrangement of single neurons in orientation pinwheels. *Nature* *442*, 925-928.
- Okabe, M., Ikawa, M., Kominami, K., Nakanishi, T., and Nishimune, Y. (1997). [']Green mice' as a source of ubiquitous green cells. *FEBS Letters* *407*, 313-319.
- Ormö, M., Cubitt, A. B., Kallio, K., Gross, L. A., Tsien, R. Y., and Remington, S. J. (1996). Crystal Structure of the *Aequorea victoria* Green Fluorescent Protein. *Science* *273*, 1392 - 1395.
- Osipchuk, Y., and Cahalan, M. (1992). Cell-to-cell spread of calcium signals mediated by ATP receptors in mast cells. *Nature* *359*, 241-244.
- Palmer, A. E., and Tsien, R. Y. (2006). Measuring calcium signaling using genetically targetable fluorescent indicators. *Nat. Protocols* *1*, 1057-1065.
- Pellow, S., Chopin, P., File, S. E., and Briley, M. (1985). Validation of open : closed arm entries in an elevated plus-maze as a measure of anxiety in the rat. *Journal of Neuroscience Methods* *14*, 149-167.
- Piston, D. W., and Kremers, G.-J. (2007). Fluorescent protein FRET: the good, the bad and the ugly. *Trends in Biochemical Sciences* *32*, 407-414.
- Prasher, D. C., Eckenrode, V. K., Ward, W. W., Prendergast, F. G., and Cormier, M. J. (1992). Primary structure of the *Aequorea victoria* green-fluorescent protein. *Gene* *111*, 229-233.

REFERENCES

- Preitner, N., Damiola, F., Luis-Lopez-Molina, Zakany, J., Duboule, D., Albrecht, U., and Schibler, U. (2002). The Orphan Nuclear Receptor REV-ERB α Controls Circadian Transcription within the Positive Limb of the Mammalian Circadian Oscillator. *Cell* *110*, 251-260.
- Rizzo, M. A., Springer, G. H., Granada, B., and Piston, D. W. (2004). An improved cyan fluorescent protein variant useful for FRET. *Nat Biotech* *22*, 445-449.
- Russell, J. T. (2011). Imaging calcium signals in vivo: a powerful tool in physiology and pharmacology. *British Journal of Pharmacology* *163*, 1605-1625.
- Sakamoto, K., and Ishida, N. (2000). Light-induced phase-shifts in the circadian expression rhythm of mammalian Period genes in the mouse heart. *European Journal of Neuroscience* *12*, 4003-4006.
- Sambrook, J., and Russell, D. (2001a). Gel electrophoresis of DNA and pulsed-field agarose gelelectrophoresis. In *Molecular Cloning: A Laboratory Manual* (Cold Spring Harbor: CSHL Press), pp. 5.1-5.58.
- Sambrook, J., and Russell, D. (2001b). Preparation and analysis of eukaryotic genomic DNA. In *Molecular Cloning: A Laboratory Manual* (Cold Spring Harbor: CSHL Press), pp. 6.1- 6.64.
- Shaner, N. C., Campbell, R. E., Steinbach, P. A., Giepmans, B. N. G., Palmer, A. E., and Tsien, R. Y. (2004). Improved monomeric red, orange and yellow fluorescent proteins derived from *Discosoma* sp. red fluorescent protein. *Nat Biotech* *22*, 1567-1572.
- Shimomura, O., Johnson, F. H., and Saiga, Y. (1962). Extraction, purification and properties of aequorin, a bioluminescent protein from the luminous hydromedusan, *Aequorea*. *J Cell Comp Physiol* *59*, 223-239.
- Song, L., Hennink, E. J., Young, I. T., and Tanke, H. J. (1995). Photobleaching kinetics of fluorescein in quantitative fluorescence microscopy. *Biophys J* *68*, 2588-2600.
- Stadtman, E. R. (2001). Protein Oxidation in Aging and Age-Related Diseases. *Annals of the New York Academy of Sciences* *928*, 22-38.
- Stieber, J., Herrmann, S., Feil, S., Löster, J., Feil, R., Biel, M., Hofmann, F., and Ludwig, A. (2003). The hyperpolarization-activated channel HCN4 is required for the generation of pacemaker action potentials in the embryonic heart. *Proceedings of the National Academy of Sciences of the United States of America* *100*, 15235-15240.
- Stosiek, C., Garaschuk, O., Holthoff, K., and Konnerth, A. (2003). In vivo two-photon calcium imaging of neuronal networks. *Proceedings of the National Academy of Sciences* *100*, 7319 -7324.
- Stryer, L. (1978). Fluorescence Energy Transfer as a Spectroscopic Ruler. *Annual Review of Biochemistry* *47*, 819-846.

REFERENCES

- Sugino, H., Yoshihara, Y., Copeland, N. G., Gilbert, D. J., Jenkins, N. A., and Mori, K. (1997). Genomic organization and chromosomal localization of the mouse telencephalin gene, a neuronal member of the ICAM family. *Genomics* 43, 209-215.
- Sullivan, M. R., Nimmerjahn, A., Sarkisov, D. V., Helmchen, F., and Wang, S. S.-H. (2005). In Vivo Calcium Imaging of Circuit Activity in Cerebellar Cortex. *Journal of Neurophysiology* 94, 1636 -1644.
- Svoboda, K., Helmchen, F., Denk, W., and Tank, D. W. (1999). Spread of dendritic excitation in layer 2/3 pyramidal neurons in rat barrel cortex in vivo. *Nat. Neurosci.* 2, 65-73.
- Swaminathan, R., Hoang, C. P., and Verkman, A. S. (1997). Photobleaching recovery and anisotropy decay of green fluorescent protein GFP-S65T in solution and cells: cytoplasmic viscosity probed by green fluorescent protein translational and rotational diffusion. *Biophysical Journal* 72, 1900-1907.
- Tallini, Y. N., Ohkura, M., Choi, B.-R., Ji, G., Imoto, K., Doran, R., Lee, J., Plan, P., Wilson, J., Xin, H.-B., et al. (2006). Imaging cellular signals in the heart in vivo: Cardiac expression of the high-signal Ca²⁺ indicator GCaMP2. *Proceedings of the National Academy of Sciences of the United States of America* 103, 4753-4758.
- Tian, L., Hires, S. A., Mao, T., Huber, D., Chiappe, M. E., Chalasani, S. H., Petreanu, L., Akerboom, J., McKinney, S. A., Schreier, E. R., et al. (2009). Imaging neural activity in worms, flies and mice with improved GCaMP calcium indicators. *Nat Meth advance online publication*. Available at: <http://dx.doi.org/10.1038/nmeth.1398> [Accessed November 9, 2009].
- Treves, S., Anderson, A. A., Ducreux, S., Divet, A., Bleunven, C., Grasso, C., Paesante, S., and Zorzato, F. (2005). Ryanodine receptor 1 mutations, dysregulation of calcium homeostasis and neuromuscular disorders. *Neuromuscular Disorders* 15, 577-587.
- Tripathi, K., and Parnaik, V. K. (2008). Differential dynamics of splicing factor SC35 during the cell cycle. *J. Biosci* 33, 345-354.
- Tsien, R. Y. (1981). A non-disruptive technique for loading calcium buffers and indicators into cells. *Nature* 290, 527-528.
- Tsien, R. Y. (1998). The green fluorescent protein. *Annu Rev Biochem* 67, 509-44.
- Wachter, R. M., Elsliger, M. A., Kallio, K., Hanson, G. T., and Remington, S. J. (1998). Structural basis of spectral shifts in the yellow-emission variants of green fluorescent protein. *Structure* 6, 1267-1277.
- Wallace, D. J., zum Alten Borgloh, S. M., Astori, S., Yang, Y., Bausen, M., Kugler, S., Palmer, A. E., Tsien, R. Y., Sprengel, R., Kerr, J. N. D., et al. (2008). Single-spike detection in vitro and in vivo with a genetic Ca²⁺ sensor. *Nat Meth advanced online publication*. Available at: <http://dx.doi.org/10.1038/nmeth.1242> [Accessed August 12, 2008].

REFERENCES

- Wehrens, X. H. T., Lehnart, S. E., and Marks, A. R. (2005). INTRACELLULAR CALCIUM RELEASE AND CARDIAC DISEASE. *Annual Review of Physiology* 67, 69-98.
- Werner, M., Kraunus, J., Baum, C., and Brocker, T. (2004). B-cell-specific transgene expression using a self-inactivating retroviral vector with human CD19 promoter and viral post-transcriptional regulatory element. *Gene Ther* 11, 992-1000.
- Wojda, U., Salinska, E., and Kuznicki, J. (2008). Calcium ions in neuronal degeneration. *IUBMB Life* 60, 575-590.
- Yang, F., Moss, L. G., and Phillips, G. N., Jr (1996). The molecular structure of green fluorescent protein. *Nat. Biotechnol.* 14, 1246-1251.
- Zufferey, R., Donello, J. E., Trono, D., and Hope, T. J. (1999). Woodchuck Hepatitis Virus Posttranscriptional Regulatory Element Enhances Expression of Transgenes Delivered by Retroviral Vectors. *J. Virol.* 73, 2886-2892.

Acknowledgements

First I want to thank my supervisor Oliver Griesbeck for giving me the opportunity performing this work and for his great guidance and creative input to my project(s) which were not always straight forward approaches. I further want to express my gratitude to Axel Borst who assumed office of being an outstanding 'Doktorvater' and always being supportive even in times of struggle and frustration.

Moreover I'd like to thank all se Griesbecks for sharing one of the best times I had in my life and your support and assistance regarding scientific problems and mind-blowing, hilarious conversations especially the crazy lunch-talks. Special honors go to the Kicker- aka Smicker- aka Wuzzel-Team colleagues Thomas aka 'Danish', Jonny aka 'Scottish', Anselm aka 'Oselm', and our cheerleaders Martina aka 'maRtiNA', Julia aka 'Austria' and Gayane aka 'Mother Russia' and of course thanks to Anja for keeping the lab in order and for her wonderful typically edible gifts for the chauffeur services during cold winter month. I further have to thank Birgit our 'Lab Mom' who always supported me and my work during the last years by handling, chopping and cuddling the mice, pampering the cell cultures and sharing endless hours at the confocal.

Throughout my 6 years here, climbing the ladder from a HiWi to a PhD I often cudgeled my brain in the P1 – the dungeon of creativity – hence coffee breaks were the only escape during hard times which I enjoyed in old days with Nina, Nicola, Alex, Adrian and Marco the former 'P1 coffee crew'. Later on we got offspring named Giovanni who made us all happy by providing the liquid elixir of life.

I further want to thank the entire Borst Department for creating a wonderful working atmosphere and fruitful chats about pretty much every topic one can think of. Special thanks also goes to Jones and his engineering skills helping out fixing cables, other broken stuff and taking care of his beer supply for late working hours.

Furthermore, I want to thank all my friends for great fun and parties especially in the WG 'FCH27'. Special thanks goes to Stefan and Christoph for providing the best fresh 'Gehacktes', Sandro my basketball mate and Uli, Marion, Claudia, Niggi and Osmin – to mention a few – for becoming close friends within the last years.

And of course I have to thank my 'Schatzi' Caro; I wouldn't have made it through these rough times without you; thanks a lot ☺. In the end I also want to thank my family who always supported and believed in me no matter what I was doing throughout my whole life.

Curriculum Vitae

EDUCATION:

Since Sept. 2007: PhD thesis at the Max-Planck-Institute of Neurobiology, Martinsried, Germany under supervision of Dr. Oliver Griesbeck and Prof. Dr. Alexander Borst: *“Investigating Expression, Function and Biocompatibility of the Genetically Encoded Calcium Indicator TN-XXL in Transgenic Mice”*

Aug. 06 – May 2007: Diploma thesis at the Max-Planck-Institute of Neurobiology, Martinsried, Germany under supervision of Dr. Oliver Griesbeck: *“Elektrophysiologische Ableitungen und Fluoreszenz-Imaging von Hippocampalen Neuronen zur Charakterisierung eines neuen Genetisch Codierten Calcium Indikators”*

Okt. 01 – Aug. 2006: Undergraduate studies in Biology at the Ludwig-Maximilians-University Munich, Germany.

June 2000: Graduation from High School: Wilhelm-Hausenstein-Gymnasium, Munich, Germany.

PUBLICATIONS:

Direnberger S, Mues M, Micale V, Wotjak C, Dietzel S, Schubert M, Scharr A, Wahl-Schott C, Biel M, Krishnamoorthy G and Griesbeck O (2011) *Biocompatibility of a genetically encoded calcium indicator in a transgenic mouse model*. Manuscript submitted.

Mank M, Santos AF, **Direnberger S**, Mrcic-Flogel TD, Hofer SB, Stein V, Hendel T, Reiff DF, Levelt C, Borst A, Bonhoeffer T, Hübener M, Griesbeck O (2008) *A genetically encoded calcium indicator for chronic in vivo two-photon imaging*. Nature Methods 5, 805 – 811.

Versicherung

Eidesstattliche Versicherung

Ich versichere hiermit an Eides statt, dass die vorgelegte Dissertation von mir selbständig und ohne unerlaubte Hilfe angefertigt ist.

München, 19.12.2011

.....

Stephan Direnberger

Erklärung

Hiermit erkläre ich, dass die Dissertation nicht ganz oder in wesentlichen Teilen einer anderen Prüfungskommission vorgelegt worden ist und dass ich mich anderweitig einer Doktorprüfung ohne Erfolg nicht unterzogen habe.

München, 19.12.2011

.....

Stephan Direnberger